CYTOCHROME P450 3A-MEDIATED PHARMACOKINETIC VARIATIONS FOR ANTI-INFECTIVE AGENTS

By
Yanhui Lu

A dissertation submitted to Johns Hopkins University in conformity with the requirements for the degree of
Doctor of Philosophy

Baltimore, Maryland
March, 2014

Abstract

Two highly homologous enzymes, cytochrome P450 enzyme 3A4 (CYP3A4) and CYP3A5 play predominant roles in drug elimination by metabolizing more than half of the marketed drugs. This thesis focuses on pharmacokinetics of anti-infective drugs that are CYP3A4/5 substrates, inducers, or inhibitors in order to provide a mechanistic understanding of CYP3A4/5-related pharmacokinetic variations.

In a dose-escalation study in healthy volunteers for daily doses of the anti-tuberculosis drug rifapentine, we developed and validated Ultra Performance Liquid Chromatrography-Mass Spectrometry (UPLC-MS)-based quantitation assays for measurement of plasma concentrations of rifapentine and the comparator drug, rifampin, and their desacetyl metabolites. We identified a less-than-proportional increase in rifapentine plasma peak concentration (C_{max}) and area under the plasma concentration-time curve (AUC) as the rifapentine dose increased from 5 mg/kg to 20 mg/kg. Co-administration of rifapentine decreased AUC of a CYP3A4/5 substrate drug, midazolam, in a dose-independent manner and the reduction was bigger than that caused by the co-administration of rifampin.

Ritonavir is a CYP3A4/5 inhibitor used in fixed combination with several anti-HIV drugs to prolong their half-lives by inhibiting CYP3A4/5-mediated metabolism of those drugs. We conducted a drug-drug interaction study to evaluate the effect of ritonavir-boosted anti-HIV drug lopinavir (LPV/r) on the anti-malarial drug quinine, which has a narrow therapeutic window. We developed a High Performance Liquid Chromatrography (HPLC) interfaced with fluorescence detector assay for simultaneous measurement of

plasma concentrations of quinine and its major pharmacologically active metabolite, 3-hydroxyquinine. We found that LPV/r significantly decreased the exposure of quinine and 3-hydroxyquinine, in both total and protein-bound free forms. The finding highlights the complex nature of the influence exerted by LPV/r on CYP3A4/5 and other drug-metabolizing enzymes involved in quinine disposition including UDP-glucuronosyltransferase, and P-glycoprotein.

Through studying metabolism of the anti-HIV drug maraviroc, we found CYP3A5 was the principal enzyme responsible for the formation of an abundant metabolite, namely, M1. The M1 formation capacity of CYP3A5 was 23 times higher than that of CYP3A4 *in vitro*. Further, human liver microsomes isolated from donors with two loss-of-function CYP3A5*3 alleles exhibited a 79% decrease in M1 formation as compared to those with two wild-type CYP3A5*1 alleles. These results indicate that maraviroc can be used as a chemical phenotyping probe to examine CYP3A5 activity *in vitro*. The excellent safety profile of maraviroc allowed us to further examine the utility of maraviroc to assess CYP3A5 activity in clinical settings with potential for use as a phenotyping probe. Following an oral dose of 300 mg maraviroc, people with two CYP3A5*1 alleles had 41% lower maraviroc AUC and 66% higher apparent clearance compared with those who do not have CYP3A5*1 allele. Subjects who do not have CYP3A5*1 allele had > 2 times the AUC ratio of maraviroc to its M1 metabolite compared with those who carry at least one CYP3A5*1 allele. Strong correlations between plasma concentration ratios and AUC ratios of maraviroc to M1 were observed from 4 to 10 h following the dose with $R^2 >$ 0.87. These results suggest that maraviroc has the potential to be used in clinical studies,

possibly with single-point blood collections after the dose, to determine CYP3A5 activity.

In conclusion, we characterized the changes in pharmacokinetics of CYP3A4/5 substrate drugs caused by anti-infective agents that are CYP3A4/5 inducers or inhibitors; and discovered a novel use of maraviroc to assess activity of the highly variable enzyme CYP3A5 in both *in vitro* and in clinical settings. The results from this thesis inform several anti-infective dosing regimens and provide a phenotyping tool for identification of CYP3A5 substrates, inducers, or inhibitors.

Thesis Committee

Craig W. Hendrix, M.D., Professor, Division of Clinical Pharmacology, Department of Medicine, The Johns Hopkins University School of Medicine (Academic Advisor, reader)

Charles W. Flexner, M.D., Professor, Division of Clinical Pharmacology, Department of Medicine, The Johns Hopkins University School of Medicine (non-reader)

Gary L. Rosner, Sc.D., Professor of Oncology, The Johns Hopkins University School of Medicine (non-reader)

Michelle Rudek, Ph.D., Pharm.D., Associate Professor of Oncology, The Johns Hopkins University School of Medicine (reader)

Preface

This thesis is dedicated to my husband, Jian Yang, and my daughters, Alisa Yang and Hannah F. Yang, without whom this work wouldn't have been possible.

Thank you for your love and support with all that I do.

Acknowledgements

First and foremost I wish to express my deepest appreciation to my advisor, Dr. Craig W. Hendrix, who has supported me through my thesis with his vision and knowledge whilst giving me freedom to work independently. I attribute my Ph.D. degree to his encouragement and effort. You are the one who always supports my research interests unconditionally and magically creates every possible opportunity to enhance my training. I am grateful for all you have done for me.

I wish to express my heartfelt gratitude to Dr. Namandjé N. Bumpus for your guidance and support on my thesis work with maraviroc. I would not have completed this thesis work without you.

I wish to acknowledge and thank the other members of my thesis committee, Dr. Charles W. Flexner, Dr. Michelle Rudek and Dr. Gary L. Rosner. Thank you for taking time with me on my thesis committee meeting, for insightful discussions and helpful suggestions, and for providing me with guidance while granting me the freedom to pursue all of my interests and goals.

I wish to acknowledge and thank my other mentors, Dr. Walter C. Hubbard and Dr. Teresa Parson. Thank you for your time, patience, kindness, and commitment to sharing your knowledge and teaching me all the skills.

I wish to extend my sincere thanks to the faculty and staff of the Division of Clinical Pharmacology, the Johns Hopkins Drug Development Unit, and the Department of Pharmacology and Molecular Sciences at Johns Hopkins University School of Medicine for all of their great effort and kind support.

Table of Contents

List of Tables

Chapter 2 – Effects of daily dosing rifapentine on the pharmacokinetics of CYP3A substrate drug midazolam

Chapter 5 – Effect of CYP3A5 polymorphism on pharmacokinetics of maraviroc and metabolite M1

List of Figures

Chapter 2 – Effects of daily dosing rifapentine on the pharmacokinetics of CYP3A substrate drug midazolam

Chapter 1 – Introduction: Importance of Cytochrome P450 3A in Drug Metabolism and Pharmacokinetics

Cytochromes P450 (CYP) are a superfamily of heme-containing enzymes. They were discovered from rat liver microsomes in the 1950s as a pigment with a characteristic absorbance at 450 nm[1]. The CYP enzymes are found in almost all living organisms. Eukaryotic CYP enzymes are usually anchored in membranes of cellular endoplasmic reticulum[2]. In humans, they are predominantly expressed in liver but are also found in other tissues including intestine, lungs, kidneys, brain, etc[3,4]. The CYP enzymes catalyze biotransformation of large number of endogenous and exogenous compounds to more polar compounds to facilitate their excretion into bile or urine[5]. The typical reaction that a CYP enzyme catalyzes is oxidation:

similarity at amino acid level[9], thereby having a great overlap in enzyme activity and substrate spectrum. The relative contributions of CYP3A4 and CYP3A5 to drug metabolism are usually indistinguishable; the two enzymes are thus commonly described as CYP3A4/5 or CYP3A enzymes. Variations in CYP3A-mediated drug metabolism could lead to variability in pharmacokinetics of the substrate drugs. The major sources of the variations come from drug-drug interactions and genetic polymorphisms.

Drug-drug interactions account for 30% of all adverse drug reactions which are the fourth leading cause of death and cause > 100,000 annual deaths in US[10,11]. On one hand, when two or more co-administered drugs are metabolized by a single CYP enzyme, they may exhibit competitive binding to the enzyme, resulting in inhibition on metabolism of one or both of the drugs, leading to elevated plasma levels; similar results could occur when one of the co-administered drugs is a CYP substrate while the other one is an inhibitor of that enzyme. Under both situations, if the drug that has an elevated plasma concentration has a narrow therapeutic index, drug-related toxicities could occur. On the other hand, however, the substrate drug plasma concentrations may decrease to sub-therapeutic level if it was co-administered with an enzyme inducer, leading to loss of desired drug response. Sometimes, changes of plasma concentrations towards either direction lead to undesired situations. For CYP3A enzymes, over a half of the marketed drugs are their substrates. Moreover, a large amount of drugs in the market have been identified as CYP3A inducers or inhibitors. In addition, citrus fruit, alcohol, herbal and dietary supplements also have modulatory effects on CYP3A activity[12,13]. Therefore, CYP3A-mediated drug-drug interactions are highly likely to happen, which warrants clinical

studies to characterize the inductive or inhibitory effect of CYP3A to inform dosing regimens so that undesirable consequences can be prevented.

CYP3A5 exhibits highly variable expression due to its genetic polymorphism. The wild type CYP3A5*1 allele is associated with the highest expression level whereas changes in the mRNA splicing site due to single nucleotide polymorphisms (CYP3A5*3, CYP3A5*6) or in the reading frame due to a T insertion (CYP3A5*7) result in lower expression or no activity[14-17]. CYP3A5*2 had a nucleotide transition from C to A, causing an amino acid change from threonine to asparagine in the CYP3A5 protein so that the enzyme is not fully functional[18]. The most common nonfunctional allele CYP3A5*3 is abundantly present in the European American population 80-90% of whom are CYP3A5 non-expressors because they are homozygous carriers of CYP3A5*3 alleles. In contrast, CYP3A5*1 has high frequency in the African American population and > 60% of them express CYP3A5 by carrying at least one wild-type allele CYP3A5*1[16,18-20]. In individuals who are expressors, CYP3A5 protein accounts for > 50% of total liver CYP3A and even several-fold higher than that of CYP3A4[21,22]. Increased risk of toxicities for some drugs has been reported in people with low CYP3A5 expression[23-26]. Conversely, unexpected high expression of CYP3A5 could result in low blood drug concentrations leading to compromised drug efficacy and even life-threatening treatment failure. Therefore, measuring CYP3A5 activity using a selective substrate has the potential to inform the rational design of drugs that can be preferentially metabolized by CYP3A4 versus the highly variable CYP3A5. Such a substrate will also help to identify drugs that are CYP3A5 inhibitors or inducers to prevent toxicity or treatment failure in multi-drug using patients.

The following four chapters in this thesis aim to study pharmacokinetic variations introduced by CYP3A-mediated drug-drug interactions and CYP3A5 genetic polymorphisms, and to identify a selective substrate drug that can be used both *in vitro* and *in vivo* to determine activity of the highly variable enzyme CYP3A5. Chapter 2 and Chapter 3 investigate the pharmacokinetic changes of CYP3A substrate drugs when they are co-administered with a CYP3A inducer and a CYP3A inhibitor, respectively; Chapter 4 investigates the anti-HIV drug maraviroc as a chemical probe that can differentiate the metabolic activity of CYP3A5 from that of CYP3A4; and finally, in Chapter 5, we extended the use of maraviroc as a CYP3A5 phenotyping probe from *in vitro* to *in vivo* by evaluating the effects of genetic variations of CYP3A5 on pharmacokinetics of maraviroc and its major oxidative metabolite. Our findings from this thesis will help to understand and characterize pharmacokinetic variations introduced by CYP3A enzymes to prevent disease treatment failure and drug-related toxicities.

Chapter 2 –Effects of daily dosing regimen of rifapentine on the pharmacokinetics of itself and CYP3A substrate drug midazolam

Dolley KE, Bliven-Sizemore EE, Weiner M, **Lu Y**, Nuermberger EL, Hubbard WC, Fuchs EJ, Melia MT, Burman WJ, Dorman SE. *Clin Pharmacol Ther.* 2012; 91(5): 881-8.

Abstract

Rifapentine is an antituberculosis drug that may shorten treatment duration when substituted for rifampin. The maximal tolerated daily dose of rifapentine and its potential for cytochrome 3A4 induction and autoinduction at clinically relevant doses are unknown. We performed a phase I dose-escalation study in healthy volunteers with daily doses ranging from 5 to 20 mg/kg. Using 10 mg/kg rifampin as a comparator drug and midazolam as a CYP3A probe, we evaluated the effect of rifapentine on CYP3A activity. UPLC-MS/MS based quantitation methods were developed and validated to measure plasma concentrations of rifapentine, rifampin, and their desacetyl metabolites. Rifapentine was tolerated at doses as high as 20 mg/kg/day. Steady-state rifapentine concentrations increased with dose from 5 to 15 mg/kg, but area under the plasma concentration–time curve ($AUC_{0–24}$) and maximum concentration (C_{max}) were similar in the 15- and 20-mg/kg cohorts. Although rifapentine pharmacokinetics appeared to be time-dependent, accumulation occurred with daily dosing. The mean $AUC_{0–12}$ of oral midazolam was reduced by 93% with the coadministration of rifapentine and by 74% with the coadministration of rifampin ($p < 0.01$). Changes in the oral clearance of midazolam did not vary by rifapentine dose. In conclusion, rifapentine pharmacokinetics was less than dose-proportional, and its CYP3A induction was robust.

Abbreviations

UPLC-MS/MS, ultra-performance liquid chromatography–tandem mass spectrometry; MRM, multiple reaction monitoring; ESI, electrospray ionization; QC, quality control; LLOQ, low limit of quantitation; $AUC_{0–24}$, area under the plasma concentration–time

curve from time 0 to 24hr; C_{max}, maximum or peak concentration; DMSO, dimethyl sulfoxide; FDA, Food and Drug Administration

Introduction

Tuberculosis is a major global health problem and remains a leading cause of death from an infectious disease[27]. In 2009, there were an estimated 9.4 million new cases and 1.7 million deaths from tuberculosis[28]. The current first-line regimen for tuberculosis was developed decades ago, and standard "short course" therapy with isoniazid, rifampin, pyrazinamide, and ethambutol must be given for 6 months. The long duration is challenging for patients and costly to tuberculosis programs.

Rifapentine belongs to family of rifamycin antibiotics. It is a cyclopentyl analogue of rifampin, the key sterilizing agent in the standard tuberculosis treatment regimen that kills bacteria by inhibiting DNA dependent RNA polymerase. Rifapentine has higher anti-microbial potency with a lower mean inhibitory concentration against Mycobacterium tuberculosis and a longer half-life than rifampin. It was approved by the Food and Drug Administration (FDA) for treatment of tuberculosis at a dose of 600 mg twice weekly (in intensive phase) and once weekly (in continuation phase). Rifapentine is being investigated as a potent tuberculosis drug that may allow reduction in the duration of tuberculosis treatment required for cure.

In a well-established mouse model of tuberculosis, bactericidal and sterilizing activity of rifapentine was enhanced as dose and frequency of administration increased. Therapeutic regimens that include rifapentine can cure tuberculosis in mice in 3 months or less when at least 10 mg/kg are given daily in combination with pyrazinamide and either moxifloxacin or isoniazid[29,30]. Recent studies in immunodeficient mice have shown that,

at the same mg/kg dose, rifapentine produces negative lung cultures more quickly and protects better against the emergence of isoniazid resistance as compared with rifampin[31]. Therefore, rifapentine holds promise as a drug agent that can shorten treatment duration in an exposure-dependent manner.

In humans, the optimal rifapentine dose and regimen are unknown. Clinical trials using current rifapentine dosing regimen have shown unacceptably high relapse rates in some patient populations, and the use of higher and/or more frequent doses is probably necessary to achieve acceptable cure rates[32-34]. Because rifapentine was initially developed and licensed as an intermittently dosed tuberculosis drug, the maximally tolerated daily dose has not been determined, and the dose-linearity of rifapentine concentrations with daily dosing has not been established. Furthermore, the impact of increasing rifapentine doses on induction of cytochrome P450 metabolizing enzyme activity has not been assessed. Like rifampin, rifapentine induces cytochrome P450 enzyme activity and may also induce its own metabolism or clearance[35-38].

We conducted a phase I, open-label, dose-escalation trial of rifapentine in healthy volunteers to evaluate the maximal tolerated daily dose of rifapentine (up to a maximum of 20 mg/kg); the pharmacokinetics of higher daily doses of rifapentine; the relationship between dose and autoinduction of rifapentine metabolism or clearance; and the association between rifapentine dose and induction of CYP3A metabolizing enzymes. We used oral midazolam as a probe drug and rifampin as a comparator drug.

Materials and Methods

Reagents

HPLC-grade solvents were obtained from the following suppliers: acetonitrile from J. T. Baker; dimethyl sulfoxide (DMSO) from Sigma-Aldrich; water from Thermo Fisher Scientific Inc. Ammonium formate was purchased from Sigma-Aldrich; internal standards rifampicin-d3 and rifaximin-d6 from Toronto Research Chemicals Inc. (Toronto, ON, Canada; **Figure 2-1**). Rifapentine, desacetyl rifapentine, rifampin and desacetyl rifampin were provided by sanofi-aventis (**Figure 2-2**).

Methods

Study population

The subjects were healthy adults 18–65 years of age, recruited in Baltimore, MD. The eligibility criteria included negative tests for HIV and hepatitis C virus antibodies, and normal liver function tests. Those with serum creatinine > 1.5 mg/dl, albumin < 3.5 g/dl, hemoglobin < 12.0 g/dl (men) or < 11.0 g/dl (women), neutrophil count < 1,250/mm^3, platelet count < 125,000/mm^3, or positive pregnancy test were excluded. All eligible subjects provided written informed consent. The study was approved by the institutional review boards of the Johns Hopkins University School of Medicine and the Centers for Disease Control and Prevention, and registered at http://www.clinicaltrials.gov (NCT01162486).

Figure 2-1. Chemical structures of internal standards. (**A**) Rifampicin-d3 for assay of rifapentine and desacetyl rifapentine. (**B**) Rifaximin-d6 for assay of rifampin and desacetyl rifampin.

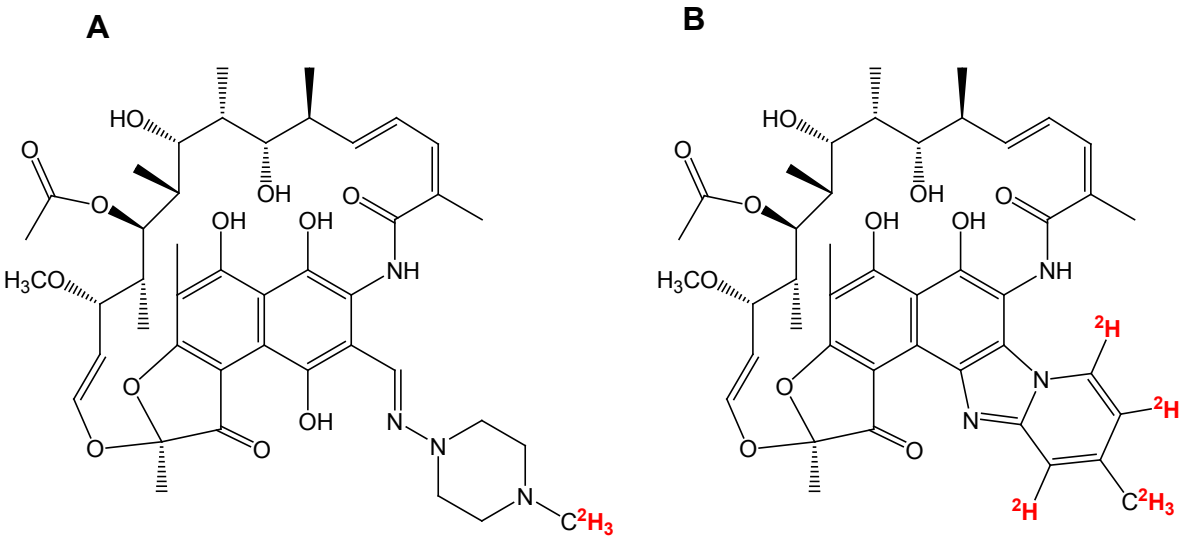

Figure 2-2. Rifamycin drugs and their metabolites in this study.

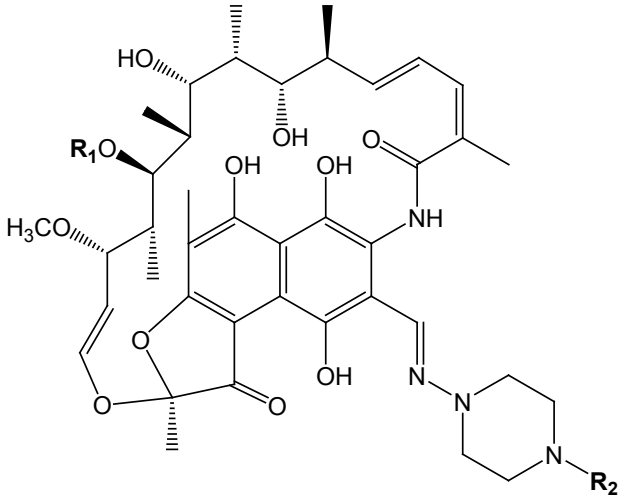

	R_1	R_2
Rifapentine	$COCH_3$	
Desacetyl rifapentine	H	
Rifampin	$COCH_3$	CH_3
Desacetyl rifampin	H	CH_3

Clinical study design

This was a phase I open-label, multiple-dose, pharmacokinetic dose-escalation study. Sequential cohorts of six subjects received oral rifapentine at 5, 10, 15, or 20 mg/kg daily. Another six subjects were enrolled in a 10 mg/kg rifampin comparator arm. All the subjects received two single oral doses of midazolam 15 mg on study days 1 (administered alone) and 15 (coadministered with rifapentine or rifampin) (**Figure 2-3**). The assigned dose of rifapentine or rifampin was administered after a low-fat (865 kcal, 20% (20 g) fat, 5.1 g fiber) breakfast on study days 2–15. Plasma samples for pharmacokinetic analysis were collected before and at 0.5, 1, 2, 4, 5, 8, 12 and 24 h after each midazolam dose and the first doses of rifapentine or rifampin. Blood samples at 34, 48, and 72 h were also collected after the last doses of rifapentine or rifampin. Samples for calculating trough concentrations were collected after 1, 5, 8, and 13 doses of rifapentine. rifapentine dosing started at 5 mg/kg and was escalated by 5 mg/kg for each successive cohort either up to 20 mg/kg or until the maximal tolerated dose, the dose at which dose-limiting toxicities (grade $\geq$ 3 drug-related adverse events occurred in at least two subjects) was reached. Adverse events were graded in accordance with the National Cancer Institute Common Toxicity Criteria, version 2.0. In this study, the prespecified maximum rifapentine daily dose was 20 mg/kg because the results of preclinical toxicology studies did not support the testing of higher doses.

Figure 2-3. Schematic of the dosing regimen and sample collection for pharmacokinetic testing.

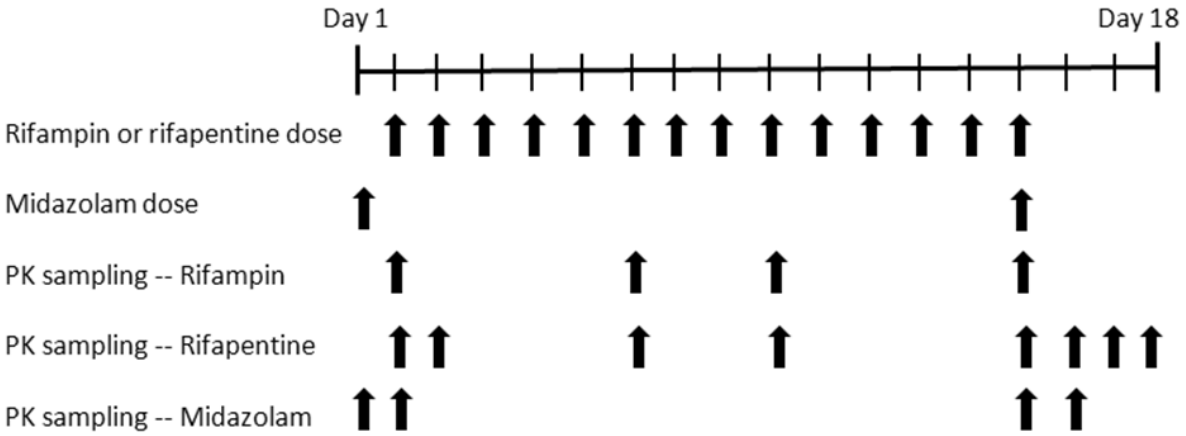

Blood sample processing

Ten ml of blood was collected by venipuncture into a BD Vacutainer tube containing 158 USP units sodium heparin. After collection, the tube was inverted gently 10 times to mix the anticoagulant, and placed on ice. Within 30 min of collection, samples were centrifuged (1500 × *g*, 10 min, 4°C), supernatant plasma was equally aliquotted into two sterile 1.8 ml cryovials, and stored at −80°C in the dark.

Preparation of stock solutions, calibration standards and quality control samples

All master stock solutions were prepared in DMSO: rifapentine and desacetyl rifapentine at 10 mg/ml; rifampin and desacetyl rifampin at 2 mg/ml; internal standards rifampicin-d3 and rifaximin-d6 at 1 mg/ml. Working solutions were serial dilutions of master stocks into DMSO. Calibration standards and quality controls were prepared by spiking freshly-made working solutions into heparinized plasma. Calibration range was linear from 100−50,000 ng/ml for rifapentine; 70−35,000 ng/ml for desacetyl rifapentine; and 100−25,000 ng/ml for rifampin and desacetyl rifampin. Stock solutions, calibration standards and quality control samples were stored at −80°C in the dark until use.

Measurement of plasma concentrations for drugs and metabolites

Plasma midazolam and 1-OH-midazolam concentration levels were determined using a validated high-performance liquid chromatography–mass spectrometry procedure that has been previously described[39]. Absolute recovery of midazolam and 1-OH-midazolam from plasma was 95% and 92%, respectively. The plasma standard curve ranged from 0.1 ng/mL to 500 ng/mL for midazolam and 1-OH-midazolam. For midazolam, intra-day

and inter-day precisions were within 11.4%. For 1-OH-midazolam, intra-day and inter-day precisions were within 11.7%. Accuracy was within 10% for both midazolam and 1-OH-midazolam.

To determine concentrations of rifapentine, rifampin and their metabolites, patient samples, standards, and quality controls were thawed (1 h, dark), vortexed, and processed at room temperature. For rifapentine and its desacetyl metabolite, 20 µL of plasma was placed into a glass tube and 350 µL of acetonitrile containing 17 ng/mL internal standard rifampicin-d3 was added. To remove denatured proteins, samples were vortexed (5 s) then centrifuged (3000 × *g*, 10 min) and supernatant was transferred into HPLC vials (Waters, Milford, MA). Samples above the upper limit of quantitation were diluted, 1:3 sample:heparinized blank plasma, and re-evaluated. For rifampin and its desacetyl metabolite, 50 µL of plasma was combined with 20 µl of 250 ng/mL internal standard rifaximin-6, in wells of a 96-well plate. The plate was vortexed, 30 µL aliquots were transferred into a 96-well filtration plate (Agilent Captiva 0.45 µm polypropylene, Lake Forest, CA), diluted with 350 µL acetonitrile containing 0.5 mg/mL ascorbic acid, vortexed and vacuum filtered. Filtrates were collected into a round collection plate (1 mL, Waters) which was sealed with a pierceable adhesive foil sheet. The autosampler was maintained at 7 ºC.

Chromatographic and mass spectrometric conditions

Plasma concentrations of rifapentine, rifampin, and their desacetyl metabolites were determined by a liquid chromatography-mass spectrometry assay with Waters ACQUITY UPLC interfaced to an AB SCIEX QTRAP 5500 mass spectrometer. The autosampler was covered with foil to protect samples from light. Aliquots of 1 µL were injected onto a

2.5 μm Waters XTerra MS 2.1 × 50 mm C_{18} column. Analytic resolution was achieved at a flow rate of 0.4 ml/min with chromatography at room temperature. Mobile phases were 5 mM ammonium formate in water (A) and 3% DMSO in acetonitrile (B), programmed at 10% B from 0 to 1.6 min, 10−99% B from 1.6 to 3 min, 99% B from 3 to 9 min, and 10% B from 9.1 to 10 min. The liquid chromatography was continued several minutes after elution of analytes and internal standards for minimization of sample carryover. Detection of the analytes and internal standards was achieved via multiple reaction monitoring. The mass-to-charge ratios of characteristic ion pairs (precursor > product) and individually optimized voltages are presented in **Table 2-1**. Retention times for analytes and internal standards are in Table **2-1**.

Table 2-1. Retention times and mass spectrometric conditions.

Compounds	Retention Time* (min)	*m/z*† of Ions		Operating Parameters		
		Precursor	Product	DP‡	CE§	CXP‖
Rifapentine	2.90 ± 0.005	877.4	845.4	106	27	24
Desacetyl rifapentine	2.73 ± 0.005	835.3	803.4	76	21	22
Rifampin	2.75 ± 0.004	823.3	791.4	21	23	30
Desacetyl rifampin	2.61 ± 0.005	781.3	749.4	31	17	42
Rifampicin-d3	2.75 ± 0.004	826.4	794.3	46	25	22
Rifaximin-d6	3.04 ± 0.005	792.2	760.3	11	33	18

*Mean ± standard deviation

†*m/z*, mass-to-charge ratio

‡DP, Declustering Potential, V

§CE, Collision Energy, eV

‖CXP, Collision Cell Exit Potential, V

Mass spectrometry data processing and quantitation

The data were acquired and analyzed by Analyst® software (Version 1.5.1, AB Sciex, Foster City, CA)) in Windows XP Professional Version 2002. Using the peak areas, the peak area ratios of analyte to internal standard were determined for each calibrator to generate the calibration curves. The $1/x^2$ weighting was selected for the best fit of the data. The peak area ratio, intercept and slope (y = mx+b, y = peak area ratio, m = slope, x = concentration, and b = intercept) were used to determine the QCs and unknown specimen concentrations.

Determination of accuracy and precision

Accuracy, the measure of exactness to the target concentration, is reflected by deviation (%) and calculated by dividing the difference between the experimental concentration (EC) and the theoretical concentration (TC) by the theoretical concentration and finally multiplying by 100 (Equation 5-1).

$$\% \text{ Dev} = [(EC - TC)/TC] \times 100 \qquad \text{Equation 5-1}$$

Precision, the measure of the degree of repeatability, is defined as the coefficient of variation (%CV), which is the standard deviation (SD) divided by the mean (M) multiplied by 100 (Equation 5-2).

$$\%CV = (SD/M) \times 100 \qquad \text{Equation 5-2}$$

The precision and accuracy was determined using the 5 different runs that assessed linearity. Within each run, LLOQ, low QC, medium QC, and high QC were analyzed six

times. The intra-run precision and accuracy results were calculated by using the quality control samples within each run.

Determination of Extraction Efficiency

Extraction efficiency was determined by the recovery of the analytes or internal standard using two sets of samples, pre-extracted and post-extracted samples. Each set of samples were prepared using six different lots of plasma at concentrations of low, medium and high QCs. For the first set, plasma samples were spiked with analytes or internal standard prior to the extraction; whereas for the post-extracted samples, blank plasma samples were extracted and then spiked with the analytes or internal standard. The recovery was calculated as:

Recovery (%) = (peak area of pre-extracted samples/peak area of post-extracted samples) × 100

Freeze-thaw Stability Test

Three replicates of low and high quality control samples were stored at –20°C for 24 hours then thawed on a lab bench at room temperature. When the samples were completely thawed, the same samples were put back into the freezer under the previous conditions. For rifapentine and desacetyl rifapentine, the freeze-thaw cycles were repeated 5 times for the low QC and 6 times for the high QC before the samples were analyzed. For rifampin and desacetyl rifampin, the freeze-thaw cycles were repeated for 3 times for both low and high QCs. The results of the samples that went through the freeze thaw cycle (treated) were compared to the results of the samples that were made fresh on the day of the analysis.

Sample matrix stability

Three replicates of the low QC and three replicates of the high QC samples were thawed and kept at room temperature on a laboratory bench for 2 days and then they were analyzed. The results obtained from this analysis were compared to samples of equivalent concentrations that were prepared fresh on the day of the analysis.

Injection matrix stability

The stability of rifampin, rifapentine and their desacetyl metabolites in the injection matrix was assessed by analyzing the samples immediately and then allowing them to remain at room temperature for three days. The samples were then reanalyzed and their concentrations calculated using the calibration curve from the first analysis. These results were then compared to the samples that were made on the original day of the analysis.

Partial volume validation

Partial volume validation was conducted in two different ways. To mimic samples that may be beyond the range of the calibration curve, human heparin plasma samples were spiked with the analytes at 3 times the highest calibrator concentration and then diluted with blank plasma at ratios of 1:4, 1:8 and 1:16; to mimic samples that may have insufficient sample volume for analysis, the medium and high QCs were diluted with blank plasma at ratios of 1:2 and 1:4. Six replicates of each sample were diluted and analyzed.

Statistical considerations and pharmacokinetic analysis

Pharmacokinetic parameters of rifapentine, rifampin, and midazolam (and their metabolites), including AUC, C_{max}, $T_{1/2}$, apparent clearance (CL/F), and volume of distribution (V/F), were calculated using standard noncompartmental methods and WinNonlin software, version 6.1 (Pharsight, Cary, NC). The values of time to C_{max} were computed from the respective concentration-time curves. The mean accumulation index, R_{ac}, namely, the ratio of the multiple-dose $AUC_{0–24}$ to the single-dose $AUC_{0–24}$, was calculated for each dosing cohort. For testing the time invariance of the drug kinetics, the mean ratio of the multiple-dose $AUC_{0–24}$ to the single-dose $AUC_{0–inf}$ ($AUC_{0–24hss}/AUC_{0–infsd}$) was estimated. Statistical analyses were performed using SAS (version 9.2; SAS Institute, Cary, NC). The Student's t-test was used for comparison of pharmacokinetic parameters and an analysis of variance test for analyzing the differences in pharmacokinetic parameters among dose cohorts.

Results

Noise background, chromatography and linearity of quantitation assays

The noise background for the interested analytes and internal standard was first evaluated in the blank plasma. The signals were minimal at the expected retention time of the analytes and the internal standard. Representative chromatograms of rifapentine, desacetyl rifapentine, and the internal standard are shown in **Figure 2-4**. The signal to noise ratios of LLOQ for all four analytes are ≥ 3 (**Figure 2-5**). Calibration range was linear from 100−50,000 ng/mL for rifapentine; 70−35,000 ng/mL for desacetyl rifapentine; and 100−25,000 ng/mL for rifampin and desacetyl rifampin. Depiction of the linearity of the assay is presented in **Figure 2-6**. The r^2 values from five independently repeated runs for each analyte were all ≥ 0.996.

Figure 2-4. Chromatograms of the analytes and internal standard in blank plasma. The data are the extracted ion currents of each of the transitions employed for the LC-MS/MS analysis. Top to bottom are rifapentine (RPT) at 877.378>845.401, desacetyl rifapentine (des-RPT) at 835.344>803.402 and internal standard rifampin-d3 (RIF-d3) at 826.357>794.300.

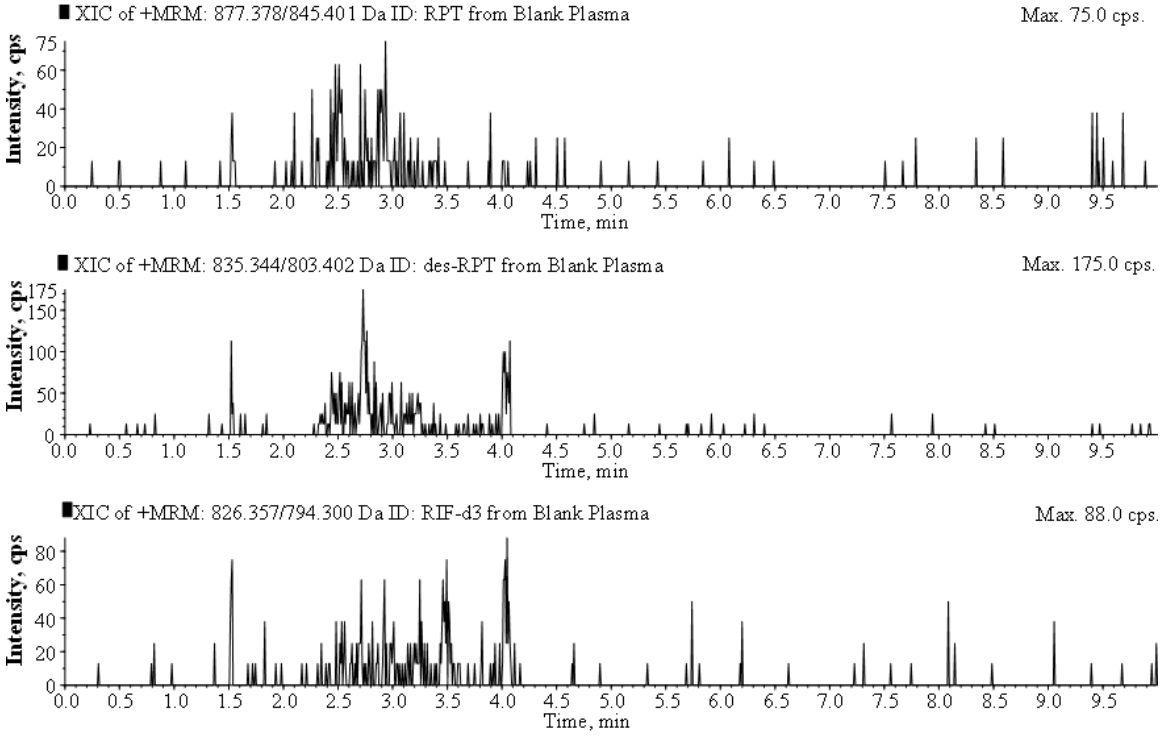

Figure 2-5. Chromatograms of rifapentine and des-rifapentine and internal standard at LLOQ. Concentrations of rifapentine and desacetyl rifapentine are 100 ng/mL and 70 ng/mL, respectively. Top to bottom are rifapentine (RPT), desacetyl rifapentine (des-RPT) and rifampin-d3 (RIF-d3).

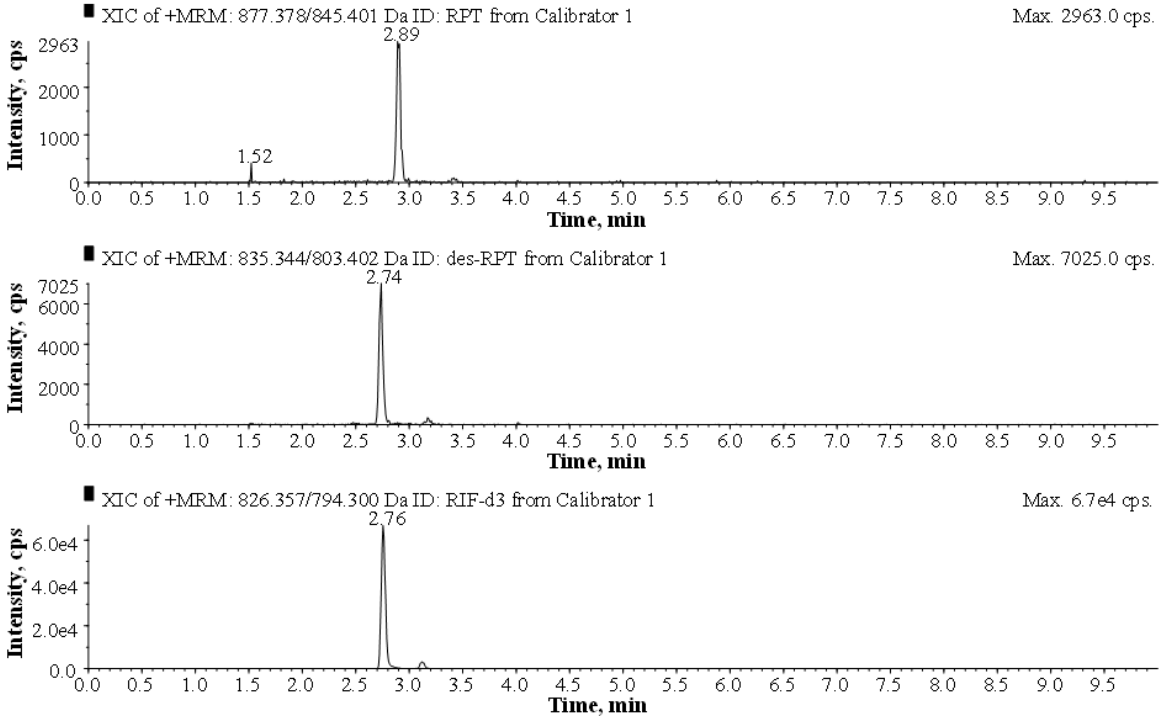

Figure 2-6. Representative calibration curves of rifapentine and desacetyl rifapentine. Top panel is rifapentine (RPT) and bottom panel is desacetyl rifapentine des-RPT). The y-axis represents the peak area ratio of corresponding analytes to the internal standard, rifampin-d3.

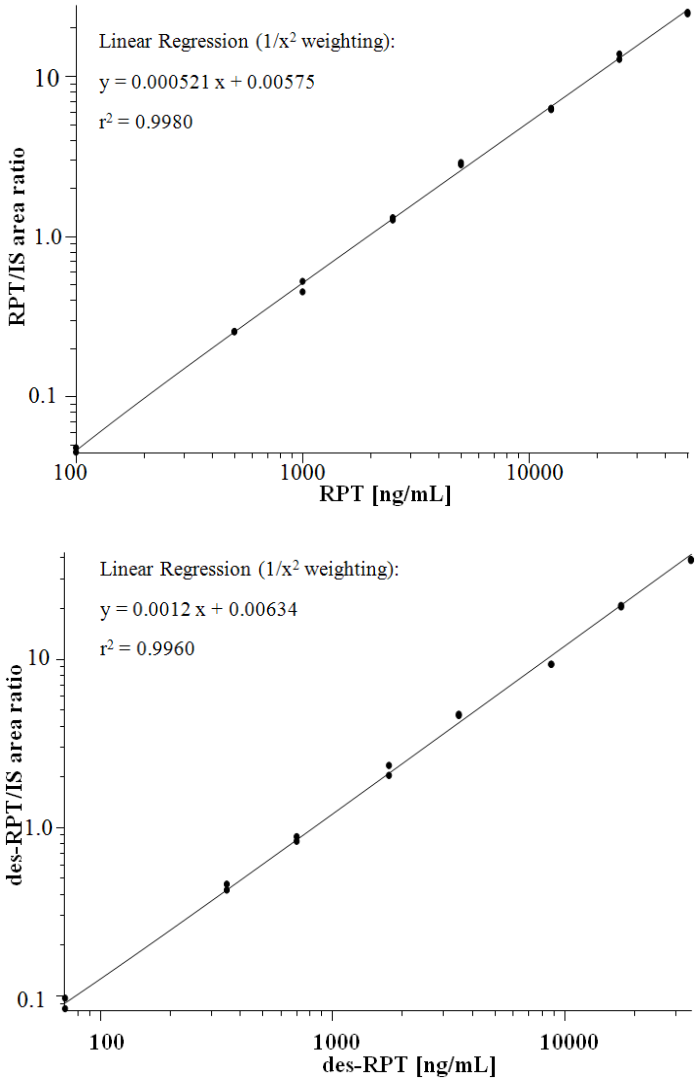

Precision, accuracy, recovery, and stability of the quantitation assays

For rifapentine, as shown in **Table 2-2**, the inter-run precision and accuracy of the LLOQ were 8.6% and 2.3%, respectively; the intra-run precision of LLOQ ranges from 3.0% to 10%; the inter-run precision and accuracy values for the low, medium, and high QCs were ≤ 7.9% for precision and within ± 9.9% for accuracy; and the intra-run precision values of the QCs were ≤ 11%. The recovery of rifapentine from human plasma was ≥ 75% from the test of low, medium and high QCs. After repeated freeze-thaw cycles, the low and high QCs only had 5% and 1.1% changes, respectively, when compared to the samples that did not go through these procedures. This indicated that the freeze-thaw did not significantly affect the stability of rifapentine. For the sample matrix test, rifapentine was stable at room temperature in dark in plasma for 2 days with the % change of the low QC and high QC at -5.6% and -2.7%, respectively. Furthermore, after the samples were processed and left in the injection matrix at room temperature for 3 days, the changes of rifapentine low and high QCs were 0.34 % and -4.7%, respectively. For partial volume validation test, the precision for rifapentine was ≤ 5.5 %, while the accuracies were all within ± 8.0% for all dilutions (**Table 2-3)**.

For desacetyl rifapentine, as shown in **Table 2-4**, the inter-run precision and accuracy of the LLOQ were 13% and 3.9%, respectively; the intra-run precision of LLOQ ranges from 6.3% to 17%; the inter-run precision and accuracy values for the low, medium, and high QCs were ≤ 8.2% for precision and within ± 7.4% for accuracy; and the intra-run precision values of the QCs were ≤ 13%. The recovery of desacetyl rifapentine from human plasma was found to be ≥ 83% by testing low, medium and high QCs. After 3 repeated freeze-thaw cycles, the low and high QCs only had changes of 0.7% and 0.4%,

respectively, comparing to the samples that did not go through these procedures. For the sample matrix test, rifapentine was stable at room temperature in dark in plasma for 2 days with the % change of the low QC and high QC at -8.0% and -7.3%, respectively. Furthermore, sample injection matrix test suggested that the changes of desacetyl rifapentine concentrations were -11.6 % and -7.1%, respectively, for low and high QCs, after the samples were processed and left in the solution at room temperature for 3 days. For partial volume validation test, desacetyl rifapentine had precisions of ≤ 6.5 % and accuracies of within ± 5.0 % for all sample dilutions (**Table 2-5)**.

For rifampin, as shown in **Table 2-6**, the inter-run precision and accuracy of the LLOQ were 10% and -5.8%, respectively; the intra-run precision of LLOQ ranges from 6.9% to 13%; the inter-run precision and accuracy values for the low, medium, and high QCs were ≤ 7.2% for precision and within ± 4.0% for accuracy; and the intra-run precision values of the QCs were ≤ 9.1%. The recovery of rifampin from human plasma was ≥ 105% for low, medium and high QCs. After repeated freeze-thaw cycles, the concentration changes of low and high QCs were 3.0% and 7% changes, respectively, comparing to the samples that did not go through these procedures. For the sample matrix test, rifampin was stable at room temperature in dark in plasma for 1 day with the % change of the low QC and high QC at -7.5% and -4.3%, respectively. Furthermore, after the samples were processed and left in the injection matrix at room temperature for 4 days, the changes of rifampin concentrations at low, medium, and high QCs were -10.9%, 7.7%, and -9.24%, respectively. For partial volume validation test, the precision of rifampin was ≤ 7.8 %, while the accuracies were all within ± 3.7% for all dilutions (**Table 2-7)**.

For desacetyl rifampin, as shown in **Table 2-8**, the inter-run precision and accuracy of the LLOQ were 11% and -2.4%, respectively; the intra-run precision of LLOQ ranges from 2.4% to 16%; the inter-run precision and accuracy values for the low, medium, and high QCs were ≤ 8.7% for precision and within ± 9.2% for accuracy; and the intra-run precision values of the QCs were ≤ 12%. The recovery of desacetyl rifampin from human plasma was ≥98% for low, medium and high QCs. After 3 repeated freeze-thaw cycles, the concentration changes of low and high QCs were 6.0% and 4.1%, respectively, comparing to the samples that did not go through these procedures. For the sample matrix test, desacetyl rifampin was stable at room temperature in dark in plasma for 1 day with concentration changes of the low QC and high QC at -3.8% and -7.7%, respectively. In addition, the changes in desacetyl rifampin concentrations for low, medium and high QCs were -1.0%, -11.3, and -10.5%, respectively, after the samples were processed and left in the solution at room temperature for 4 days. For partial volume validation test, desacetyl rifampin had precisions of ≤ 9.5 % and accuracies of within ± 5.2 % for all sample dilutions (**Table 2-9)**.

The data indicated that we have successfully developed and validated this method for the analysis of rifapentine, rifampin and their desacetyl metabolites in plasma samples. These results are within the acceptance criteria contained in the FDA Guidelines[40].

Table 2-2. Stability, recovery, accuracy, and precision of rifapentine.

Items	LLOQ	Low	Med	High
Concentrations (ng/ml)	100	300	25,000	40,000
Freeze-Thaw* (% change)	N	5.0	N	1.1
Stability† (% change)	N	-5.6	N	-2.7
Recovery (%)	N	75	78	86
Accuracy‡ (%)	2.3	9.9	3.0	-2.5
Intra-run Precision‡ (ranges of CV)	3.0-10	2.9-11	0.1-7.8	4.5-7.9
Inter-run Precision‡ (CV)	8.6	7.9	7.0	6.3
Injection Matrix Stability#	N	0.34	N	-0.73

Abbreviations: LLOQ = Lowest Limit of Quantitation; Low = Low Quality Control; Med = Medium Quality Control; High = High Quality Control

*Low, 5 cycles; High, 6 cycles; N = not determined

†Room temperature in dark for 2 days

‡From 5 independent runs with 6 replicates per run of each quality control concentration

#Samples were processed and left in the solution at room temperature in dark for 3 days

Table 2-3. Partial volume validation results of rifapentine.

	Medium QC		High QC		3 × ULOQ		
Dilution	**1:2**	**1:4**	**1:2**	**1:4**	**1:4**	**1:8**	**1:16**
Repeated Measurements (ng/mL)	24000	25120	42200	42400	145600	163200	168000
	26200	25160	38000	42800	156400	164800	144320
	26200	27600	39200	40400	152800	158400	161600
	25000	26440	38000	40800	154400	163200	159360
	25600	28040	39200	42400	144800	163200	168000
	24400	26360	42400	39920	156800	159200	164800
Theoretical Value (ng/mL)	25000	25000	40000	40000	150000	150000	150000
Mean (ng/mL)	25233	26453	39833	41453	151800	162000	161013
SD	924	1208	1986	1224	5317	2567	8874
% CV	3.7	4.6	5.0	3.0	3.5	1.6	5.5
% Dev	0.9	5.8	-0.4	3.6	1.2	8.0	7.3
n	6	6	6	6	6	6	6

Table 2-4. Stability, recovery, accuracy, and precision of desacetyl rifapentine.

Items	LLOQ	Low	Med	High
Concentrations (ng/ml)	70	210	17,500	28,000
Freeze-Thaw* (% change)	N	0.7	N	0.4
Stability† (% change)	N	-8.0	N	-7.3
Recovery (%)	N	98	83	90
Accuracy‡ (%)	3.9	7.4	-0.2	-5.1
Intra-run Precision‡ (ranges of CV)	6.3-17	2.3-13	3.2-7.7	2.3-6.0
Inter-run Precision‡ (CV)	13	8.2	6.6	6.4
Injection Matrix Stability#	N	-11.6	N	-7.1

Abbreviations: LLOQ = Lowest Limit of Quantitation; Low = Low Quality Control; Med = Medium Quality Control; High = High Quality Control

*Low, 5 cycles; High, 6 cycles; N = not determined

†Room temperature in dark for 2 days

‡From 5 independent runs with 6 replicates per run of each quality control concentration

#Samples were processed and left in the solution at room temperature in dark for 3 days

Table 2-5. Partial volume validation results of desacetyl rifapentine.

	Medium QC		High QC		3 × ULOQ		
Dilution	**1:2**	**1:4**	**1:2**	**1:4**	**1:4**	**1:8**	**1:16**
Repeated Measurements (ng/mL)	17480	17240	26400	30360	100000	115200	112480
	17220	17960	25800	26760	96000	108000	102080
	17000	17800	26400	29200	103600	104800	102400
	16860	17560	25600	25160	104000	104000	110080
	15800	18120	28200	28320	100400	110400	110080
	17000	17880	27400	27960	100000	119200	115200
Theoretical Value (ng/mL)	17500	17500	28000	28000	105000	105000	105000
Mean (ng/mL)	16893	17760	26633	27960	100667	110267	108720
SD	578	315	991	1828	2914	5974	5364
% CV	3.4	1.8	3.7	6.5	2.9	5.4	4.9
% Dev	-3.5	1.5	-4.9	-0.1	-4.1	5.0	3.5
n	6	6	6	6	6	6	6

Table 2-6. Stability, recovery, accuracy, and precision of rifampin.

Items	LLOQ	Low	Med	High
Concentrations (ng/ml)	100	300	12,500	20,000
Freeze-Thaw* (% change)	N	3.0	N	7.0
Stability† (% change)	N	-7.5	N	-4.3
Recovery (%)	N	126	105	107
Accuracy‡ (%)	-5.8	-3.9	4.0	0.2
Intra-run Precision‡ (ranges of CV)	6.9-13	5.0-8.0	0.2-7.2	3.8-9.1
Inter-run Precision‡ (CV)	10	7.2	6.4	6.9
Injection Matrix Stability#	N	-10.9	7.7	9.2

Abbreviations: LLOQ = Lowest Limit of Quantitation; Low = Low Quality Control; Med = Medium Quality Control; High = High Quality Control

*Low and High, 3 cycles; N = not determined

†Room temperature in dark for 1 day

‡From 5 independent runs with 6 replicates per run of each quality control concentration

#Samples were processed and left in the solution at room temperature in dark for 4 days

Table 2-7. Partial volume validation results of rifampin.

	Medium QC		High QC		3 × ULOQ		
Dilution	**1:2**	**1:4**	**1:2**	**1:4**	**1:4**	**1:8**	**1:16**
Repeated Measurements (ng/mL)	11880	13160	18640	18920	70800	74640	75520
	12800	13400	18580	18120	72800	70240	81920
	11940	12720	20400	18520	76400	75040	69120
	12160	12440	19220	19880	75200	82400	73920
	11560	12640	21400	21240	80400	78240	80640
	11880	11600	19760	21920	74000	78640	83040
Theoretical Value (ng/mL)	12500	12500	20000	20000	75000	75000	75000
Mean (ng/mL)	12037	12660	19667	19767	74933	76533	77360
SD	420	628	1094	1536	3305	4176	5421
% CV	3.5	5.0	5.6	7.8	4.4	5.5	7.0
% Dev	-3.7	1.3	-1.7	-1.2	-0.1	2.0	3.2
n	6	6	6	6	6	6	6

Table 2-8. Stability, recovery, accuracy, and precision of desacetyl rifampin.

Items	LLOQ	Low	Med	High
Concentrations (ng/ml)	100	300	12,500	20,000
Freeze-Thaw* (% change)	N	6.0	N	4.1
Stability† (% change)	N	-3.8	N	-7.7
Recovery (%)	N	98	99	104
Accuracy‡ (%)	-2.4	-4.8	9.2	6.0
Intra-run Precision‡ (ranges of CV)	2.4-16	4.6-11	3.5-6.6	3.3-12
Inter-run Precision‡ (CV)	11	7.4	6.2	8.7
Injection Matrix Stability#	N	-1.0	-11.3	-10.5

Abbreviations: LLOQ = Lowest Limit of Quantitation; Low = Low Quality Control; Med = Medium Quality Control; High = High Quality Control

*Low and High, 3 cycles; N = not determined

†Room temperature in dark for 1 day

‡From 5 independent runs with 6 replicates per run of each quality control concentration

#Samples were processed and left in the solution at room temperature in dark for 4 days

Table 2-9. Partial volume validation results of desacetyl rifampin.

	Medium QC		High QC		3 × ULOQ		
Dilution	**1:2**	**1:4**	**1:2**	**1:4**	**1:4**	**1:8**	**1:16**
Repeated Measurements (ng/mL)	12480	12200	19580	18600	69600	72160	73760
	12660	13840	20600	17520	70800	71200	80800
	12520	13120	16680	21040	68400	69520	63520
	12140	12920	21600	19960	73200	83200	80000
	11960	13080	22000	22560	71600	75280	72320
	12420	10840	19680	21680	72800	73680	69760
Theoretical Value (ng/mL)	12500	12500	20000	20000	75000	75000	75000
Mean (ng/mL)	12363	12667	20023	20227	71067	74173	73360
SD	262	1037	1909	1911	1853	4848	6488
% CV	2.1	8.2	9.5	9.5	2.6	6.5	8.8
% Dev	-1.1	1.3	0.1	1.1	-5.2	-1.1	-2.2
n	6	6	6	6	6	6	6

Study population and safety of daily dosing rifapentine

Of 37 enrolled participants, 33 received at least one dose of rifapentine or rifampin. Among these 33, 7 (21%) were females, median age (interquartile range) was 45 (38, 52) years, median weight was 78 (69, 85) kg, and median body mass index was 26 (24, 29) kg/m^2; the majority were African American (22 [69%]) or Caucasian (10 [31%]). Twenty-nine completed both inpatient pharmacokinetic sampling visits, and 28 were included in the pharmacokinetic analysis (one was excluded from pharmacokinetic analyses for apparent non-adherence). Median rifapentine doses by cohort were 450, 750, 1200, and 1650 mg. Clinical symptoms related to study rifamycins were rarely reported, and there were no grade 2 or higher clinical adverse events. Grade 2 or higher laboratory toxicities occurred in 9 (27%) of the participants. Dose-limiting toxicities were observed in three subjects, one each in the rifampin, rifapentine 10 mg/kg, and rifapentine 15 mg/kg cohorts. The symptoms and laboratory abnormalities resolved without specific intervention. As there were not two or more dose-limiting toxicities in any dosing cohort, dose escalation proceeded to the predefined maximum dose of 20 mg/kg. There was no specific toxicity that increased in frequency or severity with increases in rifapentine dose.

The dose effect on pharmacokinetics of rifapentine and desacetyl rifapentine

The mean plasma concentrations of rifapentine after the first and after 14 consecutive daily doses of rifapentine are shown in **Figure 2-7**, by dosing cohort. The median rifapentine single-dose C_{max} and AUC_{0-24} increased nearly dose-proportionally from 5 mg/kg to 15 mg/kg but were similar in the 15 and 20 mg/kg cohorts (**Table 2-10**). Exposures to rifapentine at steady-state after 14 consecutive doses increased less than dose-proportionally with two-fold, three-fold, and four-fold increases in dose resulting in

only 1.38-, 2.29-, and 2.17-fold increases in C_{max} and 1.51-, 2.57-, and 2.22-fold increases in $AUC_{0-24,}$ respectively (**Table 2-11**). At the maximum dose tested (20 mg/kg), the median steady state C_{max}, AUC_{0-24}, and $T_{1/2}$ were 34.1 µg/mL, 483 µg·h/mL, and 16.0 hours, respectively. Median single-dose C_{max} and AUC_{0-24} of desacetyl rifapentine increased nearly dose-proportionally with increases in rifapentine dose from 5 to 15 mg/kg but were similar in the 15 and 20 mg/kg cohorts (**Figure 2-8** and **Table 2-12**). After 14 daily doses of rifapentine, however, desacetyl rifapentine AUC_{0-24} increased 1.31-fold, 3.21-fold, and 2.15-fold with 2-, 3-, and 4-fold increases in rifapentine dose, respectively, and ratios were similar for C_{max}. There were no significant associations between rifapentine or desacetyl rifapentine pharmacokinetic parameters and observed toxicities.

Autoinduction by rifapentine and rifampin

Upon repeated once-daily dosing, the mean (% coefficient of variation [CV]) accumulation index (R_{ac}) was 1.52 (29), 1.40 (29), 1.68 (42), and 1.27 (20); The AUC_{0-24} at steady state divided by the AUC_{0-inf} after a single dose ($AUC_{0-24h}ss/AUC_{0-inf}sd$) was 0.84 (37), 0.86 (33), 0.82 (40), and 0.56(39), for the 5, 10, 15, and 20 mg/kg rifapentine cohorts, respectively. The $AUC_{0-24h}ss/AUC_{0-inf}sd$ in 15 mg/kg and 20 mg/kg cohorts were statistically significantly different from 1 ($p = 0.049$ and 0.003, respectively). Combining the cohorts, the mean estimated $AUC_{0-24h}ss/AUC_{0-inf}sd$ was 0.76 (38), and was statistically significantly different from 1 ($p = 0.0012$), indicating that rifapentine pharmacokinetics is time-dependent. With multiple dosing, $T_{1/2}$ decreased (22.9 vs. 16.7 hs, $p = 0.01$), and clearance increased (23.5 vs. 32.0 mL/h/kg, $p = 0.02$), when compared to single dose values.

Plasma concentrations for both rifampin and desacetyl rifampin were lower after multiple doses than after a single dose (**Figure 2-9**). Five out of six patients did not have measurable rifampin and desacetyl rifampin concentrations at 24 h. Median steady-state rifampin AUC_{0-12}, C_{max}, and $T_{1/2}$ were 45.2 μg·h/mL, 7.5 μg/ml, and 2.4 h, similar to values seen in other studies (**Table 2-13**)[41]. The R_{ac} for rifampin was 0.58 (37), and the AUC_{0-12h}ss/AUC_{0-inf}sd was 0.58 (37), which was statistically different from 1 (p = 0.001).

Effects of daily dosing rifapentine or rifampin on the pharmacokinetics of CYP3A4/5 substrate drug midazolam

The plasma concentration-time curves of midazolam and its major mono-oxygenated metabolite, 1-OH-midazolam, when midazolam was taken alone and together with either rifampin or rifapentine are presented in **Figure 2-10**. Concentrations of both midazolam and the metabolite were reduced when midazolam was given together with rifamycins in all cohorts. The pharmacokinetic parameters are summarized in **Table 2-14**. Mean C_{max} of midazolam was diminished by 74% by co-administration with rifampin and by 82%, 84%, 84%, and 87% by co-administration with rifapentine 5, 10, 15, or 20 mg/kg (**Figure 2-11**). Mean AUC_{0-12} of midazolam was diminished by 75% when co-administered with rifampin and by 92%, 92%, 93%, and 91%, respectively, when given together with steady-state rifapentine dosed at 5, 10, 15, or 20 mg/kg. Combining all rifapentine dose cohorts, midazolam oral clearance increased by 1750% in the rifapentine arms and 925% in the rifampin arm (p = 0.05). The half-life of midazolam is decreased by 56% in the rifapentine arms and 59% in the rifampin arm.

Figure 2-7. Plasma concentration-time profiles of rifapentine after the first dose (A) and 14 daily doses (B) of rifapentine. The values represent arithmetic means with SE bars; RPT stands for rifapentine.

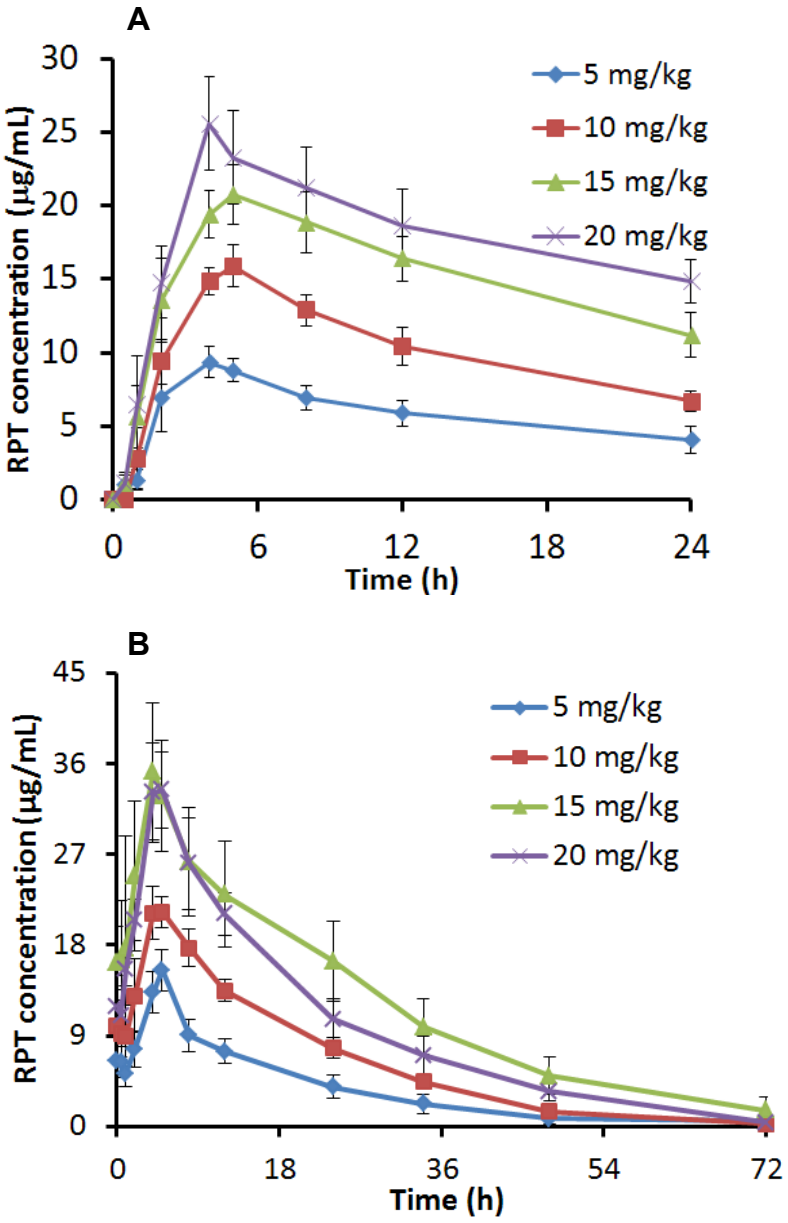

Table 2-10. Median (interquartile range, IQR) pharmacokinetic parameters of rifapentine following single doses of rifapentine.

	Single Dose of Rifapentine (mg/kg)			
	5 (N = 5)	**10 (N = 5)**	**15 (N = 6)**	**20 (N = 6)**
C_{max} (µg/mL)	9.6 (8.0-10.3)	17.1 (13.8-19.0)	25.6 (19.2-27.3)	25.0 (21.6-37.3)
T_{max}(h)	4.0 (4.0 -4.1)	5.0 (4.0-5.0)	4.5 (2.0-5.0)	4.0 (4.0-4.0)
AUC_{0-24} (µg·h/mL)	128 (101-157)	242 (231-260)	363 (310-430)	403 (357-452)
AUC_{0-inf} (µg·h/mL)	214 (187-315)	428 (375-435)	826 (750-1012)	1187 (591-1216)
$T_{1/2}$ (h)	20.4 (17.2-22.9)	16.5 (15.3-18.1)	21.3 (19.9-35.2)	25.9 (21.4-38.3)
CL/F (mL/h/kg)	23.4 (15.9-26.8)	23.4 (23.0-26.6)	18.2 (14.8-20.0)	16.9 (16.5-33.9)
V/F (mL/kg)	582 (525-622)	589 (548-611)	751 (614-753)	868 (750-937)

Table 2-11. Median (interquartile range, IQR) pharmacokinetic parameters of rifapentine following 14 consecutive doses of rifapentine.

	Daily Doses of Rifapentine (mg/kg)			
	5 (N = 5)	**10 (N = 5)**	**15 (N = 6)**	**20 (N = 6)**
C_{max} (µg/mL)	15.7 (13.0-17.7)	21.7 (21.3-22.2)	35.9 (25.1-39.4)	34.1 (29.7-42.9)
T_{max} (h)	4.1 (4.0-4.2)	5.0 (4.0-5.0)	4.2 (4.0-5.0)	4.0 (4.0-4.2)
AUC_{0-24} (µg·h/mL)	218 (142-251)	330 (284-340)	560 (401-735)	483 (414-546)
T1/2 (h)	15.4 (10.9-19.0)	13.7 (13.4-14.4)	23.3 (18.6-25.1)	16.0 (14.0-16.9)
CL/F (mL/h/kg)	23.0 (19.9-35.2)	30.3 (29.4-35.2)	22.3 (20.1-37.4)	36.8 (35.3-48.3)
V/F (mL/kg)	547 (546-556)	581 (572-636)	847 (643-980)	782 (519-1097)

Figure 2-8. Plasma concentration-time profiles of desacetyl rifapentine after the first dose (A) and 14 daily doses (B) of rifapentine. The values shown represent arithmetic

means with SE bars; desRPT stands for desacetyl rifapentine. Y axis is in different scales in A and B.

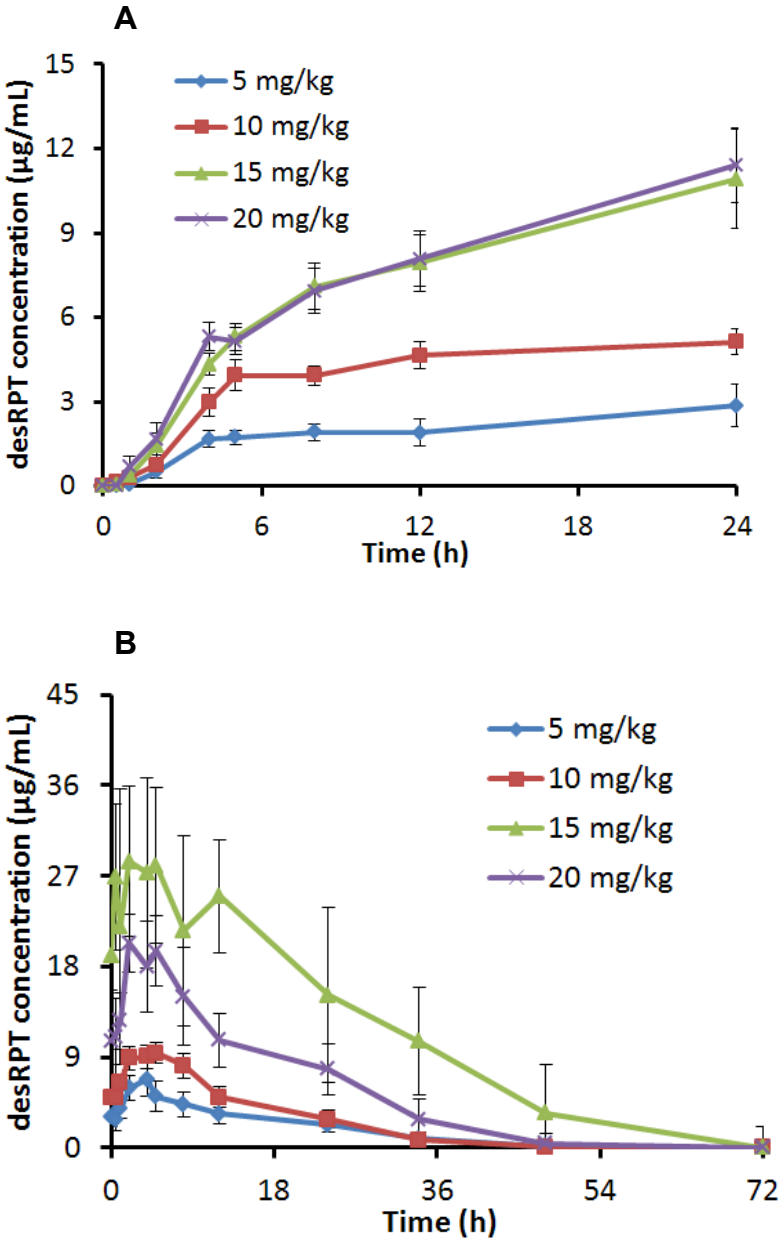

Table 2-12. Median (interquartile range, IQR) pharmacokinetic parameters of desacetyl rifapentine.

Rifapentine (mg/kg)	5 (N = 5)	10 (N = 5)	15 (N = 6)	20 (N = 6)
After single dose of rifapentine				
C_{max} (µg/mL)	2.8 (1.8-3.0)	4.7 (4.4-4.7)	12.1 (7.2-13.5)	10.6 (8.1-13.8)
T_{max} (h)	24.0 (12.0-24.0)	24.0 (12.1-24.0)	24.0 (24.0-24.0)	24.0 (12.0-24.1)
AUC_{0-24} (µg·h/mL)	49.2 (35.5-49.7)	84.3 (80.3-87.5)	153 (130-207)	182 (138-207)
After 14 daily doses of rifapentine				
C_{max} (µg/mL)	8.7 (4.9-9.4)	10.5 (9.5-12.2)	23.6 (15.1-40.1)	19.9 (14.4-29.8)
T_{max} (h)	4.1 (4.0-4.2)	5.7 (5.0-8.0)	4.5 (4.0-8.1)	5.0 (4.2-8.0)
AUC_{0-24} (µg·h/mL)	148 (70.2-148)	194 (178-202)	476 (264-890)	318 (223-461)

Figure 2-9. Plasma concentration-time profiles of rifampin (A) and desacetyl rifampin (B) after the first dose and 14 daily doses of rifampin. The values shown represent arithmetic means with SE bars; RIF stands for rifampin; desRIF stands for desacetyl rifampin.

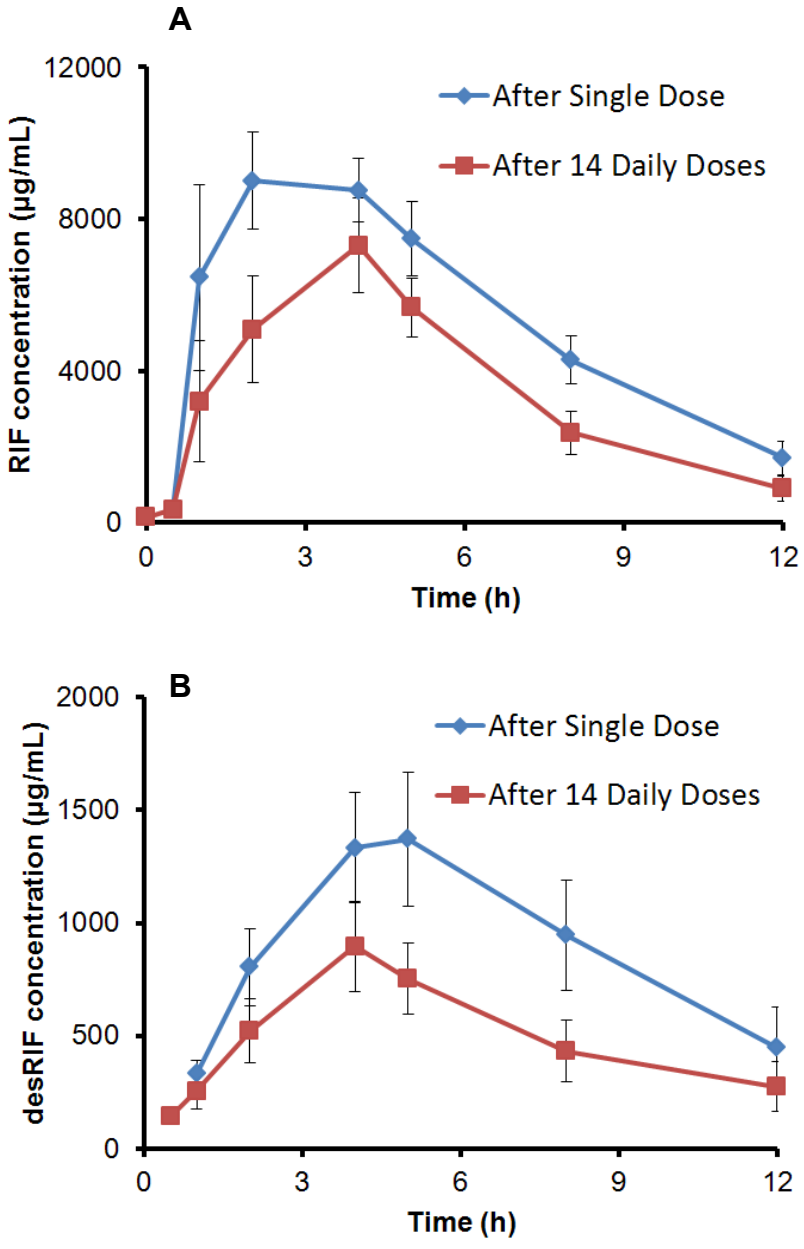

Table 2-13. Median (IQR) pharmacokinetic parameters of rifampin and desacetyl rifampin after a single dose and after 14 consecutive daily doses of 10 mg/kg rifampin.

Parameter	Single dose	Multiple doses
Rifampin		
C_{max} (µg/mL)	10.5 (9.3-12.3)	7.5 (5.5-10.1)
T_{max} (h)	2.0 (1.0-4.0)	4.0 (1.9-4. 0)
AUC_{0-12} (µg·h/mL)	57.5 (55.9-66.2)	45.2 (26.4-53.9)
AUC_{inf} (µg·h/mL)	66.4 (58.5-72.4)	47.4 (27.1-59.7)
$T_{1/2}$ (h)	3.0 (2.6-4. 0)	2.4 (1.9-3.1)
Clearance (mL/h/kg)	9.2 (8. 3-10.3)	13.0 (10.1-22.1)
V/F (mL/kg)	36.8 (33.7-46.0)	49.2 (44.7-57.6)
Desacetyl rifampin		
C_{max} (µg /mL)	1.3 (1.0-1.8)	0.9 (0.4-1.3)
T_{max} (h)	4.0 (4.0-5.0)	4.0 (4.0-5.0)
AUC_{0-12} (µg·h/mL)	8.4 (7.1-10.3)	5.4 (2.2-6.1)

Figure 2-10. Plasma concentration-time profiles of midazolam (A) and 1-OH-midazolam. The values shown represent arithmetic means with SE bars; MDZ, MDZOH, RIF, and RPT stand for midazolam, 1-OH-midazolam, rifampin, and rifapentine, respectively.

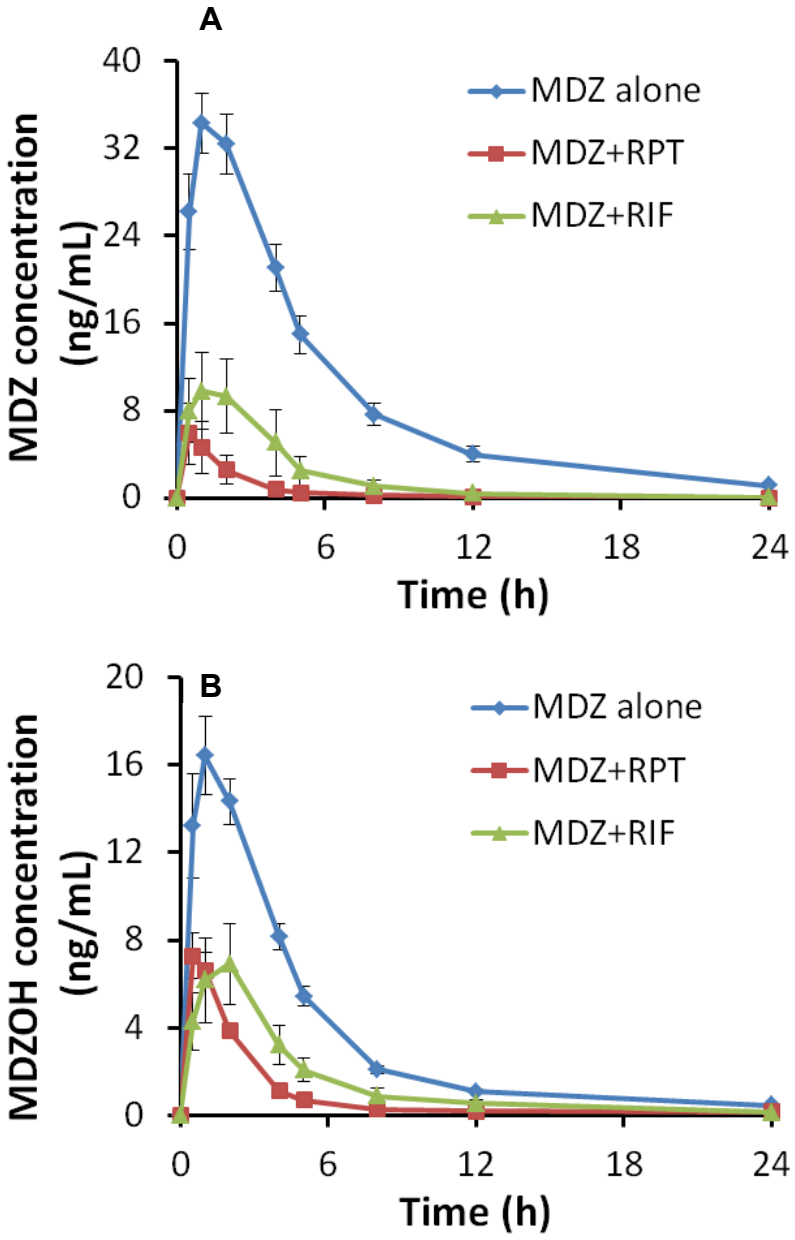

Table 2-14. Median (IQR) midazolam and 1-OH-midazolam pharmacokinetic parameters alone and together with rifapentine by dosing cohort.

Doses	5 mg/kg (N=5)		10 mg/kg (N=5)		15 mg/kg (N=6)		20 mg/kg (N=6)	
	Alone	With RPT	Alone	With RPT	Alone	With RPT	Alone	With RPT
Midazolam								
C_{max}	46.9	8.5	21.1	4.2	45.7	6.2	46.8	5.0
(ng/mL)	(29.1-56.3)	(3.8-11.1)	(20.7-25.6)	(4.1-4.9)	(35.6-52.7)	(5.1-8.8)	(28.9-60.0)	(4.1-5.5)
AUC_{0-12}	150	14.2	114	10.2	204	14.0	173	11.7
(ng·h/mL)	(108-238)	(7.34-20.1)	(111-128)	(10.0-10.4)	(158-255)	(12.6-15.2)	(118-270)	(8.8-14.6)
$T_{1/2}$	6.6	1.9	3.7	2.0	5.2	2.3	4.9	2.4
(h)	(3.6-6.7)	(1.4-2.6)	(2.7-3.8)	(1.6-2.0)	(3.8-6.4)	(1.2-2.8)	(4.0-6.0)	(2.0-2.9)
CL/F	86.1	1051	112	1436	61.5	1038	83.9	1249
(mL/h/kg)	(50.1-129)	(732-2025)	(105-125)	(1433-1489)	(44.2-87.8)	(969-1189)	(44.3-109)	(998-1528)

V/F	565	2849	578	4265	443	3065	496	3749
(mL/kg)	(475-668)	(2708-4125)	(493-660)	(4144-6658)	(381-477)	(2814-3471)	(352-1024)	(3322-4164)
1-OH-midazolam								
C_{max}	12.4	6.2	13.7	4.9	20.1	9.9	18.6	4.8
(ng/mL)	(7.2-17.8)	(5.8-9.8)	(11.5-18.3)	(2.9-9.1)	(14.5-23.0)	(7.4-12.5)	(10.7-23.2)	(3.8-5.9)
T_{max}	2.0	1.0	1.0	1.0	1.0	0.5	1.5	1.0
(h)	(1.0-2.0)	(0.5-1.1)	(1.0-2.1)	(0.6-2.0)	(0.5-2.0)	(0.5-0.5)	(0.5-2.0)	(1.0-1.0)
AUC_{0-12}	60.2	15.3	62.2	13.0	61.9	22.2	63.6	12.7
(ng·h/mL)	(34.7-70.1)	(12.7-16.3)	(52.4-92.5)	(10.7-16.7)	(60.3-76.4)	(18.5-25.8)	(43.5-84.3)	(9.6-16.1)

Table 2-15. Median (IQR) midazolam and 1-OH-midazolam pharmacokinetic parameters alone and together with rifampin.

	Alone	With Rifampin
Midazolam		
C_{max} (ng/mL)	40.8 (34.8-48.7)	9.8(7.2-13.6)
AUC_{0-12} (ng·h/mL)	151 (116-197)	26.9 (10.0-55.8)
$T_{1/2}$ (h)	4.1 (3.5-5.7)	1.7(1.1-4.4)
CL/F (mL/h/kg)	93.3 (70.1-125)	560 (243-1503)
V/F (mL/kg)	501 (381-596)	1289 (795-2155)
1-OH-midazolam		
C_{max} (ng/mL)	20.3 (13.8-23.4)	7.1 (2.7-12.3)
T_{max} (h)	1.1 (1.0-1.9)	2.0(1.0-2.0)
AUC_{0-12} (ng·h/mL)	64.7 (54.9-88.2)	30.1 (9.7-38.0)

Figure 2-11. Decreased C_{max} and $AUC_{0–12}$ of midazolam and 1-OH-midazolam by rifampin or rifapentine. C_{max} (**A**) or AUC_{0-12} (**B**) values of midazolam co-administered with steady-state rifampin or rifapentine relative to midazolam administered alone are shown on vertical axis. The horizontal axis was labeled with the amount of dosing (mg/kg) followed by the drug name rifampin (RIF) or rifapentine (RPT). AUC_{0-12}, area under the concentration–time curve from time 0 to 12 h; C_{max}, maximum concentration; midazolam, midazolam; OHMDZ, 1-OH-midazolam. Data are presented as mean ± SE.

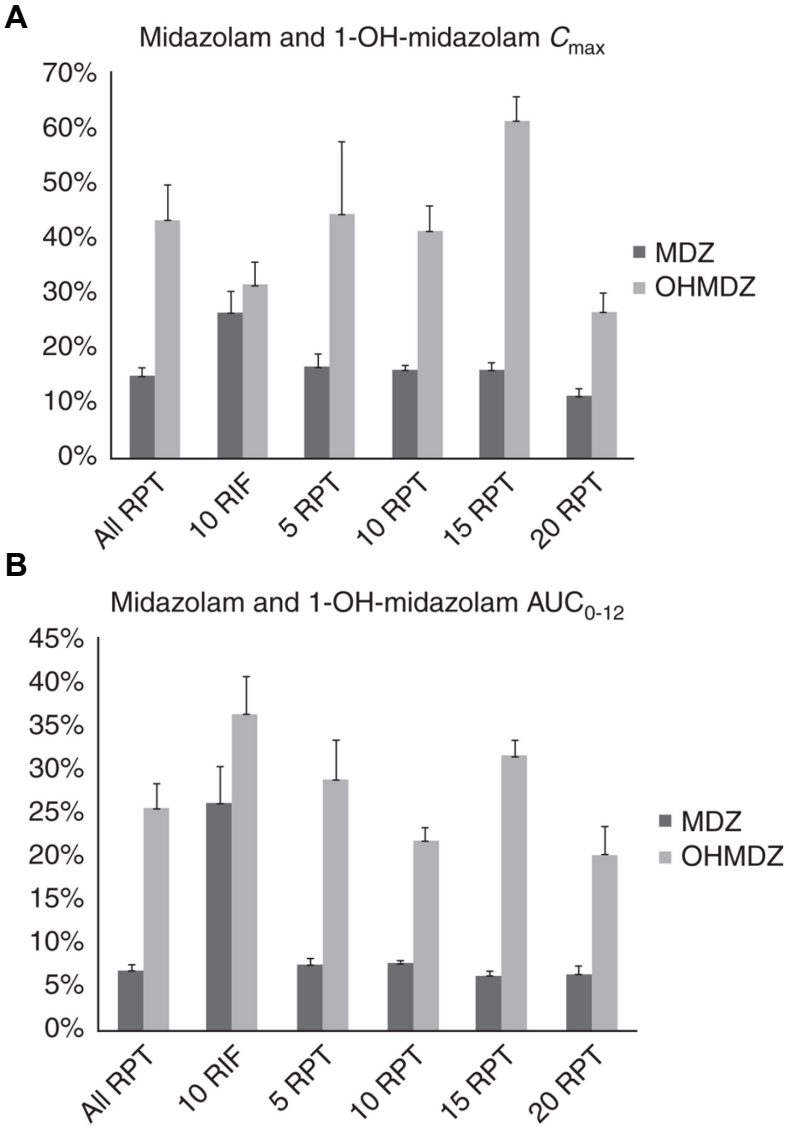

Discussion

In this dose-escalation study in healthy volunteers, the maximal tolerated daily dose of rifapentine was at least 20 mg/kg. The average dose administered in this cohort (1,650 mg daily) is the highest daily dose of rifapentine tested to date in humans and substantially higher than the Food and Drug Administration–approved dose of 600 mg twice weekly. The approved dose has been associated with increased risk of tuberculosis relapse among high-risk patients with tuberculosis and, in some populations, with relapse with acquired rifamycin monoresistance[32,34,42,43]. The optimal rifapentine dose and schedule for treating tuberculosis in humans have not been established, but the mouse model suggests that rifapentine bactericidal and sterilizing activity increases virtually without plateau up to doses of 160 mg/kg and that daily dosing improves outcomes[29,31,38,44]. The pharmacokinetic/pharmacodynamic parameters and targets necessary to achieve cure without relapse in humans are yet to be determined, but *in vitro* and *in vivo* pharmacodynamic studies suggest that the killing of the bacilli by rifamycins is concentration dependent[45]. Taken together, the preclinical and clinical data suggest that the likelihood of rifapentine contributing to a treatment-shortening regimen would be highest if rifapentine is given at the highest dose consistent with acceptable safety. In this study, we found no specific toxicities that increased with increasing rifapentine dose. The safety profile of rifapentine appeared to be similar to that of rifampin 10 mg/kg, which is a widely used rifamycin dose; however, the sample size was too small to allow for firm conclusions to be made about safety. The safety and pharmacokinetic data from this study support the evaluation of daily doses of rifapentine as high as 20 mg/kg in patients with tuberculosis. Safety can be assessed more fully among patients taking multidrug therapy

of standard duration, and pharmacokinetic/pharmacodynamic correlates can be explored to optimize dosing for future pivotal studies.

From a pharmacokinetic perspective, we found that increases in rifapentine dosage resulted in less-than-dose-proportional increases in single-dose and multiple-dose C_{max}. This suggests a decrease in bioavailability with increasing doses, especially at the highest doses. The mechanisms for this are not readily obvious but may include solubility and dissolution limits of multiple coadministered rifapentine tablets; saturability of transport across the gut wall; dose-dependent upregulation of hepatic or gut presystemic biotransformation or clearance (although this effect would have to occur even with a single dose); and sampling error. Rifampin, a close structural analog of rifapentine, is subject to a first-pass effect (presystemic biotransformation or clearance) that is saturated at a daily dose of 300–450 mg, resulting in higher-than-dose-proportional increases in concentrations at daily doses > 450 mg[46]. Our data suggest that this phenomenon does not extend to rifapentine, at least at the doses tested in this study. This may be of clinical concern if the treatment-shortening potential of rifapentine can be achieved only with exposures higher than those achieved by a dose of 15 mg/kg. A given mg/kg dose may result in lower rifapentine concentrations in patients with tuberculosis than in healthy volunteers, and therefore the dose at which maximum exposures will be achieved may be higher in patients with tuberculosis[47].

With repeated dosing, concentrations of rifampin decreased, accompanied by shorter half-life and higher oral clearance when compared with single doses, demonstrating that rifampin's pharmacokinetics is time-dependent, which is consistent with previous observations[48]. As described previously, decreases in exposure levels of rifampin and its

metabolite at steady state probably result from increased gut and/or hepatic clearance with or without secondary biotransformation of the metabolite[46,49]. In our study, there was evidence that the pharmacokinetics of rifapentine was time-dependent, with shorter half-life and higher clearance at steady state as compared with after a single dose, and with $AUC_{0-24hss}/AUC_{0-infsd} < 1$. The mechanism for time-dependent pharmacokinetics (or autoinduction) has not been fully elucidated with respect to either rifampin or rifapentine, but rifamycins are known to be strong inducers of pregnane X receptor, the activation of which leads to a cascade of downstream events, including upregulation of P450 enzymes, phase II enzymes, and transporters[50,51]. Up-regulation of metabolizing enzymes or transporters (including gut or hepatic P-glycoprotein efflux transporters or hepatic OATP1B1 influx transporters) could be responsible for the increases in clearance seen with multiple dosing[51,52]. However, increased production of the enzymes that metabolize rifamycins is unlikely to be solely responsible for this because concentrations of the desacetyl rifapentine metabolite also decline with multiple dosing. Increased biliary clearance of desacetyl rifampin occurs with multiple dosing[53], and this phenomenon may partially explain decreases in desacetyl rifapentine in response to increases in the dose of the parent drug from 15 to 20 mg/kg. Further work is needed to elucidate the mechanisms through which rifamycins "autoinduce" their metabolism and/or clearance. Of note, despite evidence of time-dependent oral clearance, accumulation of rifapentine occurred with daily dosing in contrast to rifampin, a drug with a much shorter half-life. Rifamycins are promiscuous, potent inducers of metabolizing enzymes and transporters. The use of a rifamycin-containing tuberculosis regimen complicates medical therapy of other diseases by reducing the concentrations of coadministered drugs, such as

antiretrovirals used in treating HIV. CYP3A enzymes are expressed in both enterocytes and hepatocytes and are involved in the metabolism of approximately half of all currently licensed drugs. Midazolam is a benzodiazepine that is metabolized by hydroxylation to 1-OH-midazolam, a reaction mediated almost exclusively by CYP3A[54,55]. Midazolam is commonly used as a probe drug to determine whether a candidate drug affects CYP3A enzyme activity and therefore would be expected to affect drug clearance of a CYP3A substrate[56]. When administered orally, midazolam can be used to evaluate the effect of a drug on overall CYP3A activity (presystemic plus systemic, comprising induction or inhibition of both gut and liver CYP3A)[55]. In this study, rifampin at standard doses increased midazolam clearance eight fold, as has been seen in other studies[57,58]; 1-OH-midazolam concentrations were also reduced when midazolam was coadministered with rifampin or rifapentine. Increases in midazolam clearance were higher with coadministered rifapentine than with coadministered rifampin. This was an unexpected finding because *in vitro* studies have shown rifampin to be more potent than rifapentine in inducing CYP3A[59]. However, this is not surprising, given that steady-state concentrations of rifapentine (C_{max}: 22 μg/mL and area under the plasma concentration–time curve (AUC): 330 μg· h/mL) are much higher than for rifampin (C_{max}: 7.5 μg/mL and AUC: 45 μg· h/mL) for the same mg/kg dose. On a micromolar scale, the average concentrations of rifampin and rifapentine at 10 mg/kg were 2.3 and 15.7 μmol/L, respectively. There was no evidence of a dose–response relationship between rifapentine dose and CYP3A induction at the doses studied. These data suggest that recommendations for dose adjustments resulting from drug–drug interaction studies involving rifampin and companion drugs may not lend themselves to ready extrapolation

to rifapentine. Careful testing of interactions involving rifapentine at clinically relevant doses and drugs metabolized by key cytochrome P450 enzymes will help guide dosing considerations in the future.

Our study had some limitations. First, the small sample size did not allow for full characterization of the safety and toxicity of rifapentine at different doses. However, there was no evidence of dose-dependent increases in specific toxicities that are common to the rifamycin class. To assess safety fully, these doses could be tested for a longer duration in patients with tuberculosis who are on multidrug therapy. Second, the single-dose sampling scheme may have prevented accurate estimation of the $AUC_{0–inf}$, thereby affecting evaluation of the time dependence of rifapentine pharmacokinetics. However, there was no evidence of a gamma elimination phase after 24 h in the multiple-dose data, and it is therefore likely that single-dose $AUC_{0–inf}$ estimates using 24 h data were reasonably well approximated. Third, the complex relationships between rifapentine dose and the pharmacokinetics of the parent drug and its metabolite, including time and dose dependencies and covariate effects are best assessed using nonlinear mixed effects modeling. These secondary analyses will be reported separately. Finally, preclinical toxicology studies did not support the testing of doses higher than 20 mg/kg in humans; therefore, although the maximum tolerable dose was not established, it is at least 20 mg/kg/day.

In conclusion, rifapentine, an antituberculosis drug with potential treatment-shortening properties, was tolerated by healthy adults at doses as high as 20 mg/kg/day. Average drug exposures were similar at the two highest doses tested. In humans, rifapentine is at least as strong a CYP3A inducer as rifampin when administered orally at the same mg/kg

dose. These results provide safety and tolerability data to support clinical trials of rifapentine at high daily doses among patients with tuberculosis who are on multidrug regimens.

Chapter 3 – Effects of HIV protease inhibitors lopinavir/ritonavir on the pharmacokinetics of CYP3A substrate drug quinine

Nyunt MM, **Lu Y**, Yu Q, El-Gasim M, Parsons TL, Petty BG, Hendrix CW. *Clin Pharmacol Ther.* 2012; 91(5): 889-95.

Abstract

The centuries-old antimalarial drug, quinine, continues to play a critical role in the treatment of severe falciparum malaria and uncomplicated malaria in pregnant women. It shares cytochrome P450 mediated metabolic pathways with several commonly used antiretroviral drugs, raising the potential for clinically important drug–drug interactions. A phase I pharmacokinetic study was conducted to assess the impact of long-term use of ritonavir-boosted lopinavir (LPV/r) on quinine pharmacokinetics in healthy volunteers. LPV/r significantly decreased the exposure of quinine and its major active metabolite, 3-hydroxyquinine, in both total and free (unbound) forms. These findings highlight the complex nature of the influence exerted by LPV/r on several of the drug-metabolizing enzymes involved in quinine disposition, including CYP3A4, UDP-glucuronosyltransferase, and P-glycoprotein. A decline in quinine exposure may compromise clinical efficacy. Further studies are warranted to assess changes in quinine pharmacokinetics and treatment outcomes in patients with acute malaria receiving antiretroviral therapy that includes LPV/r.

Abbreviations

AAG, α-1-acid glycoprotein; AUC, area under the plasma concentration-time curve; UGT, UDP- glucuronosyltransferase; P-gp, P-glycoprotein; PIs, protease inhibitors; LPV/r, ritonavir-boosted lopinavir.

Introduction

The exaggerated burden of falciparum malaria in the presence of HIV is widely discussed in the literature and is best documented in individuals with limited or impaired immunity to malaria, such as pregnant women[60]. Concomitant use of antimalarial and antiretroviral drugs is becoming increasingly frequent in areas where malaria and HIV coexist, most

notably in many countries in sub-Saharan Africa. There is mounting evidence to suggest that clinically important pharmacokinetic interactions between these two classes of drugs may play a critical role in modifying the nature and degree of antimalarial drug exposure, safety, and efficacy[61-63].

Quinine is one of the most commonly used antimalarial drugs for the treatment of severe malaria as well as for the treatment of uncomplicated malaria in pregnancy. It is extensively metabolized, primarily by the hepatic CYP3A, to the major metabolite, 3-hydroxyquinine[64]. This metabolite contributes 5–15% of antimalarial activity[65]. Both the parent drug and its metabolites are eliminated from the body through glucuronidation; up to 60% of the administered dose is recovered as urinary glucuronides and ~20–25% is excreted as unchanged quinine[66]. As with many CYP3A4 substrates, the P-glycoprotein (P-gp) drug transporter has also been implicated in quinine disposition[67,68]. Quinine is predominantly bound to α-1-acid glycoprotein (AAG)[69], a type 1 acute-phase protein that is upregulated during acute inflammatory states and infection, such as in untreated HIV[70] and malaria infection[71]. AAG binding to quinine is moderate in healthy individuals but may increase to > 90% in patients with acute malaria[69].

Ritonavir-boosted lopinavir (LPV/r) is a fixed-dose combination of HIV protease inhibitors that is commonly included in first-line HIV therapy regimens. Both compounds are primarily metabolized by the CYP3A family and bind to AAG with high affinity[72]. Ritonavir, best known for its potent inhibitory effects on CYP3A4 and CYP3A5[73,74], is now widely used to enhance the systemic bioavailability of other HIV protease inhibitors (PIs) such as lopinavir. However, ritonavir, alone or in combination with other PIs, also

exhibits a complex mixed inhibition–induction effect on several drug-metabolizing enzymes including, but not limited to, UDP-glucuronosyltransferases (UGTs)[75] and membrane transporter P-gp[76,77]. Some of these activities of ritonavir result in a clinically important reduction in plasma drug concentrations[75], raising concerns of a potential decline in therapeutic efficacy.

Recently, a significant increase in quinine exposure was reported in healthy volunteers when quinine was coadministered with ritonavir[78]. Ritonavir's inhibition of CYP3A4 was thought to be responsible for this effect, and the investigators recommended a decrease in quinine dosing. However, ritonavir is essentially always used in combination with other protease inhibitors, often resulting in more complex CYP3A4- and UGT-related drug interactions. To our knowledge, there are no published data on the impact of LPV/r (the commonly used ritonavir/PI combination in current clinical practice) on the disposition of quinine. We conducted a phase I, two-phase, sequential-design pharmacokinetics study in healthy volunteers to assess the impact of LPV/r on quinine pharmacokinetics.

Materials and Methods

Reagents

Quinine and its internal standard quinidine were obtained from Sigma-Aldrich (St. Louis, Missouri); and 3-hydroxyquine was from Toronto Research Chemicals Inc. (North York, Ontario, Canada). Their chemical structures are shown in **Figure 3-1.** Lopinavir, ritonavir, and their internal standard, A-86093.0, were obtained from Abbott Laboratories. High-

performance liquid chromatography–grade methanol, acetonitrile, phosphoric acid, triethylamine and water were supplied by J.T. Baker (Phillipsburg, NJ).

Figure 3-1. Chemical structures of 3-hydroxyquinine, quinine and the internal standard quinidine.

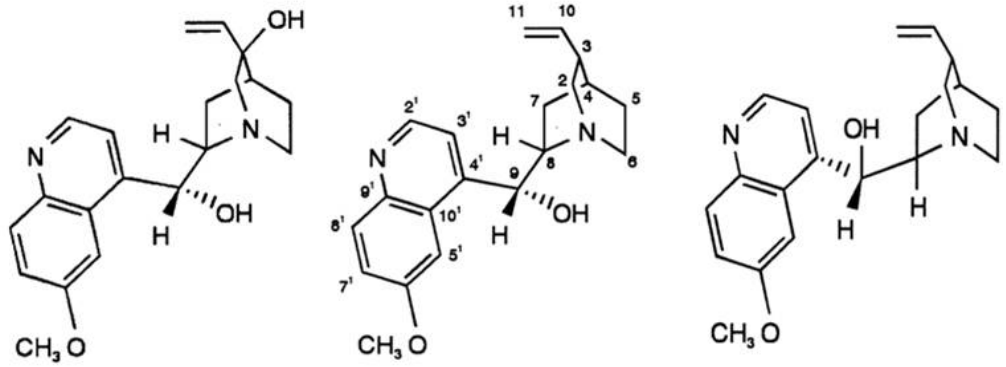

Study design

A phase I, single-center, open-label, sequential pharmacokinetics study was conducted to assess the impact of LPV/r on the pharmacokinetics of quinine in healthy volunteers. The study was reviewed and approved by the institutional review board of Johns Hopkins Medical Institutions and was conducted in compliance with national and local institutional guidelines.

Participants

Inclusion criteria included age 18–55 years, body mass index 18–32 kg/m^2, no evidence of medical illness on the comprehensive history and physical examination, normal readings on the 12-lead EKG, and normal laboratory test values (complete blood count, blood chemistry (Chem12), including serum electrolytes, hepatic enzymes, serum creatinine, pancreatic enzymes, G6PD, HIV and hepatitis panel, coagulation factors, and lipid profile). All participants gave consent in writing. Any prescribed or over-the-counter medications, alcohol, tobacco, and any food or beverage containing substances known or suspected to interact with the CYP3A family were prohibited for 2 weeks prior to and during the study. Premenopausal women were required to have a negative pregnancy test and use two methods of nonhormonal contraception. The participants were admitted as inpatients on study days 0–4 and days 14–15 and monitored in an outpatient setting on days 8, 10, 12, 18, 29, and as clinically indicated.

Administration of study drugs and collection of blood samples for pharmacokinetic testing

The participants received a single oral dose of quinine sulfate 648 mg (538 mg base) on study days 1 and 15, a single oral dose of LPV/r (400/100 mg) on day 4, and LPV/r twice a day on days 5–17 (inclusive). Quinine sulfate was purchased from Ar Scientific (Philadelphia, PA) and was manufactured for Mutual Pharmaceutical (Philadelphia, PA). LPV/r was purchased from Abbott Laboratories (Abbott Park, IL) via the Johns Hopkins Investigational Drug Service.

The participants fasted overnight and up to 4 h after drug administration on study days 1 and 15. Quinine and the first dose of LPV/r were administered with 8 oz of water under direct supervision. The time points for venous blood collection for the pharmacokinetics analysis were as follows: for quinine, within 15 min before the dose (pre-dose) and at 0.5, 1, 2, 3, 4, 6, 8, 12, 24, 48, and 72 h after the dose on study days 1 and 15; for LPV/r, pre-dose, and at 0.5, 1, 2, 3, 4, 6, 8, 12, and 24 h after the dose on day 4; predose, 0.5, 1, 2, 3, 4, 6, 8, and 12 h after the dose on day 15; and before the morning doses on days 8, 10, 12, and 14. Blood was collected in a vacutainer containing sodium heparin. Plasma was separated by centrifugation (1,500 × *g* for 10 min at 4 °C) within 30 min of collection and stored at −80 °C until analysis.

Measurement of plasma concentrations of drugs and their metabolites

Concentrations of quinine/3-hydroxyquinine in plasma were determined using a validated high-performance liquid chromatography method with fluorescent detection, using modifications to a previously reported method[79]. To obtain protein-bound free quinine/3-hydroxyquinine, 1 ml of plasma samples were equilibrated for 30 min at 37°C and transferred to Amicon Centrifree filters (30,000 MWCO; Millipore, Billerica, MA)[80]

followed by ultrafiltration at the same temperature in a fixed angle rotor centrifuge at 1000 × g for 10 min. A volume of 300 µL of the ultrafiltrates was then assayed for free drug concentration determination.

A protein precipitation technique was used in the preparation of calibrators, QCs, the unknown plasma samples and the ultrafiltrates from human subjects. Plasma or filtrate, calibrators, or QCs (300 µl) were put into 12 × 75 mm glass tubes; and 100 µl of the internal standard solution (1 µg/ml quinidine in methanol) were added and mixed. Then 800 µl of methanol were added and vortexed for 10 s followed by centrifugation at 3000 × g for 10 min. Supernatants were transferred to a new tube, dried in SpeedVac (Thermo Electron Corp., San Jose, CA) at 75°C for 2 h and reconstituted in 250 µl of mobile phase A (water/triethylamine (99:1, v/v) at pH 2.5 adjusted with phosphoric acid). The samples were transferred and 200 µl of samples were injected into a Ultrasphere C18 ODS 4.6 × 250 mm (5 µm particle size) column with a responding guard cartridge (7.5 × 4.6 mm, 5µm particle size) (Beckman, Brea, California). Mobile phase B was acetonitrile/ triethylamine (99:1, v/v). The program for the gradient mobile phase is shown as **Table 3-1.** The flow rate was 1.5 ml/min. Acquisition of chromatographic data was obtained using Waters 2695 high performance liquid chromatography (HPLC) system with a Waters 474 fluorescence detector interfaced with Waters Empower 2 software (Milford, Massachusetts). Fluorescence detection was performed at 350 nm (excitation) and 450 nm (emission). The HPLC analysis was conducted at room temperature. The concentrations of quinine and 3-hydroxyquinine were determined from calibration plots of the chromatographic peak height ratios to that of quinidine versus concentration.

Measurements of lopinavir and ritonavir were performed using a validated HPLC method conjugated with ultraviolet detection, as previously reported[81]. The linear range was 100–15,000 ng/ml for both lopinavir and ritonavir.

Pharmacokinetic and statistical data analyses

Data were double key–entered into Microsoft Excel (Microsoft Office Professional, Microsoft, Redmond, WA). Pharmacokinetic parameters were estimated using noncompartmental methods (WinNonlin Professional, version 5.3, Pharsight, Mountain View, CA). Statistical analyses were performed using Stata (version 10.0; Stata, College Station, TX). Because the continuous data were skewed, medians and IQRs were used to summarize the data. The Wilcoxon signed-rank test was used to test the statistical significance of differences in the pharmacokinetic parameters between test conditions. The geometric mean ratio and 90% confidence interval were used to describe the ratio of the pharmacokinetics of quinine plus LPV/r to that of quinine alone. Random-effects models were used to evaluate the attainment of steady state for lopinavir and ritonavir[82]. The estimated coefficient of time (slope) was interpreted as the rate of change in log–plasma trough concentrations over time, where time is a predictor of change. Sample size was selected based on the intra-individual coefficient of variation of quinine area under the plasma concentration-time curve (AUC) observed in a ketoconazole interaction study[83]; the sample size was selected to detect at least a 35% difference (with a 5% type I error for a two-sided test and 80% power) in the AUC of quinine administered alone or with LPV/r.

Table 3-1. The program of the gradient mobile phase of HPLC assay.

Time (min)	A%	B%
0.0	96	4
0.1	94	6
1.1	92	8
14.0	92	8
14.5	20	80
17.5	20	80
18.0	96	4

Results

An assay was developed and validated for simultaneous determination of plasma quinine and 3-hydroxyquinine. Under the chromatographic conditions, the two analytes were well separated from the internal standard, quinidine (**Figure 3-2**). LPV and RTV did not affect the fluorescence signal of quinine and 3-hydroxyquinine (data not shown). The retention times for 3-hydroxyquinine, quinidine and quinine were 5.0 min, 12.4 min and 14.8 min, respectively (**Figure 3-2**). The lower limits of quantification (LLOQs) for quinine and 3-hydroxyquinine were 30 and 20 ng/ml, respectively. The linear ranges for quinine and 3-hydroxyquinine were 30-5000 ng/ml and 20-5000 ng/ml, respectively. The representative calibration curves are shown in **Figure 3-3**.

The intra-run coefficient of variation and accuracy of quality controls ranged from 1.3 to 9.5% and −4.7 to 7.1%, respectively, for quinine (**Table 3-2**), and from 1.2 to 6.0% and −6.0 to 5.4%, respectively, for 3-hydroxyquinine (**Table 3-3**). The inter-run coefficient of variation and accuracy of quality controls ranged from 2.6 to 5.3% and −1.6 to 1.8%, respectively, for quinine, and from 4.0 to 4.1% and −1.8 to 0.6%, respectively, for 3-hydroxyquinine. Stability tests showed that quinine and 3-hydroxyquinine were stable at room temperature in both plasma and injection matrix for 3 days; and they were stable through 3 freeze-thaw cycles. The recovery of quinine, 3-hydroxy quinine and the internal standard for the extraction method was ≥ 79 %. For partial volume validation test, quinine had precisions of ≤ 4.8 % and accuracies of within ± 10.3 % for all sample dilutions (**Table 3-4)**; and 3-hydroxyquinine had precisions of ≤ 5.3 % and accuracies of within ± 7.3 % (**Table 3-5)**.

Figure 3-2. HPLC chromatogram of quinine and 3-hydroxyquinine and the internal standard, quinidine. Human plasma (300 µl) was spiked with 250 ng/mL of QN and 3-OHQN. One hundred µl of 1000 ng/mL quinidine were added and mixed followed by extraction. The retention time of drugs in minutes were labeled on the top of relative peaks. QN, 3-OHQN, and QD stand for quinine, 3-hydroxyquinine, and quinidine, respectively.

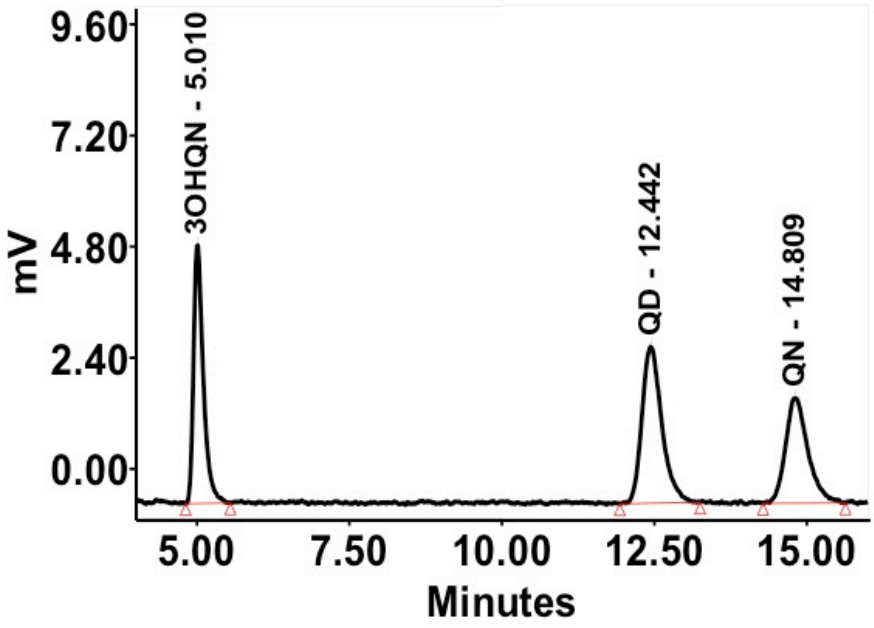

Figure 3-3. Representative calibration curves. Top and bottom panels are quinine (QN) and 3-hydroxyqinine (3-OHQN), respectively. The y-axis is the peak height ratio of analyte to the internal standard, quinidine. Equations and values of r^2 for linear regression are shown as insert.

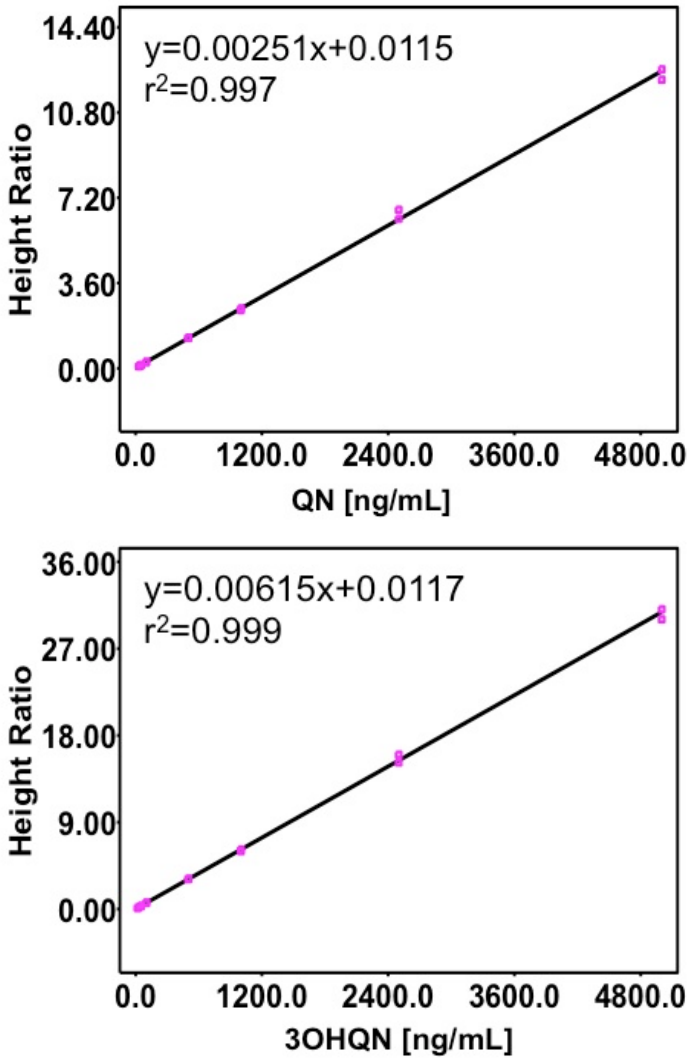

Table 3-2. Stability, recovery, accuracy, and precision of quinine.

Items	LLOQ	Low	Med	High
Concentrations (ng/ml)	30	90	250	4,000
Freeze-Thaw* (% change)	N	0.3	N	0.8
Stability† (% change)	N	-3.3	N	-0.1
Recovery (%)	N	79	N	81
Intra-run Precision‡ (ranges of CV)	4.6-10	1.9-9.5	1.8-3.4	1.3-2.6
Intra-run Accuracy‡ (ranges, %)	-6.6-15	-4.7-0.7	-1.9-7.1	-1.4-3.5
Inter-run Precision‡ (CV)	9.1	4.1	4.0	4.0
Inter-run Accuracy‡ (%)	4.1	-1.6	1.8	1.4
Injection Matrix Stability#	N	1.7	N	0.8

Abbreviations: LLOQ = Lowest Limit of Quantitation; Low = Low Quality Control; Med = Medium Quality Control; High = High Quality Control

*3 cycles; N = not determined

†Room temperature for 3 days

‡From 5 independent runs with 6 replicates per run of each quality control concentration

#Samples were processed and left in the solution at room temperature for 3 days

Table 3-3. Partial volume validation results of quinine.

	Medium QC		High QC		3 × ULOQ		
Dilution	**1:2**	**1:4**	**1:2**	**1:4**	**1:4**	**1:8**	**1:16**
Repeated Measurements (ng/mL)	270 269 267	277 261 252	3968 4039 4036	4152 4131 4250	16148 16286 16341	16723 16470 16458	15504 15649 15562
Theoretical Value (ng/mL)	250	250	4000	4000	15000	15000	15000
Mean (ng/mL)	269	263	4015	4178	16259	16550	15572
SD	1	13	40	64	100	150	73
% CV	0.5	4.8	1.0	1.5	0.6	0.9	0.5
% Dev	7.5	5.2	0.4	4.4	8.4	10.3	3.8
n	3	3	3	3	3	3	3

Table 3-4. Stability, recovery, accuracy, and precision of 3-hydroxyquinine.

Items	LLOQ	Low	Med	High
Concentrations (ng/ml)	20	60	250	4,000
Freeze-Thaw* (% change)	N	1.1	N	-0.9
Stability† (% change)	N	9.3	N	1.4
Recovery (%)	N	86	N	80
Accuracy‡ (%)	1.1	-1.6	0.6	-1.8
Intra-run Precision‡ (ranges of CV)	4.0-9.0	3.2-6.0	1.2-3.5	1.9-4.3
Inter-run Precision‡ (CV)	13	8.2	6.6	6.4
Injection Matrix Stability#	N	-1.2	N	-4.2

Abbreviations: LLOQ = Lowest Limit of Quantitation; Low = Low Quality Control; Med = Medium Quality Control; High = High Quality Control
*3 cycles; N = not determined
†Room temperature for 3 days
‡From 5 independent runs with 6 replicates per run of each quality control concentration
#Samples were processed and left at room temperature for 3 days

Table 3-5. Partial volume validation results of 3-hydroxyquinine.

	Medium QC		High QC		3 × ULOQ		
Dilution	**1:2**	**1:4**	**1:2**	**1:4**	**1:4**	**1:8**	**1:16**
Repeated Measurements (ng/mL)	258 255 278	277 259 250	4100 4222 4201	4268 4266 4331	15785 15838 15742	16273 15918 16036	15409 15480 15490
Theoretical Value (ng/mL)	250	250	4000	4000	15000	15000	15000
Mean (ng/mL)	264	262	4174	4288	15788	16076	15460
SD	13	14	65	37	48	181	44
% CV	4.8	5.3	1.6	0.9	0.3	1.1	0.3
% Dev	5.5	4.7	4.4	7.2	5.3	7.3	3.1
n	3	3	3	3	3	3	3

Pharmacokinetics of quinine and its major active metabolite 3-hydroxyquinine

In the presence of steady-state LPV/r, plasma concentrations decreased for both quinine (**Figure 3-4**) and 3-hydroxyquinine (**Figure 3-5**) compared with those when quinine was administrated alone. The changes in protein-bound free concentrations followed the same pattern. The maximal concentration (C_{max}) and the total drug exposure measured as the area under the plasma concentration–time curve extrapolated to infinity ($AUC_{0–inf}$) decreased both for quinine (48% and 50% reduction in total quinine C_{max} and $AUC_{0–inf}$, respectively, **Table 3-6**) and for 3-hydroxyquinine (69% reduction in both total 3-hydroxyquinine C_{max} and $AUC_{0–inf}$) (**Table 3-7**). The concentrations of the drug and its metabolite in plasma at 8 h after dosing (8 h being the time at which trough concentration is reached after dosing in the standard malaria treatment) were also reduced (45% for total quinine and 67% for 3-hydroxyquinine). Both total clearance and apparent volume of distribution increased, with the extent of increase being larger for total clearance than for apparent volume of distribution, resulting in a decrease in the terminal half-life. However, this decline in half-life was not statistically significant either for total quinine or for total 3-hydroxyquinine. The change in free quinine (**Table 3-8**) and free 3-hydroxyquinine (**Table 3-9**) concentrations was statistically significant for all pharmacokinetic parameters measured, although slightly smaller in magnitude than for the total drug.

Figure 3-4. Plasma concentration-time profiles. Top and bottom panels are for quinine and 3-hydroxyqinine, respectively. Solid lines represent quinine alone; broken lines represent quinine plus LPV/r. Plots with filled circles represent total drug concentrations, and those with open circles represent free drug concentrations. LPV/r, ritonavir-boosted lopinavir.

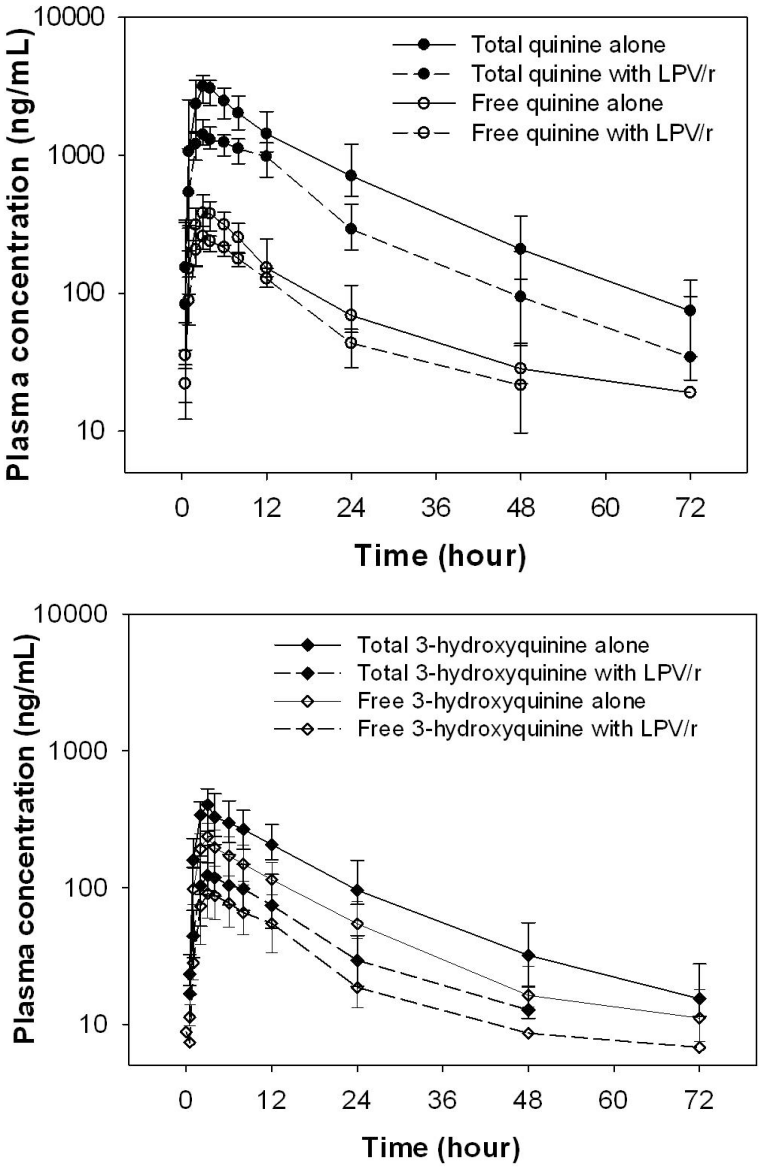

Table 3-6. Pharmacokinetic parameters of total quinine when quinine was administered alone and in the presence of steady-state LPV/r.

PK parameter	Total Quinine*		GMR – tQN (95% CI)	*p*-value
	Alone (N=13)	With LPV/r (N=12)		
T_{max} (h)	3.0 (3.0–3.0)	3.0 (3.0–3.3)	1.09 (0.86–1.40)	0.39
C_{max} (mg/L)	3.2 (2.5–3.7)	1.5 (1.3–2.0)	0.52 (0.44–0.61)	0.001
$AUC_{0\text{-}inf}$ (mg·h/L)	46.7 (41.1–79.2)	24.6 (22.0–30.1)	0.50 (0.39–0.64)	0.0003
$T_{1/2}$ (h)	13.7 (11.1–15.8)	10.4 (7.4–14.0)	0.84 (0.71–1.0)	0.192
V/F (L)	184 (131–272)	316 (272–430)	1.68 (1.37–2.07)	0.0023
CL/F (L/h)	11.5 (6.8–13.1)	22.0 (17.9–24.5)	2.0 (1.56–2.57)	0.0003
C8 (mg/L)	2.0 (1.6–2.5)	1.12 (0.91–1.30)	0.55 (0.45–0.67)	0.0003

$AUC_{0–inf}$, area under the plasma concentration–time curve extrapolated to infinity; C8, plasma concentration at 8 h after quinine administration, representing the end of a dosing interval in standard malaria treatment; CI, confidence interval; CL/F, apparent clearance; C_{max}, maximal concentration; GMR–tQN, geometric mean ratio of total quinine in presence of LPV/r to administration of quinine alone; LPV/r, ritonavir-boosted lopinavir; PK, pharmacokinetic; T_{max}, time to C_{max}; $T_{1/2}$, terminal elimination half-life; V/F apparent volume of distribution.

*Values expressed in median (interquartile range).

Table 3-7. Pharmacokinetic parameters of total 3-hydroxyquinine when quinine was administered alone and in the presence of steady-state LPV/r.

PK parameter	Total 3-hydroxyquinine*		GMR – t3OH (95% CI)	p-value
	Alone (N = 13)	With LPV/r (N = 12)		
T_{max} (h)	3.0 (2.0–3.0)	3.0 (3.0–3.3)	1.26 (0.94–1.69)	0.083
C_{max} (mg/L)	0.40 (0.29–0.52)	0.13 (0.10–0.22)	0.31 (0.25–0.38)	0.0001
$AUC_{0\text{-}inf}$ (mg·h/L)	6.3 (6.1–9.0)	2.0 (1.6–3.2)	0.31 (0.27–0.35)	0.0001
$T_{1/2}$ (h)	11.9 (11.0–16.4)	10.6 (8.8–13.6)	0.87 (0.76–1.0)	0.174
V/F (L)	1474 (939–1944)	3610(2702–4862)	2.86(2.39–3.42)	0.0002
CL/F (L/h)	85.8 (59.6–88.6)	275 (167–338)	3.27 (2.88–3.70)	0.0001
C8 (mg/L)	0.25 (0.19–0.32)	0.18 (0.17–0.19)	0.72 (0.59–0.87)	0.0039

$AUC_{0–inf}$, area under the plasma concentration–time curve extrapolated to infinity; C8, plasma concentration at 8 h after quinine administration, representing the end of a dosing interval in standard malaria treatment; CI, confidence interval; CL/F, apparent clearance; C_{max}, maximal concentration; GMR–t3OH, geometric mean ratio of total 3-hydroxyquinine in presence of LPV/r to administration of quinine alone; LPV/r, ritonavir-boosted lopinavir; PK, pharmacokinetic; T_{max}, time to C_{max}; $T_{1/2}$, terminal elimination half-life; V/F apparent volume of distribution.
*Values expressed in median (interquartile range).

Table 3-8. Pharmacokinetic parameters of free quinine when quinine was administered alone and in the presence of steady-state LPV/r.

PK parameter	Free Quinine*		GMR – fQN (95% CI)	*p*-value
	Alone (N=13)	With LPV/r (N=12)		
T_{max} (h)	3.0 (3.0–3.0)	3.0 (3.0–3.0)	1.06 (0.95–1.19)	0.513
C_{max} (mg/L)	0.38 (0.36–0.51)	0.26 (0.24–0.31)	0.67 (0.57–0.78)	0.0013
$AUC_{0\text{-}inf}$ (mg·h/L)	5.0 (4.4–8.9)	3.7 (3.1–4.0)	0.64 (0.49–0.85)	0.0019
$T_{1/2}$ (h)	9.4 (8.4–13.7)	8.1 (5.8–9.7)	0.80 (0.66–0.96)	0.103
V/F (L)	1345 (1063–1655)	1752(1513–1974)	1.24 (1.06–1.45)	0.064
CL/F (L/h)	108 (60.4–122)	146 (134–175)	1.55 (1.18–2.04)	0.0019
C8 (mg/L)	0.27 (0.19–0.36)	0.10 (0.07–0.15)	0.33 (0.28–0.39)	0.0001

$AUC_{0–inf}$, area under the plasma concentration–time curve extrapolated to infinity; C8, plasma concentration at 8 h after quinine administration, representing the end of a dosing interval in standard malaria treatment; CI, confidence interval; CL/F, apparent clearance; C_{max}, maximal concentration; GMR–fQN, geometric mean ratio of free quinine in presence of LPV/r to administration of quinine alone; LPV/r, ritonavir-boosted lopinavir; PK, pharmacokinetic; T_{max}, time to C_{max}; $T_{1/2}$, terminal elimination half-life; V/F apparent volume of distribution.

*Values expressed in median (interquartile range).

Table 3-9. Pharmacokinetic parameters of free 3-hydroxyquinine when quinine was administered alone and in the presence of steady-state LPV/r.

PK parameter	Free 3-hydroxyquinine*		GMR – f3OH (95% CI)	*p*-value
	Alone (N = 13)	With LPV/r (N = 12)		
T_{max} (h)	3.0 (2.0–3.0)	3.0 (3.0–3.0)	1.2 (1.0–1.4)	0.0399
C_{max} (mg/L)	0.24 (0.17–0.29)	0.10 (0.08–0.15)	0.41 (0.35–0.48)	0.0007
$AUC_{0\text{-}inf}$ (mg·h/L)	4.3 (3.5–5.1)	1.9 (1.1–2.2)	0.35 (0.29–0.43)	0.0001
$T_{1/2}$ (h)	12.6 (10.8–17.6)	8.0 (7.5–12.5)	0.71 (0.62–0.82)	0.0743
V/F (L)	2794(1592–3135)	4995 (3678–6167)	2.03 (1.71–2.41)	0.0081
CL/F (L/h)	125 (105–154)	281 (243–483)	2.85 (2.33–3.50)	0.0001
C8 (mg/L)	0.15 (0.12–0.20)	0.06 (0.05–0.09)	0.43 (0.37–0.50)	0.0007

$AUC_{0–inf}$, area under the plasma concentration–time curve extrapolated to infinity; C8, plasma concentration at 8 h after quinine administration, representing the end of a dosing interval in standard malaria treatment; CI, confidence interval; CL/F, apparent clearance; C_{max}, maximal concentration; GMR–f3OH, geometric mean ratio of free 3-hydroxyquinine in presence of LPV/r to administration of quinine alone; LPV/r, ritonavir-boosted lopinavir; PK, pharmacokinetic; T_{max}, time to C_{max}; $T_{1/2}$, terminal elimination half-life; V/F apparent volume of distribution.
*Values expressed in median (interquartile range).

The median (IQR) of the ratio of the AUCs of total 3-hydroxyquinine to total quinine was 0.14 (0.10–0.18) when quinine was administered alone. The ratio decreased to 0.07 (0.05–0.13) when quinine was coadministered with LPV/r ($p = 0.033$ per Wilcoxon signed-rank test). The ratio of the AUCs of free 3-hydroxyquinine AUC to free quinine was 0.53 (0.45–0.64) when quinine was administered alone, and the ratio decreased to 0.36 (0.27–0.52) in the presence of LPV/r ($p = 0.0076$). The free fraction of quinine (median (IQR)) represented ~10.8% (9.2–12.4%) of total quinine when quinine was administered alone, and it increased to 15.6% (12.6–17.7%) when quinine was coadministered with LPV/r ($p = 0.0047$). The free fraction of 3-hydroxyquinine did not change in the presence of LPV/r.

Pharmacokinetics of lopinavir and ritonavir

Single-dose and steady-state pharmacokinetics estimates of lopinavir and ritonavir are shown in **Table 3-10** and **Table 3-11,** respectively. A steady-state concentration seemed to be reached by study days 8 and 10 for ritonavir and lopinavir, respectively (**Figure 3-5**). The total exposure (median (IQR)) of lopinavir and ritonavir when LPV/r was administered alone were not significantly different from the levels when LPV/r was administered with quinine: lopinavir $AUC_{0–inf}$ 76.4 mg·h/L (55.4–114 mg·h/L) and $AUC_{0–tau}$ 93.4 mg·h/L (77.9–120 mg·h/L) ($p = 0.39$); ritonavir $AUC_{0–inf}$ 3.4 mg·h/L (3.1–5.9 mg·h/L); and $AUC_{0–tau}$ 6.1 mg·h/L (5.0–8.3 mg·h/L) ($p = 0.06$).

Table 3-10. Pharmacokinetic parameters of lopinavir following a single oral dose of LPV/r alone and at steady-state in the presence of quinine.

PK parameter	Single dose (N=13)	Steady-state* (N=12)
T_{max} (h)	3.0 (3.0 – 6.0)	2.0 (2.0 – 3.3)
C_{max} (mg/L)	6.2 (4.3 – 7.7)	10.2 (8.0 – 13.3)
C_{min} (mg/L)	N/A	4.7 (4.1 – 6.2)
AUC(mg·h/L)†	76.4 (55.4 – 114)	93.4 (77.9 – 120)
$T_{1/2}$ (h)	6.0 (5.3 – 7.5)	9.9 (7.8 – 11.4)
V/F (L)	45.7 (42.3 – 56.2)	60.1 (48.7 – 75.5)
CL/F (L/h)	5.23 (3.5 – 7.2)	4.3 (3.4 – 5.1)

Values expressed in median (interquartile range).
AUC, area under the plasma concentration–time curve; CL/F, apparent clearance; C_{max}, maximal concentration; C_{min}, minimal concentration; LPV/r, ritonavir-boosted lopinavir; N/A, not determined; PK, pharmacokinetic; T_{max}, time to C_{max}; $T_{1/2}$, terminal elimination half-life; V/F, apparent volume of distribution.
*Steady-state pharmacokinetic parameters following twice daily dosing of LPV/r in the presence of quinine.
†For single dose, AUC extrapolated to infinity ($AUC_{0\text{-}inf}$); for steady-state, AUC are calculated during a dosing interval ($AUC_{0\text{-}tau}$).

Table 3-11. Pharmacokinetic parameters of ritonavir following a single oral dose of LPV/r alone and at steady-state in the presence of quinine.

PK parameter	Single dose (N = 13)	Steady-state* (N = 12)
T_{max} (h)	4.0 (3.0 – 6.0)	2.0 (2.0 – 3.5)
C_{max} (mg/L)	0.33 (0.24 – 0.45)	1.1 (0.8 – 1.3)
C_{min} (mg/L)	N/A	0.18 (0.12 – 0.24)
AUC(mg·h/L)†	3.4 (3.1 – 5.9)	6.1 (5.0 – 8.3)
$T_{1/2}$ (h)	5.8 (4.9 – 8.0)	4.2 (3.7 – 4.7)
V/F (L)	221 (174 - 256)	98.4 (73.8 – 131)
CL/F (L/h)	29.5 (17.5 – 32.8)	16.4 (12.1 – 20.1)

Values expressed in median (interquartile range).
AUC, area under the plasma concentration–time curve; CL/F, apparent clearance; C_{max}, maximal concentration; C_{min}, minimal concentration; LPV/r, ritonavir-boosted lopinavir; N/A, not determined; PK, pharmacokinetic; T_{max}, time to C_{max}; $T_{1/2}$, terminal elimination half-life; V/F, apparent volume of distribution.
*Steady-state pharmacokinetic parameters following twice daily dosing of LPV/r in the presence of quinine.
†For single dose, AUC extrapolated to infinity ($AUC_{0\text{-}inf}$); for steady-state, AUC are calculated during a dosing interval ($AUC_{0\text{-}tau}$).

Figure 3-5. Trough plasma concentrations of lopinavir (solid line) and ritonavir (broken line) after twice-daily administration of ritonavir-boosted lopinavir (LPV/r) (400 mg/100 mg).

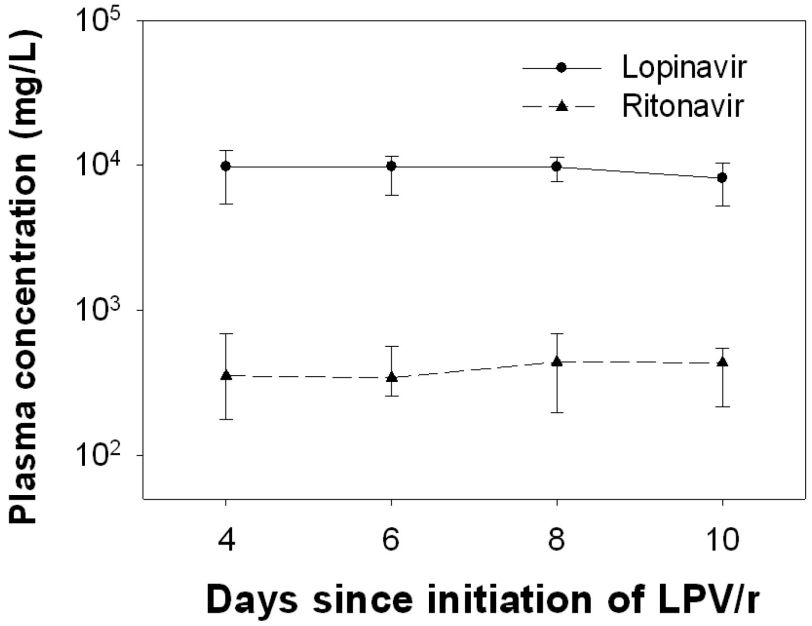

Discussion

Quinine is the oldest and probably the best characterized antimalarial drug in terms of its pharmacokinetics and pharmacodynamics. Unlike other antimalarial drugs, quinine has a relatively well defined therapeutic range of total quinine plasma trough concentration (5–15 mg/L). There is considerable overlap of the therapeutic and toxic concentrations for quinine. At about 5 mg/L, the notorious adverse effects of quinine, including the signs and symptoms of cinchonism[84], usually appear, with the result that successful therapy with quinine is almost always associated with some degree of noxious adverse effects[85]. Despite its record of poor tolerability, quinine maintains its critical role in malaria treatment because of its persistent efficacy against *Plasmodium falciparum* that has evolved resistance to most other drugs and also because of its reasonable safety profile, low cost, long shelf life, and wide availability. It is also the only antimalarial drug known to be safe in early pregnancy and widely available worldwide for parenteral use in the treatment of severe malaria. Quinine may be increasingly relied on if the recently emergent artemisinin resistance in Southeast Asia[86] disseminates more widely.

LPV/r is the most commonly used ritonavir-based combination in HIV management[87]. Our study showed that co-administration of LPV/r caused a significant decrease in exposure of both quinine and its active metabolite, 3-hydroxyquinine. This contrasts with a recent finding by Soyinka *et al.* of a large increase in quinine concentrations when quinine was administered along with ritonavir[78]. The authors concluded that potent inhibition of CYP3A4 by ritonavir was responsible for the increase in quinine exposure, and they recommended reducing quinine dosing in the presence of ritonavir. However,

the recommendation for quinine dose reduction on the basis of evaluation of ritonavir alone may be premature. The design of our study differed from that of the study by Soyinka *et al*. with respect to two important factors: (i) our study assessed the impact of ritonavir plus lopinavir on quinine pharmacokinetics, whereas Soyinka and colleagues' study evaluated ritonavir alone, and (ii) our study participants received LPV/r containing 200 mg ritonavir per day for 10 days before the second round of quinine administration, whereas the participants in the study by Soyinka *et al*. received higher doses of ritonavir (400 mg/day) for a shorter duration (6 days). One partial explanation for the differences in study findings could be that the findings by Soyinka *et al*. are the result of dominant CYP3A4 inhibition before induction was complete. The availability of metabolite and free drug concentration data in our study allowed exploration of additional mechanisms of drug interaction apart from CYP3A4 inhibition, possibly involving multiple drug-metabolizing enzymes and drug transporters including, but not limited to, phase II enzyme UGT and P-gp.

We found that the metabolic ratio of 3-hydroxyquinine to quinine was reduced by ~50% in the presence of LPV/r, consistent with ritonavir's potent inhibitory action on CYP3A4. In the presence of CYP3A4 inhibition, one would expect the exposure of the parent drug, quinine, to be increased. However, our study showed the opposite result. The exposure of both quinine and 3-hydroxyquinine were significantly decreased, and the decrease was greater for 3-hydroxyquinine (**Figure 3-4**). There was also an associated large increase in apparent distribution and total clearance for both compounds and a decrease in half-life, possibly indicating a decline in bioavailability secondary to increased pre-systemic metabolism induced by ritonavir. In the presence of other protease inhibitors, ritonavir

can also exhibit a mixed inhibition-inducing effect on several drug-metabolizing enzymes, in addition to CYP3A4. This inductive effect has been shown to reduce the exposure of several drugs, resulting in recommendations for dose adjustment or alternative therapy[75]. One of these ritonavir-induced enzymes, UGT, is also responsible for the final conjugation of quinine and 3-hydroxyquinine. Although the family or subfamily of UGTs involved in the disposition of quinine and 3-hydroxyquinine have not been clearly identified, it has been shown that up to 60% of the administered dose of quinine is recovered as glucuronides and 20–25% as unchanged quinine. We suspect that the significant reductions in quinine and 3-hydroxyquinine were mediated by the induction of UGT. A decrease in the rate of formation (because of inhibition of CYP3A4) and an increase in the metabolism of 3-hydroxyquinine (because of induction of UGTs) may account for the observed greater reduction in concentrations of 3-hydroxyquinine than in those of quinine.

Another potential pathway that may be involved in the quinine-LPV/r interaction is P-gp multidrug efflux transporter. Many substrates of CYP3A4, like quinine, are known to be substrates of P-gp as well[88], and P-gp is known to be induced by chronic administration of ritonavir[77]. The two-fold reduction in quinine concentration despite ritonavir-mediated CYP3A4 inhibition may reflect simultaneous induction of UGTs and P-gp, resulting in an increased intestinal drug efflux and presystemic metabolism leading to reduced bioavailability. Lopinavir is unlikely to be the cause of this suspected induction because it does not have inductive effects[89].

The 50% increase in the free fraction of quinine in the presence of LPV/r may have also enhanced the availability of quinine for enzymatic biotransformation and increased the volume of distribution. The reason for this increase is unclear. HIV protease inhibitors bind to AAG with high affinity[72], whereas quinine binding to AAG is moderate in healthy volunteers[69]. Although displacement of quinine from AAG by lopinavir and ritonavir is a possible explanation, it is unlikely that this change in protein binding would have caused a significant impact on the overall quinine exposure or had an important clinical implication. This is because the quinine was orally administered and has a relatively small hepatic extraction[90].

Adverse events were frequent in our study. Symptoms suggestive of quinine-induced cinchonism (headache, nausea, and tinnitus) occurred in 13% of the participants, and gastrointestinal discomfort, probably associated with LPV/r, was found in >70% of the participants. The nature of the adverse events and their frequency were similar to previous observations[91-93]. A significant QTc prolongation, which is likely to be associated with quinine treatment, was found in the two female participants who received the two highest quinine doses on a per kilogram basis. The drug concentrations in these participants were not different from those in the others, and therefore there was no evidence of a concentration–response relationship. Although the absolute length of the QTc interval did not exceed 500 ms, the maximal increase of > 60 ms from baseline raised a clinical concern. Changes of similar magnitude in the QT interval in association with quinine treatment have been reported in healthy volunteers[94-96]. Cardiac toxicity seems to be more frequent in healthy volunteers than in patients with acute malaria[97], and this raised a caution for the drug cocktail studies wherein quinine is commonly used to

probe CYP3A4[94-96]. It is also known that the baseline QT interval determines the risk of arrhythmia[98]; women have longer baseline QT intervals and are therefore at greater risk for drug-induced *torsade de pointes*[99,100]. A larger study is needed to assess the risk of quinine-related cardiac toxicity in women of reproductive age, the population most likely to be exposed to this drug in malaria-endemic countries.

One of the female participants in our study who developed QTc prolongation also developed a skin exanthema when both quinine and LPV/r were present; this made it impossible to identify the likely cause clearly. As stated earlier, quinine exposure in this participant did not differ from those in other participants, suggesting that pharmacokinetic polymorphisms were not involved. Dermatologic adverse effects have been reported in association with either quinine hypersensitivity reaction[91] or LPV/r[101]; however, the dermatologic adverse effects are believed to be uncommon with either drug[92,93]. Given the Asian ancestry of this research participant, it is worth considering the Stevens-Johnson syndrome. This syndrome has been attributed to treatment with carbamazepine[102] and allopurinol[103] in the presence of human leukocyte antigen polymorphisms *HLA-B*1502* and *HLA-B*5801*, respectively, in Han Chinese.

The major limitation of our study is that only a single dose of quinine was tested in healthy volunteers. A healthy population enables us to avoid the potential impact of illness and minimize the complexity associated with the concomitant use of multiple drugs that is typically prevalent in the HIV-infected patient population. The nature and degree of drug interactions observed in healthy volunteers are usually similar to interactions seen in HIV-infected populations[104,105], and findings in healthy volunteers are

generally being applied to individuals with HIV. However, the recent discovery of a striking discordance in results between a study in healthy volunteers[106] and one in patients with HIV and tuberculosis[107] suggests caution in extrapolating findings in healthy volunteers to populations with disease. Confirmatory studies in relevant target populations should be encouraged[108]. It is also plausible that quinine disposition could differ between healthy and malaria-infected populations because of important differences that may influence quinine metabolism, including the abundance of the major drug-binding protein AAG and underlying hepatic and renal functions. Similarly, the impact of LPV/r may be different after a single quinine dose than after multiple quinine doses (as are typically encountered in treatment regimens). For these reasons, our findings should be confirmed in patients coinfected with malaria and HIV. In addition, the metabolic pathways proposed to explain quinine disposition in our study are conjectural; the assessment of glucuronides and other metabolic products should be carried out for a full understanding of the interaction between quinine and LPV/r.

Conclusions

The HIV protease inhibitor combination LPV/r causes a significant decline in exposure (C_{max} and AUC) of quinine and its major active metabolite, 3-hydroxyquinine, after a single oral dose of 538 mg base quinine in healthy volunteers. This decline was noted in both the total and free forms of the quinine and its metabolite, and the degree of reduction was larger for the metabolite than for the parent drug. In the presence of steady-state LPV/r, the metabolic ratio of 3-hydroxyquinine to quinine decreased, and the free fraction of quinine (but not 3-hydroxyquinine) increased. A single dose of quinine did not affect the total exposure of either lopinavir or ritonavir. Because quinine is efficacious

within a relatively narrow concentration range, a routine quinine regimen in individuals who are also taking long-term LPV/r-based antiretroviral treatment may not achieve therapeutic quinine concentrations, thereby compromising the efficacy of the malaria treatment. A careful assessment of quinine pharmacokinetics in association with antimalarial treatment outcomes is needed in a relevant population of individuals living with HIV who are at risk for malaria.

Chapter 4 – CYP3A5 plays a predominant role in formation of a major mono-oxygenated metabolite of maraviroc

Lu Y, Hendrix CW, Bumpus NN. *Drug Metab Dispos.* 2012 Dec; 40 (12):2221-30.

Abstract

Maraviroc is an anti-HIV drug that acts by blocking viral entry into target cells. Using ultra performance liquid chromatography-mass spectrometry several monooxygenated, dioxygenated and glucuronidated metabolites of maraviroc were identified both in vitro and in vivo. Characterization of the enzymes involved in the production of these metabolites determined that CYP3A5 was the principal enzyme responsible for the formation of an abundant metabolite of maraviroc that resulted from oxygenation of the dichlorocyclohexane ring. For the formation of this metabolite the V_{max} values for CYP3A4 and CYP3A5 were 0.04 and 0.93 pmole/min/pmole P450, and the K_m values were 11.1 μM and 48.9 μM, respectively. Further, human liver microsomes isolated from donors homozygous for the loss-of-function CYP3A5*3 allele exhibited a 79% decrease in formation of this metabolite as compared to those homozygous for the wild-type CYP3A5*1 allele. In order to probe which divergent residues between CYP3A4 and CYP3A5 might play a role in the differential activities of these enzymes towards maraviroc mutations were introduced into both enzymes and metabolism of maraviroc was measured. A CYP3A5 L57F mutant exhibited a 61% decrease in the formation of this metabolite whereas formation by a CYP3A4 F57L mutant was increased by 337% as compared to wild-type. Taken together, these data provide novel insight into the biotransformation of maraviroc as well as the potential role of CYP3A4 and CYP3A5 divergent residues in the enzymatic activities of these two highly homologous enzymes.

Abbreviations

CYP, a cytochrome P450; UPLC-MS, ultra performance liquid chromatography-mass spectrometry; SRSs, substrate recognition sites; UDP-glucuronosyltransferase, UGT;

UDPGA, uridine disphosphoglucuronic acid.

Introduction

The cytochromes P450s are a superfamily of heme-containing monooxygenases that play a crucial role in drug clearance. The CYP3A subfamily enzymes CYP3A4 and CYP3A5 are responsible for the metabolism of more than 50% of drugs currently on the market [109]. They share 84% amino acid sequence identity and 92% similarity resulting in overlapping substrate specificities[9]. As such, defining their respective contributions to drug metabolism as well as drug-drug interactions remains challenging. It is well established that CYP3A5 is polymorphically expressed with the wild type CYP3A5*1 allele being associated with the highest amount of protein expression whereas variant alleles such as CYP3A5*3 lead to decreased expression or no activity due to alternative mRNA splicing [15,16]. In individuals that carry at least one CYP3A5*1 allele, CYP3A5 protein accounts for at least 50% of the total hepatic CYP3A content [15]. The expression of CYP3A5 is highly variable among different ethnic populations. For instance, the CYP3A5*3 allele is abundantly present in the European American population with a frequency of 85-98% while it is much less common in the African American population with a frequency of 27-48% [15,16,18,20]. In addition, increased risk of certain drug toxicities has been reported in people who have low expression of CYP3A5 [24-26].

To date, several CYP3A4 crystal structures have been solved while the structure of CYP3A5 is not yet available. Six CYP3A4 substrate recognition sites (SRS1-6) were identified and experimentally demonstrated to be important for substrate binding and catalytic activity [110-116]. Phenylalanine residues F108, F213, F215, F219, F220, F241 and F304 form a hydrophobic roof of the CYP3A4 active site above the heme between SRS1,

SRS2, SRS3 and SRS4 [117,118]. Another phenylalanine residue, F57, falls into a region recently denoted as SRS 1'a [119] and is important for CYP3A4 substrate binding [120]. In contrast, information regarding the importance of particular CYP3A5 active site residues is very limited. Due to the high similarity between CYP3A4 and CYP3A5, the overall folding of CYP3A5 has been predicted to be largely similar to that of CYP3A4 [9]. Mutation of divergent SRS residues of CYP3A4 to the corresponding amino acids of CYP3A5, P107S, F108L, N206S, L210F, V376T, S478D, and L479T, resulted in a shift of the aflatoxin B1 metabolite profile of CYP3A4 towards that of CYP3A5 [110]. However, the effects of the reverse mutations on CYP3A5 activity remain unknown.

Maraviroc is an anti-HIV drug that acts by blocking the virus co-receptor, chemokine receptor CCR5 at the viral entry step thereby preventing viral infection [121,122]. In addition, there is increased interest in the development of maraviroc as an oral and/or topical microbicide for use in HIV prevention. Maraviroc undergoes extensive metabolism in human body after oral administration. N-dealkylation and oxidation are the two major metabolizing pathways [123]. CYP3A4 was reported to be the primary enzyme for N-dealkylation whereas enzymes responsible for oxidation remain unknown (**Figure 4-1**). Monooxidation results in oxygen insertions on difluorocyclohexane ring, phenyl ring and triazol moiety of the maraviroc molecule. Dioxidative products have been found and proposed to have one oxygen insertion on difluorocyclohexane ring and the other one on triazole moiety [123].

Figure 4-1. Previously proposed pathways of maraviroc metabolism. N-dealkylation and oxidation are the two major pathways. Mono-oxidative products have oxygen insertions on three possible positions. Di-oxidative products have been proposed to have one oxygen insertion on difluorocyclohexane ring and the other one on triazole moiety. CYP3A4 is the primary enzyme for N-dealkylation. Question mark (?) represents enzymes that are still unknown. The graph is modified based on Figure 2 of the reference[123].

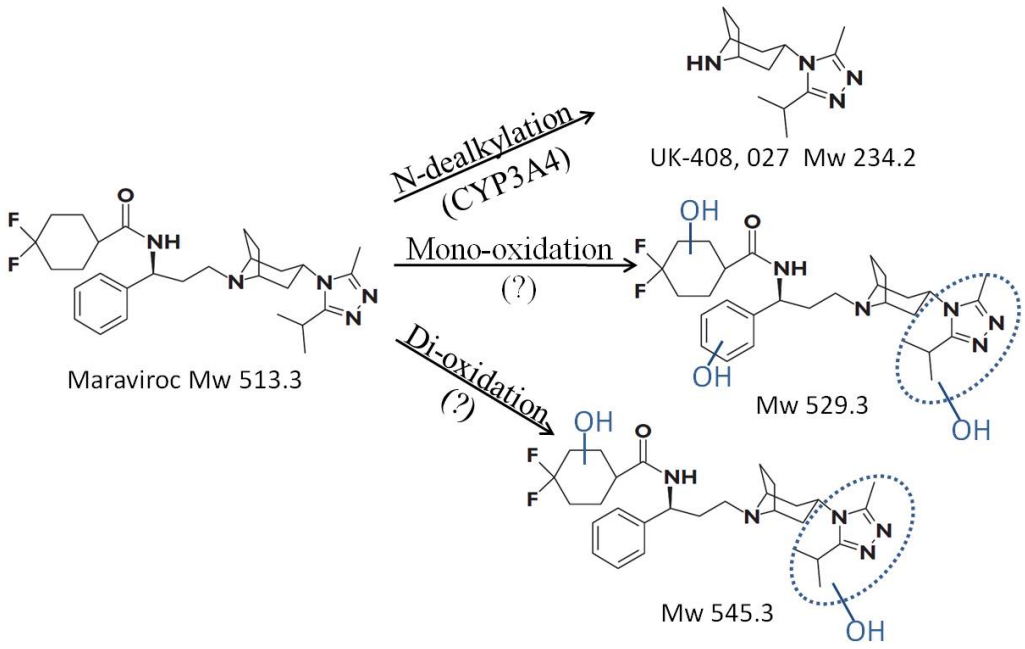

In the present study, we performed a comprehensive analysis on the enzymes involved in maraviroc oxidative metabolism. Our enzyme kinetic studies revealed that CYP3A5 has a higher capacity to metabolize maraviroc to a major monooxygenated metabolite than CYP3A4. Plasma and urine isolated from a human subject genotyped as wild type for CYP3A5 confirmed that this metabolite is, indeed, the most abundant maraviroc product formed *in vivo,* as well. Further, we then leveraged this observation and systematically mutated CYP3A5 towards CYP3A4 using formation of this metabolite as an activity probe to identify residues in CYP3A5 that confer specificity with regard to maraviroc metabolism. In addition, we identified four novel dioxygenated maraviroc metabolites and two glucuronidated metabolites and confirmed their existence in human urine samples. Collectively, these studies provide novel mechanistic insight into the phase I and phase II metabolism of maraviroc as well as the role of divergent amino acids of CYP3A4 and CYP3A5 in influencing the catalytic activities of these two highly homologous enzymes.

Materials and Methods

Materials

Maraviroc was obtained from the National Institutes of Health AIDS Research and Reference Reagent Program **(**Germantown, MD). Maraviroc-d6, 3-hydroxymethyl maraviroc, and 4-hydroxyphenyl maraviroc were obtained from Toronto Research Chemicals Inc (North York, Ontario, Canada). Chemical structures of maraviroc, 3-hydroxymethyl maraviroc, and 4-hydroxyphenyl maraviroc are shown in **Figure 4-2**. Quinidine, ketoconazole, sulfaphenazole, (+)-N-3-benzylnirvanol and furafylline were purchased from Sigma-Aldrich (St. Louis, MO). 2-phenyl-2-(1-piperidinyl) propane was bought from Santa Cruz Biotechnology (Santa Cruz, CA). Pooled human liver microsomes (20 mg/ml, pool of 200, mixed gender) and one lot of CYP3A5*3/*3 human liver microsomes were purchased from XenoTech, LLC (Lenexa, KS). The NADPH regenerating system, BD Biosciences UGT Reaction Mix (consisting of two reagents: solution A (25 mM UDPGA) and solution B (5×-UGT Assay Buffer containing alamethicin)), CYP3A4 and CYP3A5 primary antibodies, CYP3A5*1/*1 and CYP3A5*3/*3 human liver microsomes, Supersomes^{TM} containing cDNA-expressed human CYP1A2, CYP2B6, CYP2C8, CYP2C9*1, CYP2C19, CYP2D6*1, CYP3A4, and CYP3A5, co-expressed with reductase, were purchased from BD Biosciences (San Jose, CA). The β-actin antibody and cell lysis buffer were obtained from Cell Signaling Technology (Danvers, MA). The bicinchoninic acid assay kit and SuperSignal West Dura Chemiluminescent Substrate were obtained from Thermo Scientific (Rockford, IL).

Figure 4-2. Structures and molecular weights of chemicals. Structures of maraviroc (A), internal standard maraviroc-d6 (B), and commercially available oxidative metabolite standards 3-hydroxymethyl maraviroc (C) and 4-hydroxyphenyl maraviroc (D) are shown along with their molecular weights.

A

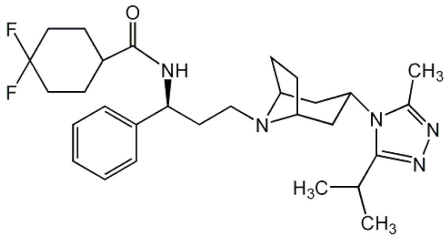

Maraviroc, Mw 513.3

B

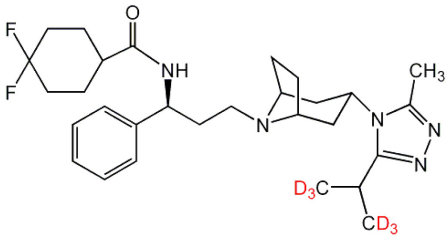

Maraviroc-d6, Mw 519.3

C

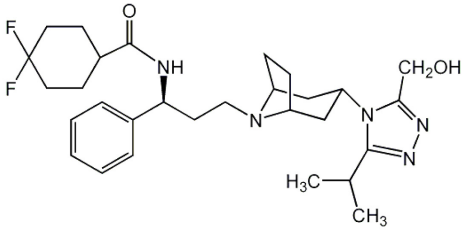

3-hydroxymethyl maraviroc, Mw 529.3

D

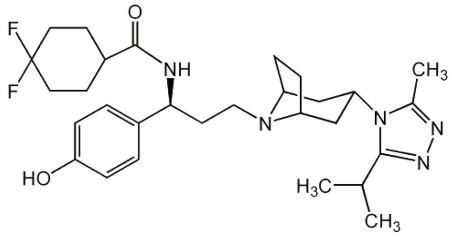

4-hydroxyphenyl maraviroc, Mw 529.3

Incubation conditions for human liver microsome metabolism experiments.

The metabolism experiments using human liver microsomes were carried out in a volume of 500 µl in 10 × 75 mm borosilicate glass tubes (Fisher Scientific). One µl of 10 mM maraviroc in methanol was added into a 500 µl reaction system containing 0.1 M potassium phosphate buffer (pH 7.4), 0.5 mg/ml human liver microsomes and incubated for 5 min at 37°C in a water bath. The reaction was initiated by addition of the NADPH regenerating system and allowed to proceed for 30 min at 37°C. For the chemical inhibition assays, furafylline (20 µM), 2-phenyl-2-(1-piperidinyl) propane (30 µM), sulfaphenazole (20 µM), (+)-N-3-benzylnirvanol (10 µM), quinidine (10 µM) and ketoconazole (10 µM) were used to inhibit CYP1A2, CYP2B6, CYP2C9, CYP2C19, CYP2D6, and CYP3A4/5, respectively, in order to investigate the involvement of these individual CYP enzymes in the formation of maraviroc oxidative metabolites. The inhibitors were pre-incubated with the human liver microsomes and NADPH regenerating system for 10 min prior to the addition of 1 µl of 10 mM maraviroc to initiate the reactions. For reactions containing CYP3A5 genotyped human liver microsomes, a final concentration of 2 µM maraviroc was used in a total reaction volume of 250 µl with other components being kept at the same concentrations as described above. For glucuronidation reactions, UGT reaction solutions containing 25 mM UDPGA and 5×-UGT assay buffer with alamethicin were added into the above pooled human liver microsome reaction systems following addition of the NADPH regenerating system.

Incubation conditions for individual cDNA-expressed P450s

One pmole of human recombinant P450 enzyme (CYP1A2, CYP2B6, CYP2C8, CYP2C9*1, CYP2C19, CYP2D6*1, CYP3A4, or CYP3A5) was pre-incubated with 20 μM maraviroc in 0.1 M potassium phosphate buffer (pH 7.4) at 37°C for 5 min and the reaction was initiated by addition of the NADPH regenerating system (final reaction volume of 100 μl) and continued for 30 min at 37 °C.

Enzyme kinetics for CYP3A4 and CYP3A5

Maraviroc stock solution (600 mM) was prepared in DMSO and diluted into working solutions (0.02, 0.2, 2, 6, 20, 60, 200 mM). The working solution (0.5 μl of each) was then pre-incubated with 13 pmole CYP3A4 or CYP3A5 at 37°C for 5 min in 0.1 M potassium phosphate buffer (pH 7.4). The final concentrations of maraviroc were 0.1, 1, 10, 30, 100, 300, and 1000 μM in a total reaction volume of 100 μl. The reaction was initiated by addition of NADPH regenerating system and allowed to proceed for 30 min at 37 °C.

The enzyme concentrations as well as the incubation time were chosen based on preliminary results demonstrating that the formation of oxidative metabolites was linear under these conditions. The metabolite concentrations were estimated against a standard curve with a range of 0.024-200 pmol maraviroc.

Sample preparation after incubation

At the end of the incubation, 2 reaction volumes of acetonitrile were added to stop the reaction. The internal standard maraviroc-d6 (100 μl of 20 ng/ml), an analogue of maraviroc labeled with six deuteriums, was added and the samples were vortexed. The mixture was then centrifuged at 3000 ×g for 10 min at 4 °C and the supernatants were

dried under a stream of nitrogen gas at 50 °C. The samples were reconstituted in 50 µl methanol and transferred to vials containing 40 µl of 5% acetonitrile/95% water/0.1% formic acid for injection onto the Ultra Performance Liquid Chromatography-Mass Spectrometry (UPLC-MS) system.

Analysis of maraviroc and metabolites using UPLC-MS

Maraviroc and its metabolites were detected by UPLC-MS using a Waters ACQUITY UPLC interfaced to an AB SCIEX QTRAP 5500 mass spectrometer. Aliquots of reconstituted samples were injected onto a 1.7 µm Waters UPLC BEH 2.1 x 100 mm C8 column. Analyte resolution was achieved at a flow rate of 0.35 ml/min with chromatography at room temperature. Mobile phases were 5% acetonitrile – 0.1% formic acid in water (A) and 5% water – 0.1% formic acid in acetonitrile (B), programmed at 0% B from 0 to 1.1 min, 20% B from 32 to 33 min, and 0% B from 33.1 to 34 min. Detection of the analytes and the internal standard was achieved via multiple reaction monitoring for quantification under positive mode. The monooxygenated maraviroc metabolites were monitored using m/z of precursor/product ion pairs at 530/296 and 530/280. The di-oxidative metabolites were monitored at m/z 546/421 and the glucuronidated metabolites were monitored at m/z 706/581 and 706/389. Maraviroc and the internal standard maraviroc-d6 were monitored at m/z of 514/389 and 520/389, respectively. The N-dealkylated metabolite of maraviroc was monitored at m/z of precursor/product ion pairs at 235/110. For maraviroc metabolite identification, MS^3 scans were performed with $1^{st}/2^{nd}$ precursor ions of maraviroc, monooxygenated, dioxygenated, and glucuronidated metabolites at m/z 514/280, 530/296 and 546/312, respectively. For glucuronides, MS^3 scans were performed with $1^{st}/2^{nd}$ precursor ions at m/z 706/581 and at m/z 706/389. All

the data were acquired under positive mode and analyzed by AB SCIEX Analyst software (Version 1.5.1) in Windows XP Professional Version 2002.

Maraviroc metabolite analysis in human plasma and urine

A healthy male subject was recruited for maraviroc oxidative metabolite analysis after providing written informed consent for participation in a protocol approved by the institutional review board of Johns Hopkins Medical Institutions. The subject was genotyped for CYP3A5 using a previously reported method [15]. A single dose of 300 mg maraviroc was administrated orally followed by blood and urine collection over a 24 h period. Blood (10 mL) samples were collected into a heparinized tube pre-dose and 1, 2, 4, 6, 8, and 24 h following the administration. Urine samples were collected with intervals of 0-2, 2-4, 4-6, 6-8, and 8-24 h after drug administration. Plasma was prepared by centrifugation of blood at 1,000 ×g for 10 min at 4 °C. For metabolite analysis, 100 µl of plasma was mixed with 300 µl methanol. Following centrifugation, the supernatant was dried and reconstituted for analysis as described above by UPLC-MS. For urine samples, 100 µl of sample was directly dried and reconstituted using methanol for metabolite analysis.

Site-directed mutagenesis and expression of CYP3A4 and CYP3A5

Plasmids pCMV6-XL4 containing CYP3A4 and CYP3A5 full length cDNAs (TrueClones®) were obtained from OriGene Technologies. Mutations were made with primers (**Table 4-1**) using a QuikChange lightning site-directed mutagenesis kit following the manufacturer's instructions. Plasmid DNA was isolated using GeneJET™ plasmid miniprep kit (Thermo Scientific) and DNA sequencing was performed to

confirm the presence of a desired mutation and the absence of extraneous mutations. The plasmid constructs (4 μg) were transfected into COS-7 cells using lipofectamine 2000 (Invitrogen) according to the manufacturer's instruction.

Table 4-1. Sequence of oligonucleotides used for site-directed mutagenesis for CYP3A4 and CYP3A5[a].

Mutation	Oligonucleotide Sequence
CYP3A5	
L57F	5'-aaatgttttgtcctatcgtcagggt**t**tctggaaatttgacac-3'
	5'-gtgtcaaatttccagaaaccctgacgataggacaaaacattt-3'
S107P	5'-cttcacaaatcgaagg**c**ctttaggcccagtggg-3'
	5'-cccactgggcctaaaggccttcgatttgtgaag-3'
L108F	5'-cttcacaaatcgaaggtctt**c**ggcccagtggg-3'
	5'-cccactgggccgaaagaccttcgatttgtgaag-3'
L120I	5'-ttatgaaaagtgccatctct**a**tagctgaggatgaagaatgg-3'
	5'-ccattcttcatcctcagctatagagatggcacttttcataa-3'
F146V	5'-gaaaactcaaggagatg**g**tccccatcattgcccag-3'
	5'-ctgggcaatgatggggaccatctccttgagtttc-3'
K166T	5'-acttgaggcgggaagcagaga**cg**ggcaagcctgt-3'
	5'-acaggcttgcccgtctctgcttcccgcctcaagt-3'
G186S	5'-cctacagcatggatgtgattact**a**gcacatcatttgga-3'
	5'-tccaaatgatgtgctagtaatcacatccatgctgtagg-3'
S206N	5'-caagacccctttgtggaga**a**cactaagaagttcctaaaa-3'
	5'-ttttaggaacttcttagtgttctccacaaaggggtcttg-3'
F210L	5'-tttgtggagagcactaagaagtt**a**ctaaaatttggtttcttagatcc-3'
	5'-ggatctaagaaaccaaattttagtaacttcttagtgctctccacaaa-3'
K212R	5'-ggagagcactaagaagttcctaa**g**atttggtttcttagatccattat-3'
	5'-ataatggatctaagaaaccaaatcttaggaacttcttagtgctctcc-3'
G214D	5'-gcactaagaagttcctaaaatttg**a**tttcttagatccattatttctctc-3'
	5'-gagagaaataatggatctaagaaatcaaattttaggaacttcttagtgc-3'
L219F	5'-cctaaaatttggtttcttagatccatt**c**tttctctcaataatactctttccatt-3'
	5'-aatggaaagagtattattgagagaaagaatggatctaagaaaccaaattttagg-3'
I224T	5'-cttagatccattatttctctcaataa**cg**ctctttccattccttaccccagt-3'
	5'-actggggtaaggaatggaaagagcgttattgagagaaataatggatctaag-3'
V238I	5'-tccttaccccagtttttgaagcattaaat**a**tctctctgtttccaa-3'
	5'-ttggaaacagagagatatttaatgcttcaaaaactggggtaagga-3'
S239C	5'-ccccagtttttgaagcattaaatgtct**g**tctgtttccaaaag-3'
	5'-cttttggaaacagacagacatttaatgcttcaaaaactgggg-3'
L240V	5'-ccccagtttttgaagcattaaatgtctct**g**tgtttccaaaagata-3'
	5'-tatcttttggaaacacagagacatttaatgcttcaaaaactgggg-3'
K243R	5'-tttgaagcattaaatgtctctctgtttccaa**g**agataccataaatttttttaagtaaat-3'
	5'-atttacttaaaaaatttatggtatctcttggaaacagagagacatttaatgcttcaaa-3'
A296V	5'-gtctgatctggagctcg**t**agcccagtcaataatct-3'
	5'-agattattgactgggctacgagctccagatcagac-3'
V369I	5'-gaaacactcagattattccca**a**ttgctattagacttgagagga-3'
	5'-tcctctcaagtctaatagcaattgggaataatctgagtgtttc-3'
I371M	5'-cactcagattattcccagttgctat**g**agacttgagagga-3'
	5'-tcctctcaagtctcatagcaactgggaataatctgagtg-3'

T376V	5'-ccagttgctattagacttgagagg**gt**ttgcaagaaagatgttgaaatcaa-3'
	5'-ttgatttcaacatctttcttgcaaaccctctcaagtctaatagcaactgg-3'
S392V	5'-gggtattcattcccaaaggg**gt**aatggtggtgattccaactt-3'
	5'-aagttggaatcaccaccattacccctttgggaatgaataccc-3'
R415L	5'-agcctgaggagttcc**t**ccctgaaaggttcag-3'
	5'-ctgaacctttcagggaggaactcctcaggct-3'
D477S	5'-tgtaaagaaacacagatccccttgaaatta**ag**cacgcaaggacttctt-3'
	5'-aagaagtccttgcgtgcttaatttcaaggggatctgtgtttctttaca-3'
T478L	5'-aacacagatccccttgaaattagac**cta**caaggacttcttcaaccagaaaaac-3'
	5'-gtttttctggttgaagaagtccttgtaggtctaatttcaaggggatctgtgtt-3'
Q479G	5'-ccccttgaaattagacacg**gg**aggacttcttcaaccagaa-3'
	5'-ttctggttgaagaagtcctcccgtgtctaatttcaagggg-3'
CYP3A4	
F57L	5'-tattttgtcctaccataagggctt**a**tgtatgtttgacatggaatg-3'
	5'-cattccatgtcaaacatacataagcccttatggtaggacaaaata-3'
P107S	5'-gtcttcacaaaccggagg**ag**ttttggtccagtgggatt-3'
	5'-aatcccactggaccaaaactcctccggtttgtgaagac-3'
F108L	5'-caaaccggaggcctt**a**ggtccagtggg-3'
	5'-cccactggacctaaaggcctccggtttg-3'
D214G	5'-caccaagaagcttttaagatttg**g**ttttttggatccattctttctct-3'
	5'-agagaaagaatggatccaaaaaaccaaatcttaaaagcttcttggtg-3'
Δ423N[b]	5'-cctgaaagattcagcaagaag**---**aaggacaacatagatccttac-3'
	5'-gtaaggatctatgttgtcctt---cttcttgctgaatctttcagg-3'
L479T	5'-cagatccccctgaaattaagc**acg**ggaggacttcttcaaccagaa-3'
	5'-ttctggttgaagaagtcctcccgtgcttaatttcaggggggatctg-3'

[a] The underlined nucleotide(s) in bold represent the introduced mutations that were used to make the desired residue changes. [b] Three nucleotides were omitted in the primer sequence in order to delete residue N423 of CYP3A4.

Analysis of metabolite formation by CYP3A4 and CYP3A5 expressed in COS-7 cells

Twenty-four hours following transfection, maraviroc was added to a final concentration of 20 μM in 1 ml of DMEM per well. After 40 min incubation, 600 μl or 300 μl medium were transferred to glass tubes and mixed with 50 μl of 20 ng/ml maraviroc-d6 for cells expressing CYP3A4 and CYP3A5, respectively. Two volumes of acetonitrile were added, vortexed, and centrifuged at 3000 ×g for 10 min at 4 °C. Supernatants were transferred, dried, reconstituted and analyzed following the procedure described above.

Immunoblot analysis of CYP3A4 and CYP3A5 expression

Cells were harvested in 1 ml PBS followed by centrifugation at 500 ×g for 5 min at 4 °C. The cell pellets were then resuspended in cell lysis buffer containing freshly added phosphatase and protease inhibitor cocktail (Thermo Scientific Halt Protein and Phosphatase Inhibitor Cocktail) and phenylmethylsulfonyl fluoride (PMSF). The resuspended cell pellets were passed 30 times through a 25G gauge needle for lysis and centrifuged at 14,000 ×g for 10 min at 4 °C. Protein concentrations were measured using a bicinchoninic acid assay kit (Thermo Scientific) and 20 μg total protein was loaded onto a 10% polyacrylamide gels for separation by SDS-PAGE. Immunoblotting was performed using anti-CYP3A4, anti-CYP3A5 antibodies and β-actin for normalization. A Carestream 4000R system was used for chemiluminescent imaging followed by densitometrical analysis.

Statistical analysis

K_m and V_{max} values were determined by nonlinear regression analysis using GraphPad Prism 5 for Windows (GraphPad Software Inc., San Diego, CA). All data presented are

means ± SD from three independent experiments performed in duplicate. Two-tailed unpaired *t* tests were performed for comparisons and $P \leq 0.05$ was considered statistically significant.

Results

Detection of monooxygenated metabolites of maraviroc using UPLC-MS

Using a novel UPLC-MS method that was specifically developed for the detection and separation of maraviroc and its oxidative metabolites, six major monooxidative metabolites were identified from incubations with human liver microsomes. Herein, these metabolites are denoted as metabolite 1- metabolite 6 (M1-M6; numbered by order of elution) with retention times of 14.9, 16.2, 16.9, 21.7, 22.6 and 27.0 min, respectively (**Figure 4-3A, B**). The retention time for maraviroc was 25.08 min (**Figure 4-3C**). Among the six metabolites, M1, M2, and M3 were the predominant metabolites. To confirm the formation of these monooxygenated products of maraviroc *in vivo*, a single 300 mg dose of maraviroc was administered orally to a healthy volunteer followed by blood and urine collection and metabolite analysis using UPLC-MS. Genotyping results of CYP3A5 determined this subject to be homozygous for wild type CYP3A5 allele *1. We found that these six metabolites were the major products present in both plasma (**Figure 4-4A**) and urine (**Figure 4-4B**). A secondary amine product resulting from N-dealkylation of maraviroc has been previously found in plasma and excreta [123,124]. Therefore, in order to gain a more comprehensive view of maraviroc biotransformation, we also monitored the formation of this metabolite using our assay. We found that the peak area ratio of formation of this N-dealkylated metabolite to M1 by human liver microsomes was 0.3. In addition, consistent with previous findings, we also detected the N-dealkylated metabolite of maraviroc in both human plasma and urine samples. The peak area ratio of the N-dealkylated maraviroc to M1 ranged from 0.3-2.6 and 1.4-6.4 in

plasma and urine samples, respectively, over a period of 24 h following a single oral dose of maraviroc administration.

CYP3A5 has a higher capacity to form M1 than CYP3A4

To determine which CYP isozymes play a role in the formation of these metabolites, maraviroc was incubated with a panel of cDNA-expressed P450s. As shown in **Figure 4-5** CYP3A4 and CYP3A5 were essentially the only enzymes that catalyzed the formation of monoxygenated products of maraviroc. Among the six metabolites, M1 was the most abundant and formation by CYP3A5 was 9.7-fold greater than by CYP3A4. To further confirm the role of CYP3A4 and CYP3A5 in M1 formation, maraviroc was incubated with human liver microsomes in the presence of inhibitors of CYP1A2, CYP2B6, CYP2C9, CYP2C19, CYP2D6, and CYP3A4/5 (**Figure 4-6**). Ketoconazole, an inhibitor of CYP3A4/5, significantly reduced the activity by 81% ($P < 0.001$). Quinidine, a CYP2D6 inhibitor, decreased formation of M1 16%, however, this was not statistically significant when compared to the vehicle control ($P = 0.12$). The V_{max} values for M1 formation by CYP3A4 and CYP3A5 were 0.04 ± 0.001 pmole/min/pmole P450 and 0.93 ± 0.04 pmole/min/pmole P450, respectively, and the K_m values were 11.1 ± 2.1 μM and 48.9 ± 7.6 μM, respectively (**Figure 4-7**). At 1 μM maraviroc, which is within the clinically useful range of maraviroc concentrations, formation by CYP3A5 was 9-fold higher than that of CYP3A4 (**Figure4-7 inset**), indicating that CYP3A5 may play a predominant role in the formation of M1 at pharmacologically relevant concentrations of maraviroc.

Figure 4-3. Separation of maraviroc oxidativemetabolites using a novel chromatographic method. Chromatograms of oxidative metabolites M1-M5 (A), oxidative metabolite M6 (B) and maraviroc (C). Retention times (min) are shown near corresponding peaks. Human liver microsmes were incubated with 20 μM maraviroc for 30 min at 37°C and reactions were terminated by acetonitrile. The analytes were separated using a Waters Acquity UPLC BEH C8 1.7mm 2.1×100 mm column and analyzed by mass spectrometry under MRM mode with transitions m/z 530→296 for M1-M5, 530→280 for M6, and 514→389 for maraviroc.

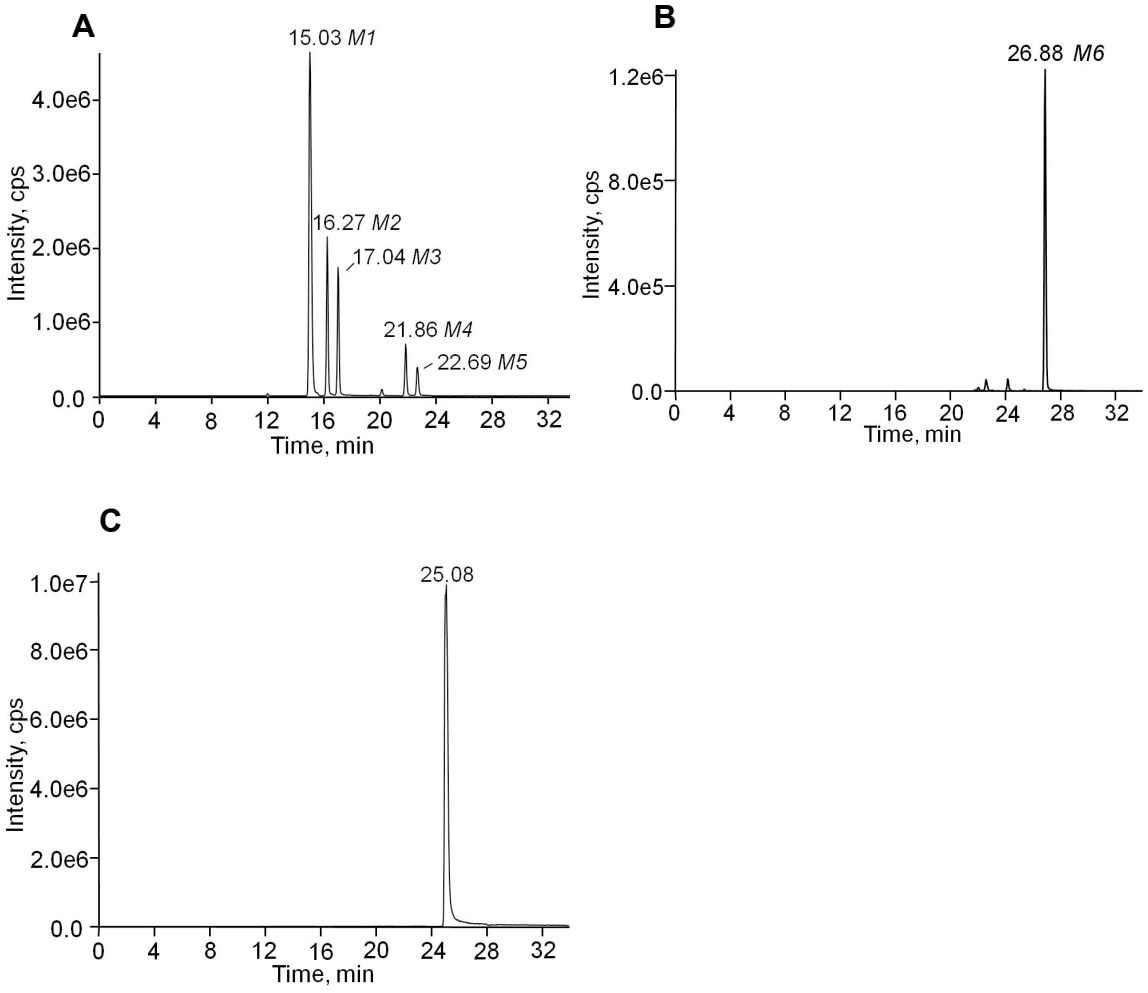

Figure 4-4. Separation of oxidative metabolites from human plasma samples after an oral dose of maraviroc. The human plasma (A) and urine (B) chromatogram are representative data obtained 2 h and 2-4 h, respectively, following a single oral dose of 300 mg maraviroc. Metabolites were analyzed by mass spectrometry using the transitions m/z 530→296 for M1-M5 and 530→280 for M6 after separation on an UPLC column.

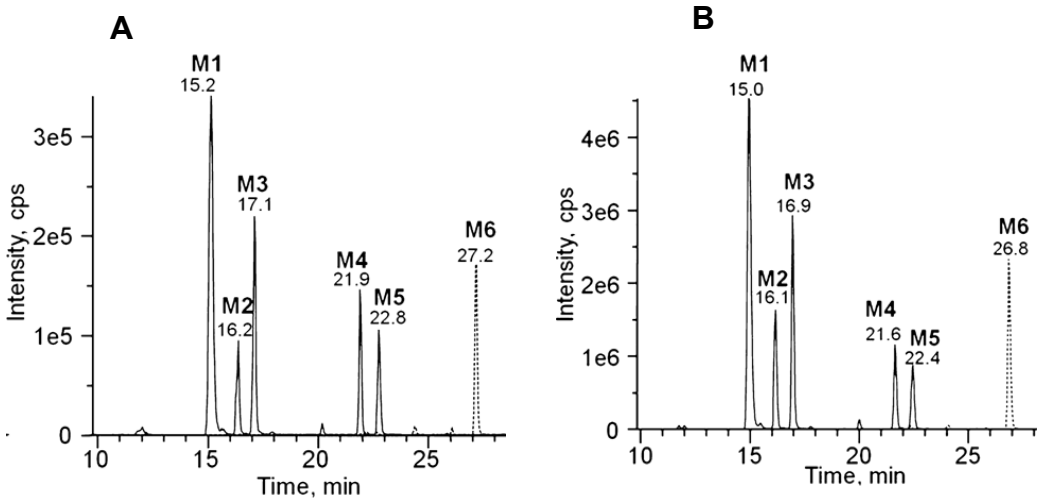

Figure 4-5. CYP3A4 and CYP3A5 are the major enzymes responsible for maraviroc oxidation. A panel of cDNA-expressed P450s was incubated with maraviroc followed by metabolite analysis.

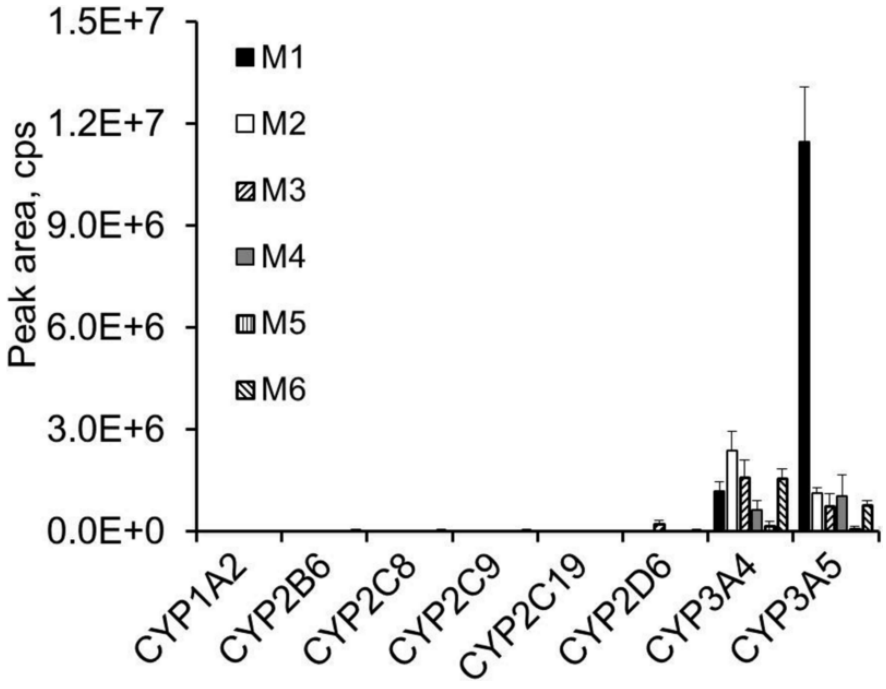

Figure 4-6. Ketoconazole inhibited M1 formation. CYP chemical inhibitors were preincubated with human liver microsomes prior to the addition of maraviroc. The data are presented as percent M1 formation activity remaining relative to vehicle control. The CYP enzyme targeted by the particular chemical inhibitor is shown at the top of the figure. PPP is the abbreviation for 2-phenyl-2-(1-piperidinyl) propane. ***$P < 0.001$ when compared to solvent control.

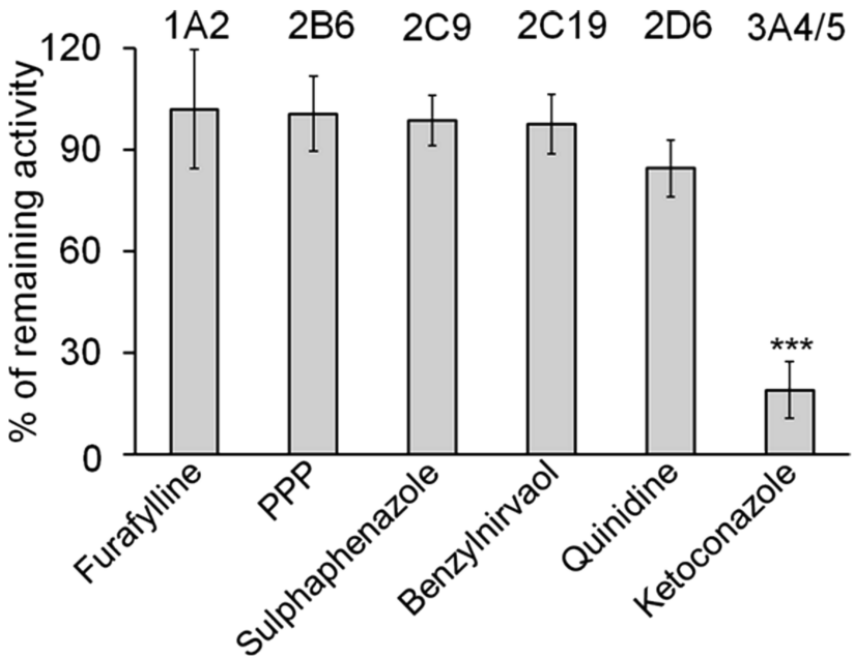

Figure 4-7. M1 formation rate by CYP3A5 is greater than that by CYP3A. cDNA-expressed CYP3A4 and CYP3A5 were incubated with 0.1-1000 μM maraviroc under initial rate conditions. M1 formation was determined using a maraviroc standard curve and maraviroc-d6 as an internal standard. Kinetics data at maraviroc concentrations in the therapeutic range are shown in the inset.

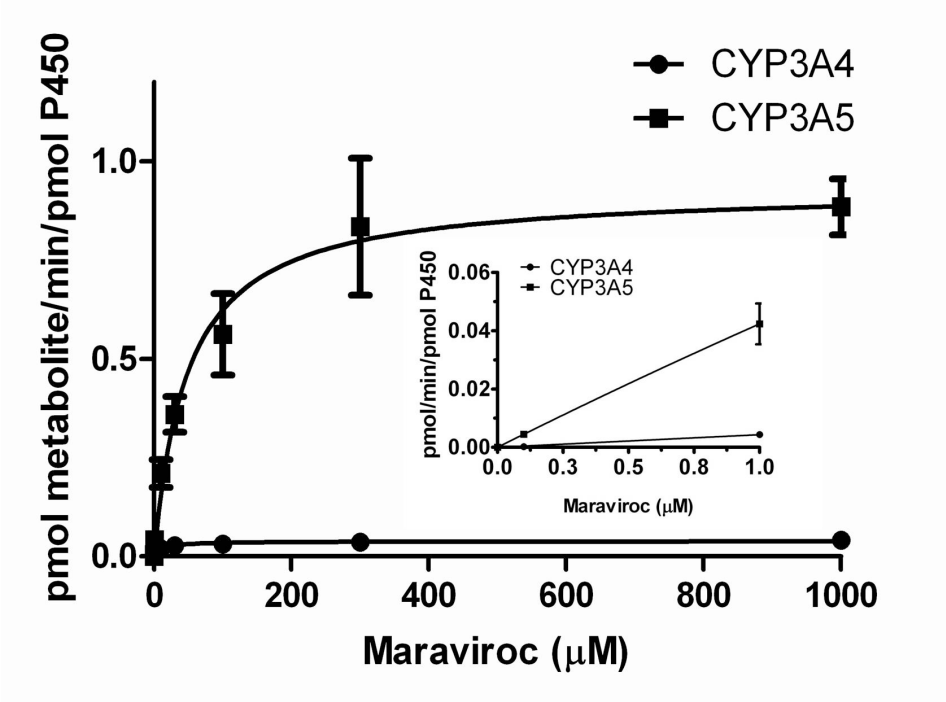

Reduced M1 formation by human liver microsomes genotyped as homozygous for the loss-of-function CYP3A5*3 allele

The expression and activity of CYP3A5 has been reported to be affected by genetic polymorphisms. Individuals who carry two CYP3A5*3 alleles (CYP3A5*3/*3) have reduced or no expression of CYP3A5 compared to those homozygous for the wild type CYP3A5*1 allele [15,16]. We measured M1 formation by human liver microsomes isolated from individuals genotyped as CYP3A5*1/*1 and individuals genotyped as CYP3A5*3/*3 in order to determine the contribution of CYP3A5 to M1 formation in a system where CYP3A4 is present while CYP3A5 expression is absent or markedly reduced. In addition, these studies were used to probe the utility of M1 formation as a CYP3A5 phenotyping tool. Following incubation with maraviroc (2 μM) the human liver microsomes isolated from donors homozygous for the CYP3A5*3 alleles, exhibited a 79% decrease in formation of M1 as compared to production by human liver microsomes isolated from donors homozygous for the CYP3A5*1 allele (**Figure 4-8A**, $p = 0.01$). Furthermore, M1 was the most abundant metabolite formed using the CYP3A5*1/*1 human liver microsomes (**Figure 4-8B**). In human liver microsomes genotyped as CYP3A5*3/*3 M1, M2, and M3 all had comparable intensities (**Figure 4-8C**).

Figure 4-8. Decreased M1 formation in human liver microsomes genotyped as CYP3A5*3/*3. (A) Reduced M1 formation by human liver microsomes homozygous for a CYP3A5 nonfunctional allele. Human liver microsomes from individuals genotyped as CYP3A5*1/*1 or CYP3A5*3/*3 were incubated with 2 μM maraviroc and M1 formation was measured. Each data point represents the peak area ratio of M1 to maraviroc-d6 (internal standard). The mean for each group is indicated by a horizontal line. (B) and (C) are representative chromatogram of oxidative metabolites from reactions of CYP3A5*1/*1 and CYP3A5*3/*3 human liver microsomes, respectively.

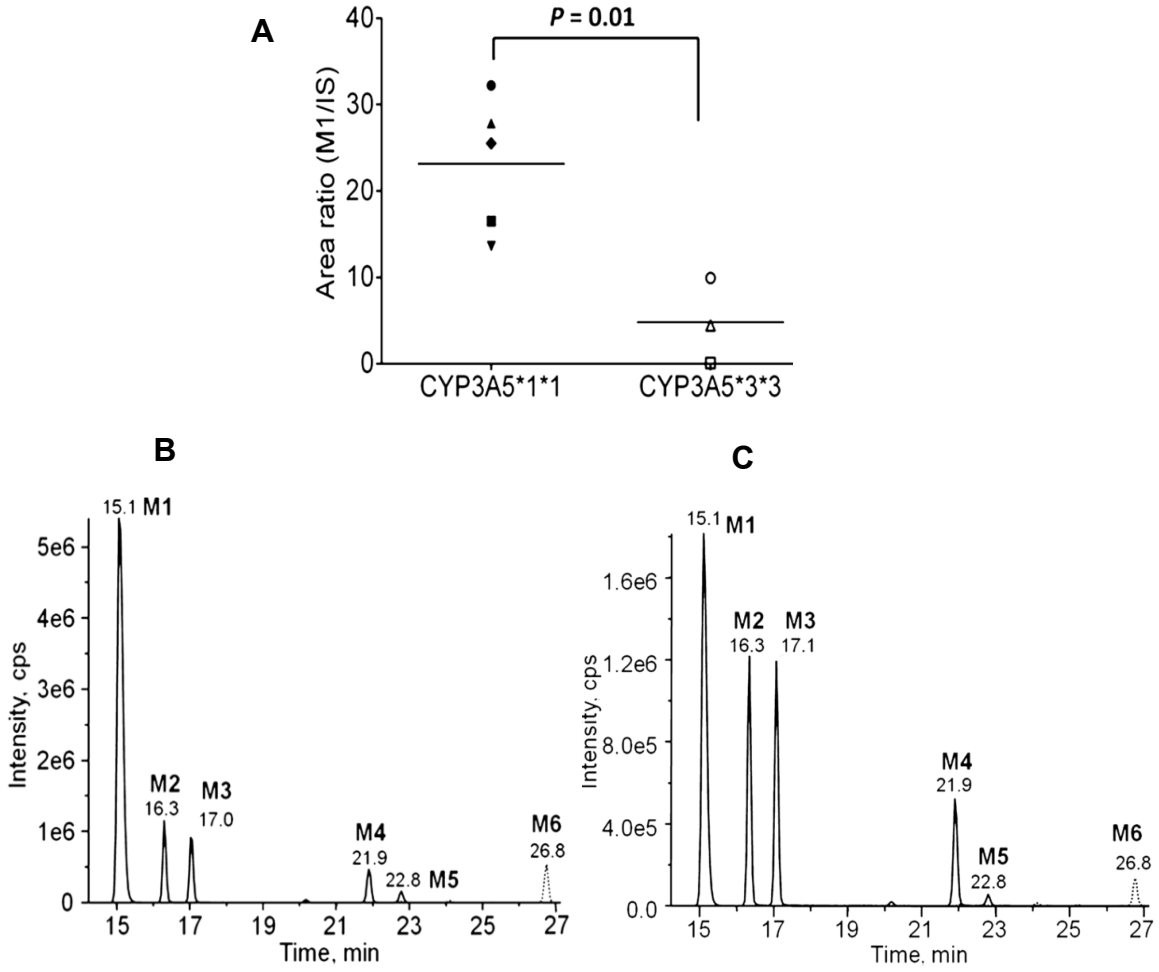

M1 is formed via hydroxylation of the difluorocyclohexane ring of maraviroc

To determine the position of the CYP-dependent monooxygenation that results in the formation of M1, mass spectrometry was performed using MS^2 and MS^3 scans following the UPLC separation of M1 from other maraviroc oxidative metabolites. These spectra were then compared to maraviroc as well as commercially available synthetic standards for 3-hydroxymethyl maraviroc, a metabolite with a hydroxyl group on the triazole moiety, and 4-hydroxyphenyl maraviroc, a metabolite with a hydroxyl group on the phenyl ring. Fragmentation of maraviroc resulted in two major daughter ions with m/z of 389 and 280, respectively, from losing the triazol moiety and the breakage at the tertiary amine nitrogen of the tropane ring (**Figure 4-9A**) [125]. The spectrum of 3-hydroxymethyl maraviroc was similar to that of maraviroc because the oxygen is on the triazol moiety, which was not included in the two major daughter ions after fragmentation. The fragmentation of M6 was similar to that of 3-hydroxymethyl maraviroc, indicating the oxygen insertion was on the triazol moiety. In contrast, fragmentation of 4-hydroxyphenyl maraviroc had two major daughter ions with m/z of 405 and 296, respectively, with 16 D increase due to an oxygen insertion on the two major daughter ions with m/z of 389 and 280. Similar to 4-hydroxyphenyl maraviroc, MS^2 scans of M1-M5 resulted in two major product ions at m/z 296 and 405 (**Figure 4-9B**), which contains the difluorocyclohexane ring and phenyl ring of maraviroc but not the triazole moiety. Thus, we propose that the m/z 296 ion of M1 represents an oxygen (16 Da) insertion into this portion of the molecule suggesting that the site of metabolism is either on difluorocyclohexane ring or on the phenyl ring but not on the triazole moiety.

Figure 4-9. MS/MS spectra of maraviroc and its hydroxylated metabolites. (A) maraviroc; (B) Monohydroxylated maraviroc M1-M5.

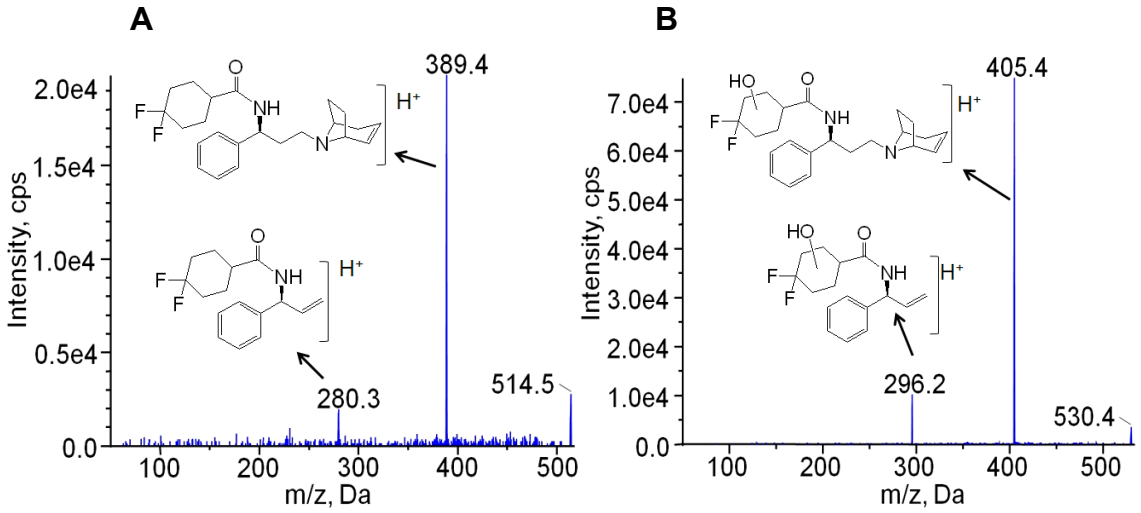

To test this further, selected daughter ions were fragmented for analysis using MS^3 scan. Maraviroc daughter ion m/z 280 produced product ions at m/z 91, 106 and 117 (**Figure 4-10A**). The ions with m/z 106 and 117 have been identified as phenyl ring containing product ions of maraviroc [125,126]. In contrast, fragmentation of 4-hydroxyphenyl maraviroc daughter ion m/z 296 generated ions at m/z 122 and 133 (**Figure 4-10B**), products resulting from one oxygen insertion on the phenyl ring containing ions m/z 106 and 117, respectively. Unlike 4-hydroxyphenyl maraviroc but similar to maraviroc, fragmentation of M1 yielded phenyl ring containing product ions at m/z 106 and 117 (**Figure 4-10C**). From these data, it was concluded that M1 formation did not involve oxygenation of the phenyl ring. Taken together, since M1 formation did not appear involved oxygen insertion on either the triazole ring or the phenyl ring of maraviroc, the oxygen insertion was assigned on the difluorocyclohexane ring (**Figure 4-10D**), which matched other product ions (**Figure 4-10C**). Fragmented ions with a loss of HF (20 Da) and CH_2=CH_2 (28 Da) from m/z 296 were found at 276 and 268, respectively. The loss of both HF and water (18 Da) from m/z 296 generated ions at m/z 258. A further loss of CH_2=CH_2 (28 Da) produced ions at m/z 230 (**Figure 4-10C**). MS^2 and MS^3 scans were also used to confirm that M2-M6 were indeed monooxygenated products as well and distinct from M1 (data not shown).

Figure 4-10. M1 results from oxygen insertion on the difluorocyclohexane ring of maraviroc as determined by mass spectrometry. MS^3 spectra of **(A)** maraviroc, **(B)** 4-hydroxyphenyl maraviroc and **(C)** M1. **(D)** The proposed structure of M1. MS^3 scans were performed using $1^{st}/2^{nd}$ precursor ions at m/z 514/280 for maraviroc and at m/z 530/296 for 4-hydroxyphenyl maraviroc and M1, respectively.

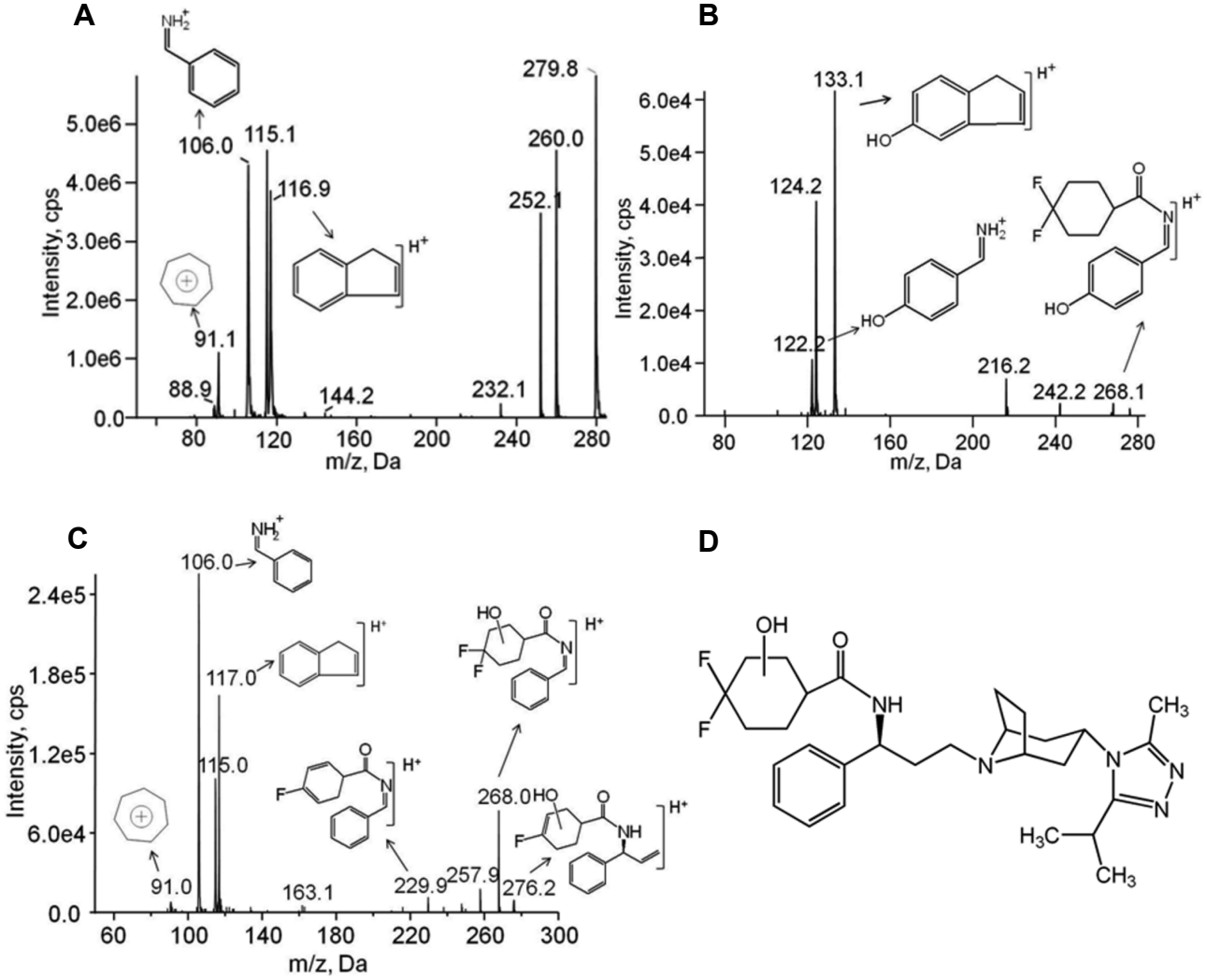

Mutation of residues that are divergent between CYP3A4 and CYP3A5 alters M1 formation

Since studies have yet to be performed to identify the CYP3A5 residues that might confer substrate specificity, we leveraged our finding that M1 is formed preferentially by CYP3A5 over CYP3A4 and mutated several CYP3A5 residues predicted to be within SRSs based on alignment with CYP3A4. A number of residues outside of the predicted CYP3A5 SRSs were mutated to the corresponding amino acids of CYP3A4 as well in order to evaluate their contribution to the differential metabolism of maraviroc by these enzymes (**Figure 4-11**).

Figure 4-11. Mutations of divergent residues between CYP3A4 and CYP3A5. The mismatched residues evaluated in this study are underlined and in bold font. The six previously reported putative substrate recognition sites SRS1-SRS6 are shown in boxes[127].

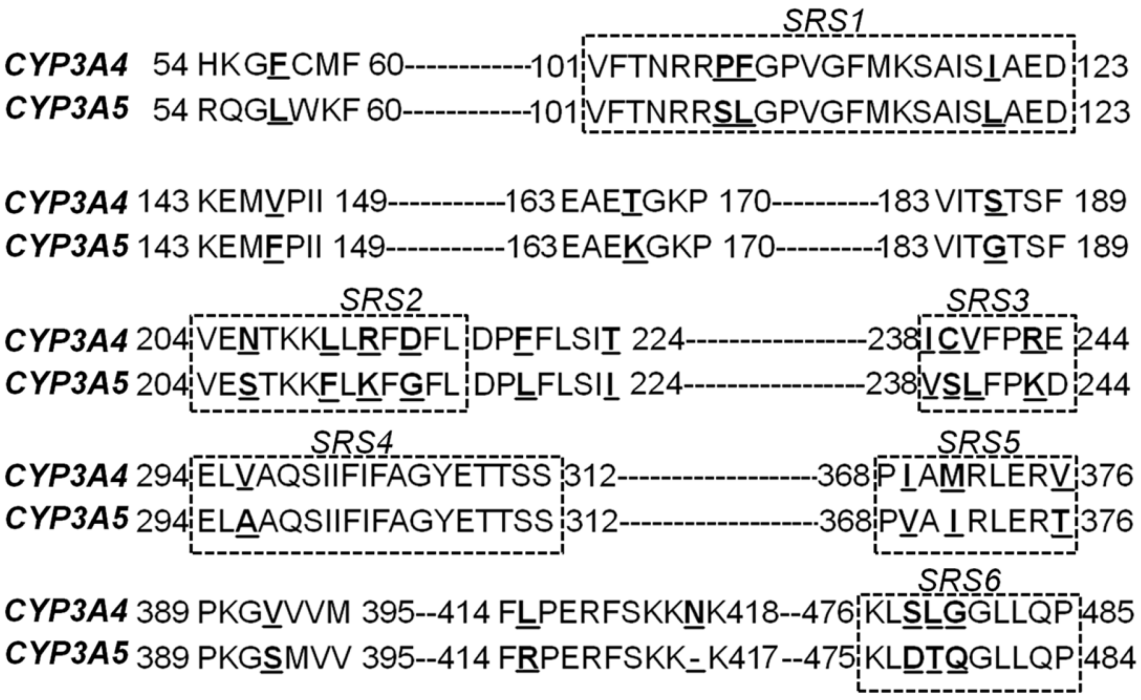

COS-7 cells were used as a model system for expression of CYP3A4 and CYP3A5 since they have been proven to express endogenous NADPH-cytochrome P450 reductase which is necessary to support CYP enzyme-mediated metabolism [128]. The untransfected cells did not exhibit activity towards maraviroc (data not shown). After transfection, protein expression of wild type CYP3A5 and all mutants was measured using immunoblotting (**Figure 4-12**). Similar to the maraviroc metabolism studies carried out using human liver microsomes, the CYP3A transfected COS-7 cells formed the oxidative metabolites of maraviroc with M1-M3 being the most predominant. Following protein normalization, a significant reduction in M1 formation by the L57F, S107P, L108F, G214D, L219F, L240V, I371M, S392V, T478L, and Q479G mutants was observed (**Figure 4-13**, $p < 0.02$). Among them, G214D exhibited the greatest reduction of 88% compared to the wild type CYP3A5. M1 formation by the L57F, L108F and S107P mutants of CYP3A5 was decreased by 61%, 59% and 72%, respectively. I224T mutation resulted in a loss of CYP3A5 expression and thus no M1 was detected. We also found that mutations F146V, G186S, S206N, A296V and V369I significantly increased M1 formation ($p < 0.05$). Mutations of F210L, S239C and K243R did not significantly change the M1 formation activity of CYP3A5 ($p = 0.16$, 0.16, and 0.20, respectively). No obvious changes were detected for other mutations including F120L, K166T, K212R, V238I, T376V, R415L, and D477S (data not shown).

Figure 4-12. Protein expression of CYP3A5 wild type and mutants. Plasmids containing wild type or mutant cDNA were transfected into COS-7 cells and maraviroc was added to the medium 24 h post-transfection. Protein expression was detected by immunoblot. Wild type (WT) was included for comparison with mutant in each experiment.

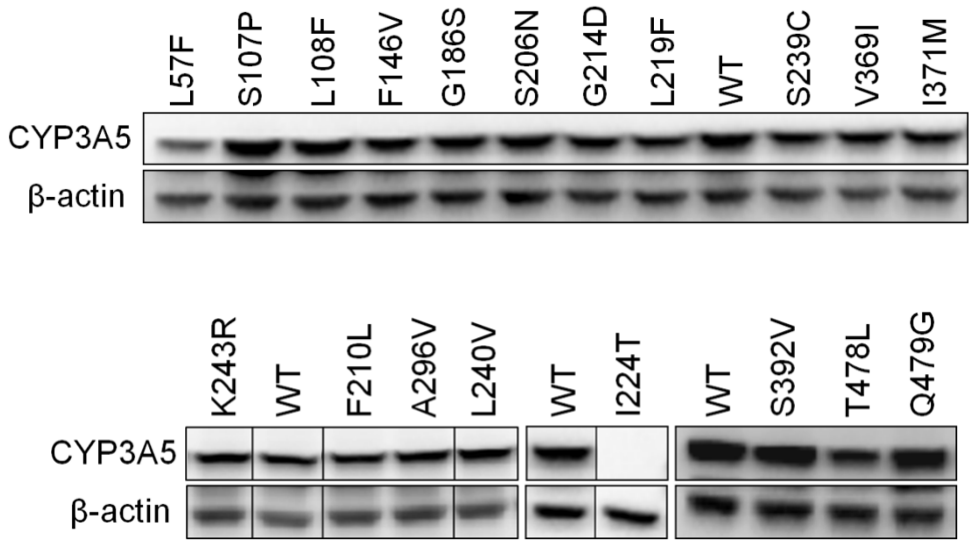

Figure 4-13. Changes in M1 formation resulting from mutation of CYP3A5 towards CYP3A4 after normalization by protein expression. At 24 h post-transfection, maraviroc was incubated with the cells for 40 min and metabolites were measured in the medium followed by protein expression measurement for normalization. SRS regions that the residues belong are denoted on the graph. $P \leq 0.05$ for all mutants, except for F210L ($p = 0.16$), S239C ($p = 0.16$), and K243R ($p = 0.20$), when compared to wild type CYP3A5.

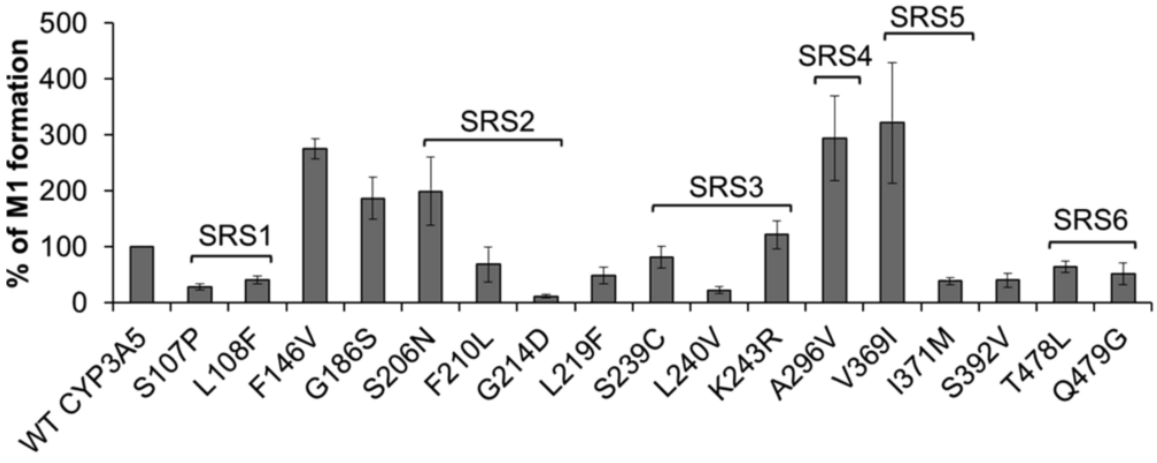

To gain a more comprehensive understanding of the effects of the mutations of CYP3A5 on catalytic activity we also measured the formation of M2 and M3 in addition to M1. Wild type CYP3A5 formed M1 at a higher level than M2 and M3 with metabolic ratios of M1/M2 and M1/M3 of 24.4 and 30.4, respectively (Table 1). In contrast, M1 formed by CYP3A4 was comparable to formation of M2 and M3 with M1/M2 and M1/M3 ratios of 1.5 and 1.6, respectively. Among the CYP3A5 mutants that were tested, L108F, G214D, and L57F resulted in a decrease in M1/M2 ratio by 95%, 75%, and 52%, respectively, as compared to wild type CY3A5. Furthermore, L108F, G214D, S107P, L57F, L240V and I371M decreased M1/M3 ratio by 95%, 85%, 64%, 55%, 51%, and 51%, respectively. Thus, these mutations of CYP3A5 shifted formation of these metabolites towards that of CYP3A4. In addition, F146V and L219F decreased the metabolic ratios of both M1/M2 and M1/M3; however, the differences from wild type CYP3A5 were less than 50%. Unlike the other mutants, S206N increased M1/M2 and M1/M3 by 39% and 57%, respectively.

Table 4-2. Comparison of metabolic ratios of CYP3A5 and its mutants to that of CYP3A4. The indicated enzymes were transiently expressed in COS-7 cells. Metabolism experiments for maraviroc were carried out and oxidative metabolites M1, M2, and M3 were measured as described under Materials and Methods. Metabolic ratios (M1/M2 and M1/M3) are presented as means ± SD.

Name	M1/M2	M1/M3
CYP3A5	24.4 ± 1.3	30.4 ± 4.2
L57F	11.8 ± 1.2	13.6 ± 1.4
S107P	24.1 ± 2.7	10.9 ± 4.0
L108F	1.29 ± 0.05	1.7 ± 0.03
F146V	20.0 ± 2.9	25.6 ± 4.0
G186S	25.4 ± 1.5	38.9 ± 3.2
S206N	34.0 ± 2.1	47.6 ± 3.6
G214D	6.14 ± 0.2	4.6 ± 0.03
L219F	17.9 ± 0.4	16.7 ± 0.1
S239C	27.3 ± 4.0	42.3 ± 3.9
L240V	13.3 ± 6.3	14.9 ± 4.9
V369I	18.2 ± 4.5	25.1 ± 2.8
I371M	20.3 ± 2.8	15.0 ± 1.5
S392V	22.5 ± 0.1	18.8 ± 2.3
T478L	25.6 ± 2.7	38.1 ± 2.7
Q479G	25.6 ± 2.2	23.4 ± 1.1
CYP3A4	1.5 ± 0.5	1.6 ± 0.8

Following the observation that mutation of certain CYP3A5 residues resulted in metabolite profile similar to that of CYP3A4 we tested whether the reverse could occur if residues in CYP3A4 were mutated to the corresponding mismatched residues in CYP3A5. We analyzed CYP3A4 mutants including F57L, P107S, F108L, D214G, L479T, and deletion of N423 (ΔN423). CYP3A4 contains 503 amino acids while CYP3A5 has 502 residues. N423 is the CYP3A4 amino acid that appears to be the additional amino acid that is not present in CYP3A5 when the two sequences are aligned. Very interestingly, we found that while the L57F mutation of CYP3A5 shifted M1 formation towards CYP3A4 with a decrease of 61% the reverse mutant of CYP3A4, F57L, had the opposite effect in that it increased M1 formation to 337% of that produced by wild type CYP3A4 (**Figure 4-14**). Other mutations including P107S, F108L, D214G, L479T, ΔN423, did not have changes on M1 formation (data not shown).

Figure 4-14. Residue 57 contributes to the differential formation of M1 by CYP3A4 and CYP3A5. Decreased M1 formation by the CYP3A5 L57F mutant ($p = 0.0002$) and increased M1 formation by the CYP3A4 F57L mutant ($p = 0.002$) relative to that by wild type CYP3A5 and CYP3A4, respectively. Protein expression of wild type (WT) CYP3A4 and the F57L mutant is shown above the right panel and expression of CYP3A5 L57F is shown in Figure 6a. Metabolite formation was normalized to protein expression as measured using immunoblotting. $^{**}p < 0.01$, $^{***}p < 0.001$ when compared to wild type.

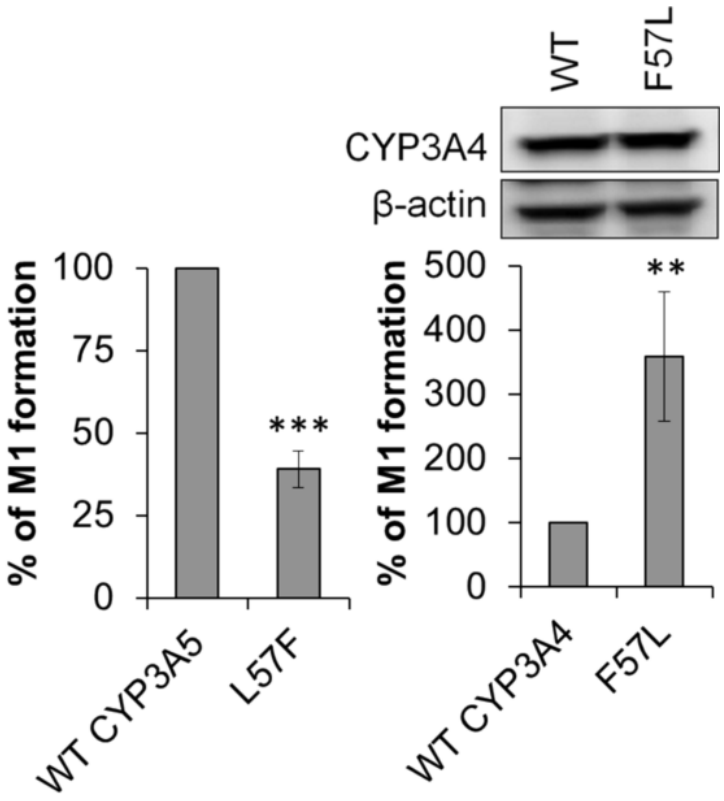

Identification of novel dioxygenated maraviroc metabolites

Using the chromatographic method for maraviroc metabolite analysis that we developed, four previously unreported maraviroc dioxygenated metabolites (M7-M10) were identified in human liver microsome reactions by monitoring the transition m/z 546/312 (**Figure 4-15A**). MS^2 fragmentation of the four metabolites all produced two major daughter ions at m/z 312 and 421, which have a 32 Da increase compared to the daughter ions of maraviroc m/z 280 and 389, respectively (**Figure 4-15B**). This suggested that the oxygen insertions were not on the triazole ring as neither of the fragment ions m/z 280 or m/z 389 contain the triazole ring. Further fragmentation of m/z 312 from M7-M10 generated product ions m/z 106 and 117 (**Figure 4-15C**), the two phenyl ring containing ions found in the MS^3 spectra of maraviroc daughter ion m/z 280 (**Figure 4-10A**), indicating that no oxygen insertions occurred on the phenyl ring of maraviroc. Therefore, the two hydroxyl groups were assigned to the difluorocyclohexane ring. The assignment was in agreement with other observed ions in the spectra namely m/z 294 and 274 that are products of the m/z 312 daughter ion that are formed after the loss of a water molecule (18 Da) and a further loss of HF (20 Da), respectively (**Figure 4-15C**). Consistent with the *in vitro* metabolism results using human liver microsomes, we found that the four dioxygenated metabolites were present in all the urine samples collected from the healthy volunteer (**Figure 4-15D**). Similar to what was observed for the monooxygenated metabolites, CYP3A5 and CYP3A4 catalyzed the formation of all of the dioxygenated metabolites (data not shown).

Figure 4-15. Chromatograms and MS^n spectra of dioxygenated metabolites. (A) Chromatogram of dioxygenated maraviroc metabolites (M7-M10) detected using the transition m/z 546→312 from metabolism reactions using human liver microsomes. (B) Representative MS^2 spectra of M7-M10 with the precursor ion m/z 546. (C) Representative MS^3 spectra of M7-M10 with 1st/2nd precursor ions at m/z 546/312. The proposed structures of fragmented ions are shown near the corresponding peaks. (D) Chromatogram of dioxygenated maraviroc metabolites (M7-M10) detected in urine collected at 0-2 h from a healthy volunteer using the transition m/z 546→312.

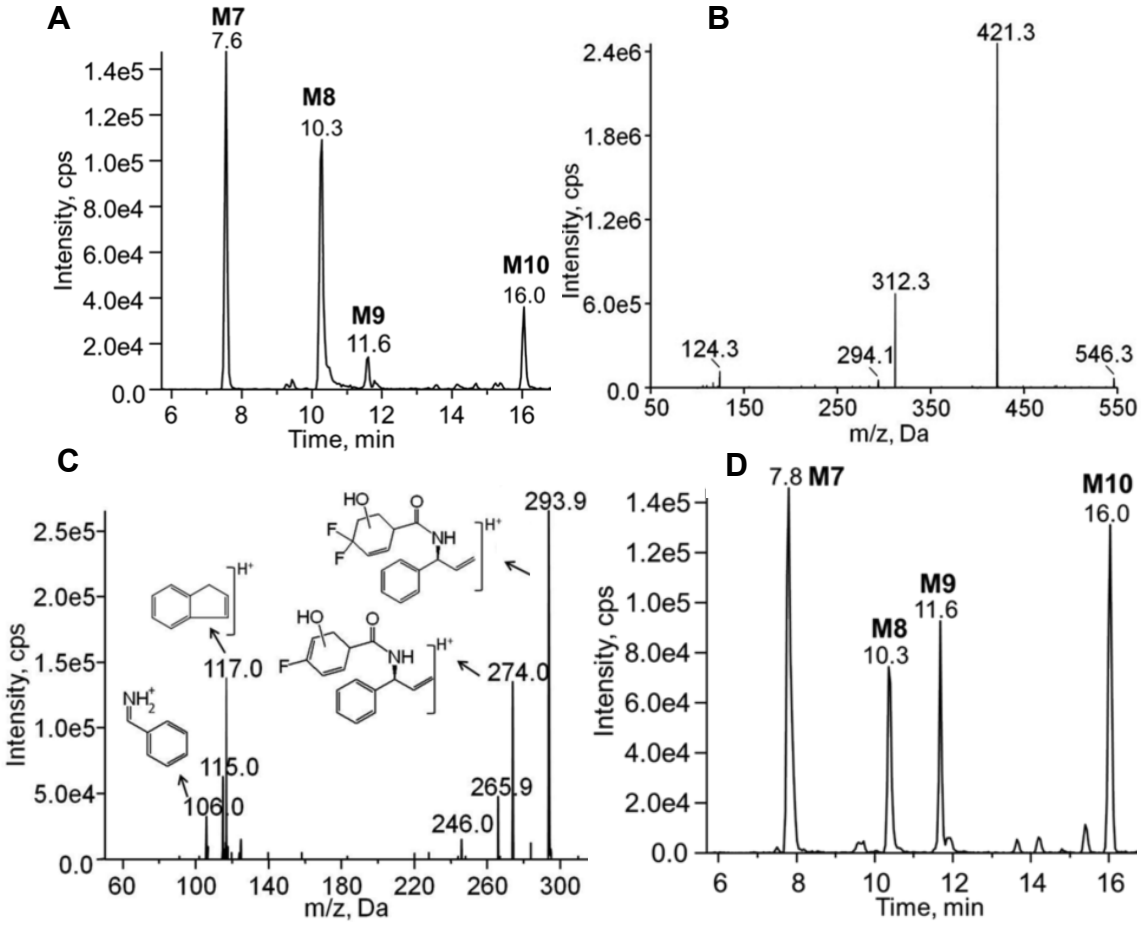

Glucuronidation of Maraviroc

Glucuronidation has been proposed as a metabolic pathway for maraviroc in mice but not in humans [129]; however, in the present study we have identified two maraviroc glucuronides that were detected using the transitions m/z 706/581 (M11, **Figure 4-16A**) and m/z 706/389 (M12, **Figure 4-16A**). MS^3 spectra of M11 with $1^{st}/2^{nd}$ precursor/product ions of 706/581 contained ions at m/z 472, 296, and 133 (**Figure 4-16B**). The ion with m/z 472 is a product resulting from a glucuronic acid (176 Da) conjugation on the ion with m/z 296, an ion with one oxygen insertion compared to maraviroc daughter ion m/z 280. The ion with m/z 133 has the same mass as a product ion (m/z 133) of 4-hydroxyphenyl-maraviroc (**Figure 4-10B**). Therefore, the conjugation of glucuronic acid was assigned to the phenyl ring. Unlike M11, fragmentation of M12 generated two major ions m/z 389 and m/z 280, the same two daughter ions produced via fragmentation of maraviroc (**Figure 4-16C**). MS^3 spectra confirmed that these two ions were indeed the same in both maraviroc and M12 suggesting that the glucuronidation occurred on the triazole moiety following oxidation. Consistently, we also found that the two glucuronides were present in the human urine samples (**Figure 4-16D**).

Figure 4-16. Chromatograms and MS^n spectra of maraviroc glucuronides. (A) MRM chromatogram of maraviroc glucuronides with transitions at m/z 706→581 (M11) and at m/z 706→389 (M12) from metabolism reactions using human liver microsomes. (B) MS^3 spectra of M11 monitoring $1^{st}/2^{nd}$ precursor ions at m/z 706/581. (C) MS^2 spectra of M12 monitoring precursor ion at m/z 706. The proposed structures of fragmented ions are shown near the corresponding peaks. (D) MRM chromatogram of maraviroc glucuronides with transition at m/z 706→581 (M11) and at m/z 706→389 (M12) in urine collected at 0-2 h from the volunteer.

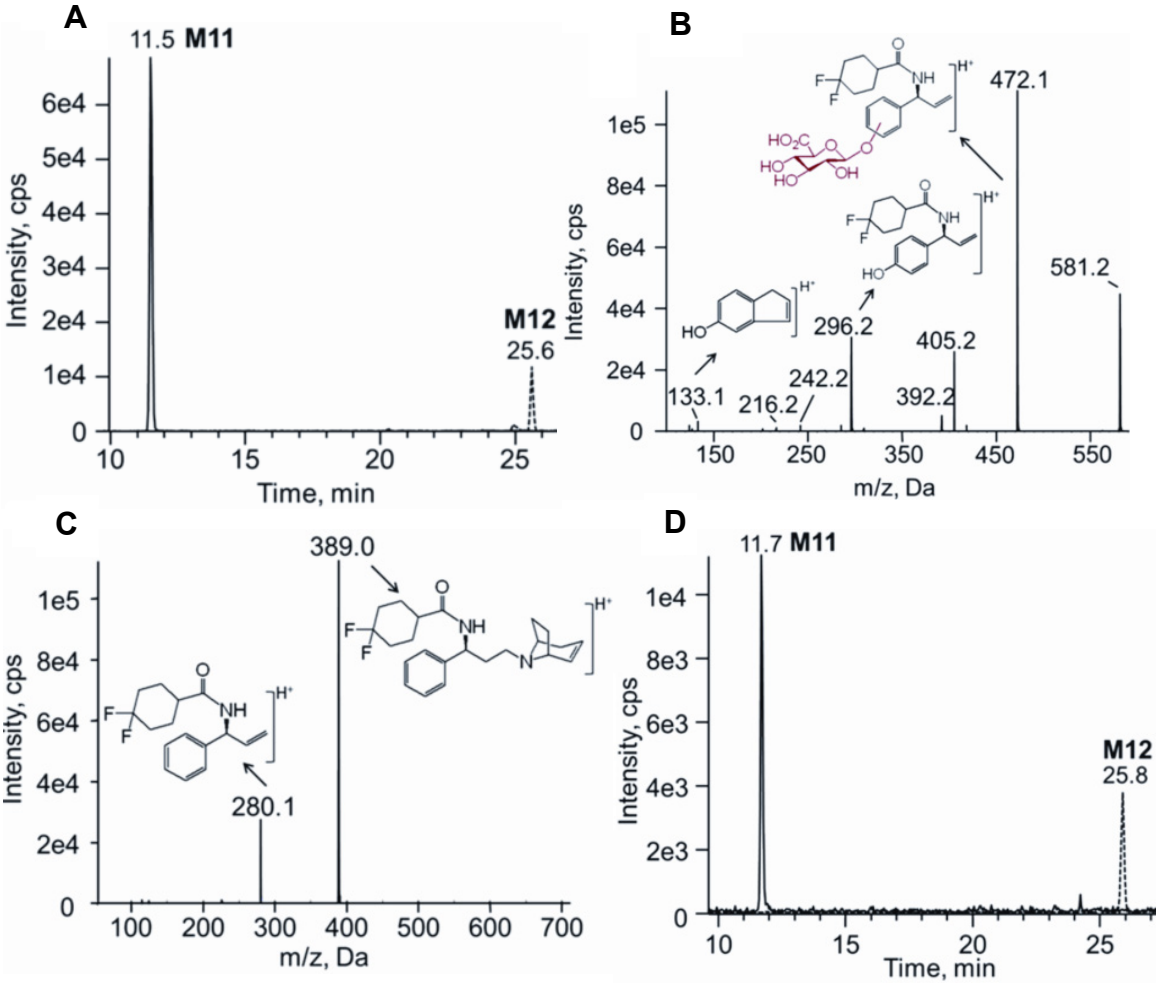

Discussion

In this study, a novel chromatographic method was developed for the separation and quantitation of oxidative metabolites and glucuronides of maraviroc. We found six major monooxygenated metabolites (M1-M6), four novel dioxygenated metabolites (M7-M10), and two previously unidentified glucuronides (M11-M12) using human liver microsomes and confirmed that the metabolite profile was similar in plasma and/or urine samples after administration of maraviroc to a healthy volunteer. The separation method that we developed has utility in future studies of maraviroc metabolism in both basic and clinical research. Further, since maraviroc is currently used clinically to treat HIV and is being investigated for additional use in HIV prevention, the data presented here are valuable in that we provide the first detailed information regarding the biotransformation of maraviroc both in vitro and in vivo.

We identified CYP3A4 and CYP3A5 as the major P450s involved in maraviroc oxidation, which will be helpful in understanding drug-drug interactions of maraviroc with other drugs. It is known that maraviroc plasma concentration and exposure are significantly changed when co-administered with CYP3A inducers or inhibitors [130,131]. The M1 formation activity of CYP3A5 exhibited an evident difference from that of CYP3A4. This was further confirmed by the observation that there was marked reduction in M1 formation by human liver microsomes genotyped as homozygous CYP3A5*3 allele that do not express CYP3A5. In addition, N-dealkylation and oxidation have been reported to be the two major pathways responsible for the metabolism-dependent clearance of maraviroc [123] . Previous studies reported a K_m of 21 μM and V_{max} of 0.45 pmole/min/pmole P450 for N-dealkylation of maraviroc using human liver microsomes

and a K_m of 13 μM and V_{max} of 3 pmole/min/pmole P450 for the formation of this same metabolite using cDNA expressed CYP3A4 [124]; here we demonstrated that CYP3A5 plays a primary role in the formation of M1 with K_m of 48.9 μM and V_{max} of 0.93 pmole/min/pmole P450. We also detected the N-dealkylated metabolite of maraviroc in both plasma and urine samples. The peak area ratio of the N-dealkylated metabolite to M1 in plasma varied from 0.3 to 2.6 with time over a period of 24 h after the dose, suggesting that monooxygenation of maraviroc may not be a minor pathway of maraviroc metabolism when compared to the N-dealkylation. This indicates that in addition to N-dealkylation, monooxygenation should also be monitored in order to gain a more complete understanding of the mechanism(s) of maraviroc clearance. Taken together, our results indicate that M1 formation is primarily mediated by CYP3A5 and thus maraviroc is potentially useful as a probe substrate for CYP3A5. The use of maraviroc as a CYP3A5 probe substrate can be applied to *in vitro* drug-drug interaction studies to identify potential inducers or inhibitors of CYP3A5 in the process of drug development.

In addition, several aspects of maraviroc make it an attractive candidate for potential consideration as a CYP3A5 clinical phenotyping probe: 1) it is an Food and Drug Administration (FDA)-approved oral drug; 2) maraviroc has an excellent clinical safety profile [132]; 3) M1 was detected as one of the major oxidative metabolites in urine as early as 0-2 h following maraviroc administration (data not shown), possibly making maraviroc a non-invasive phenotyping probe through analysis of urine samples. Several studies have shown that CYP3A5 is involved in metabolism of drugs including vincristine [133-135], tacrolimus [136,137], and cyclosporine [138]; however, these drugs all have demonstrated toxicities [139-142], making them less desirable as probe drugs for use in healthy volunteers.

We found a single residue, 57, that when mutated in CYP3A5 (L to F) shifted the CYP3A5-dependent M1 formation to mirror that of CYP3A4 and vice versa (CYP3A4 F to L). This is the first time that a residue that confers a switch in the activity between CYP3A4 and CYP3A5 has been identified. Our study provided the first experimental evidence, to the best of our knowledge, for the importance of this residue for CYP3A activity as well as its role in differentiating activities between CYP3A4 and CYP3A5. A recent crystal structure has shown that the CYP3A4 residue F57 is involved in the binding of the CYP3A4 substrate ritonavir [120].

Several studies have suggested an important role for SRS1 residue F108, which resides in the Phe-cluster (F108, F213, F215, F219, F220, F241, and F304) that forms a hydrophobic roof for the CYP3A4 active site, in CYP3A4 catalytic activity[117,118]. Replacement of F108 in CYP3A4 to the corresponding CYP3A5 residue L decreased metabolism of testosterone and aflatoxin B1 [110]. The CYP3A4-ritonavir crystal structure showed that F108 formed a hydrophobic pocket for ritonavir binding along with several other residues [120]. In addition, computational modeling predicted that F108 in CYP3A4 is involved in maraviroc binding via van der Waals interaction [143]. A previous CYP3A5 homology model constructed based on the CYP3A4 crystal structure showed that the overall folding of CYP3A5 overlaid with the folds of CYP3A4 [9], suggesting that L108 might be located in the roof of the CYP3A5 active site as it is in CYP3A4. Our current study showed that mutation L108F in CYP3A5 reduced M1 formation, confirming its importance to CYP3A5 activity. In addition, the formation of M2 and M3 was increased compared to wild type CYP3A5. The resultant metabolite profile resembles that of CYP3A4 with similar metabolic ratios. Similar to residue F108, residue F219 in the

hydrophobic pocket of CYP3A4 is replaced by L in CYP3A5. After mutation of L to F at 219 in CYP3A5, we also observed a reduction in M1 formation. The increased size in the side chain for the mutation L to F at 108 and 219 may strengthen the effects of the characteristic "Phe-cluster" thereby making the shape of CYP3A5 substrate binding pocket more like that of CYP3A4, resulting in the change of CYP3A5 activity towards that of CYP3A4.

Mutation of CYP3A5 SRS2 residue G214 to CYP3A4 residue D214, a residue located between the hydrophobic residues F213 and F215, resulted in a pronounced effect with 88% reduction of CYP3A5 activity for M1 formation. CYP3A4 SRS3 residue V240 belongs to this hydrophobic ceiling of the active site along with the Phe-cluster and was shown to contribute to progesterone binding [118]. The mutation of CYP3A5 L240V also resulted in a marked decrease in M1 formation. These data underscore the importance of the hydrophobic roof in the active site, which might play a role in CYP3A4 and CYP3A5 substrate specificity.

In summary, we found that CYP3A4 and CYP3A5 were the major enzymes responsible for maraviroc oxidation and that CYP3A5 was the primary enzyme responsible for the formation of a major monooxygenated metabolite of maraviroc; we determined that the divergent residue 57 within CYP3A4 and CYP3A5 contributed to their differential activities towards maraviroc; we also identified novel secondary deoxygenated and glucuronidated metabolites of maraviroc. Collectively, besides filling the gap in understanding of maraviroc metabolism, these studies suggest that maraviroc may have utility as a probe substrate for CYP3A5. In addition, the present study has provided novel

biochemical information regarding the contribution of divergent residues to the activity of both CYP3A4 and CYP3A5.

Chapter 5 – Effect of CYP3A5 polymorphism on pharmacokinetics of maraviroc and metabolite M1

Abstract

Cytochrome P450 3A5 (CYP3A5) is a drug metabolizing enzyme similar to CYP3A4, but, unlike CYP3A4, CYP3A5 exhibits greater polymorphic expression resulting in large variations in blood concentrations of drugs that are metabolized preferentially by CYP3A5. A selective CYP3A5 substrate is useful to determine CYP3A5 activity. Our *in vitro* metabolism study results demonstrated that CYP3A5 plays a major role in the oxidative metabolism of the anti-HIV drug maraviroc. The present study evaluated the impact of CYP3A5 genotype on the pharmacokinetics of maraviroc. After screening CYP3A5 genotyping, we evaluated twenty-four research participants in 3 groups of eight participants each: CYP3A5 homozygous wild type (two CYP3A5*1 alleles), heterozygous (one CYP3A5*1 allele and one mutant allele), and mutant (no CYP3A5*1 alleles). Participants received an oral dose of 300 mg maraviroc and blood was sampled over a period of 32 h. The homozygous wild type group had 41% lower maraviroc area under the plasma concentration-time curve from time 0 to infinity ($AUC_{0\text{-}inf}$) and 66% higher apparent clearance compared with the mutant group. Maraviroc $AUC_{0\text{-}inf}$ in the heterozygous group was 16% lower but this difference was not statistically significant when compared to the mutant group. The M1 $AUC_{0\text{-}inf}$ was 224% and 157% in the heterozygous and homozygous wild type group, respectively, relative to that in the mutant group. The $AUC_{0\text{-}inf}$ ratios of maraviroc to M1 in heterozygous and homozygous wild type group were lower by 51% and 64% when compared with the mutant group, respectively. Plasma concentration ratios and $AUC_{0\text{-}inf}$ ratios of maraviroc to M1 were well correlated at 4 h post dose administration. These results suggest that maraviroc can be used in clinical studies as a probe for CYP3A5 activity.

Abbreviations

AUC, area under the plasma concentration-time curve, AUC; $AUC_{0\text{-inf}}$, area under the curve from time to infinity; $AUC_{maraviroc}/AUC_{M1}$, $AUC_{0\text{-inf}}$ ratio of maraviroc to M1; BMI, body mass index; C_{max}, plasma peak concentration; CL/F, oral apparent clearance; CrCL, creatinine clearance; CYP3A5, Cytochrome P450 3A5; FDA, Food and Drug Administration; IQR, interquartile range; PCR, polymerase chain reactions; T_{max}, time to reach C_{max}; $T_{1/2}$, half-life; UPLC, Ultra Performance Liquid Chromatography; V/F, volume of distribution.

Introduction

Cytochromes P450 (CYP)-dependent metabolism is an important pathway for drug elimination[144]. CYP-mediated biotransformation usually converts drugs to more polar metabolites to facilitate their excretion into bile or urine. When two or more drugs are co-administered, if one drug is cleared through CYP-mediated metabolism and the other drug has an inhibitory or inductive effect on the CYP enzyme, the substrate drug blood concentration may be increased resulting in toxicity or decreased leading to treatment failure. Similarly, the variation in CYP expression also leads to changes in the blood concentration of their substrate drugs. Using a CYP substrate as a phenotyping probe to measure *in vivo* activity of a CYP enzyme is valuable in the process of drug development to identify drugs or dietary supplements that have potential modulatory effects on these enzymes, especially when the substrate drug has a narrow therapeutic window. CYP3A4 and CYP3A5, two major CYP3A subfamily enzymes, play predominant roles in drug metabolism by catalyzing the biotransformation of more than 50% of marketed drugs; however, the substrate spectra of these two enzymes largely overlap due to high

similarity at the amino acid level making discovery of selective substrates difficult. Over the years, efforts have been focused on the development of CYP3A4 phenotyping probes because CYP3A4 has been thought to be the major CYP3A isoform in liver; however, CYP3A5 has received increased attention in recent years due to the fact that it is highly polymorphic and thus, its expression is highly variable. The wild type CYP3A5*1 allele is associated with the highest expression level of CYP3A5, whereas changes in the mRNA splicing site due to single nucleotide polymorphisms (CYP3A5*3, CYP3A5*6) or in the reading frame due to a T insertion (CYP3A5*7) result in lower expression or no activity of CYP3A5 [16,19,145,146]. CYP3A5*2 had a nucleotide transition from C to A, causing an amino acid change from threonine to asparagine in the CYP3A5 protein so that the enzyme is not fully functional[18]. The most common nonfunctional allele CYP3A5*3 is abundantly present in the European American population and < 10% of them express CYP3A5. In contrast, CYP3A5*1 has high frequency in the African American population and > 60% of them express CYP3A5[16,18-20]. In individuals who are expressers, CYP3A5 protein accounts for > 50% of total liver CYP3A and even several-fold higher than that of CYP3A4[57,58]. Several studies have shown that variations in CYP3A5 expression contribute to changes in the plasma concentrations of its substrate drugs[147-151]. Increased risk of drug toxicities has been reported in people with low CYP3A5 expression. Conversely, unexpected high expression of CYP3A5 could result in low blood drug concentrations leading to compromised drug efficacy and even life-threatening treatment failures. Therefore, a clinical probe that is used to measure CYP3A5 *in vivo* activity will help to identify drugs that are CYP3A5 inhibitors or inducers in order to prevent toxicity or treatment failure in multi-drug using patients.

Our *in vitro* work showed that CYP3A5 is the major enzyme responsible for formation of the maraviroc metabolite, M1. Human liver microsomes isolated from donors homozygous for the nonfunctional CYP3A5*3 allele exhibited a significant decrease in M1 formation compared with those homozygous for the wild-type CYP3A5*1 allele, indicating that the biotransformation from maraviroc to M1 could be used to measure CYP3A5 activity. Since maraviroc is an anti-HIV drug with an excellent safety profile that could be given to healthy volunteers, it may have the potential to be used as a clinical CYP3A5 phenotyping probe. Therefore, we extended these *in vitro* observations to further investigate the clinical value of maraviroc in CYP3A5 metabolic phenotyping by evaluating the influence of CYP3A5 genotype on pharmacokinetics of maraviroc and metabolite M1.

Materials and Methods

Subjects and study design

This was an open label, single dose study. Inclusion criteria included age 18–65 years, healthy with no acute medical illness, no evidence of hepatic or renal impairment (liver function tests values < 1.5 Upper Limit of Normal (ULN), total bilirubin below ULN, creatinine clearance > 60 mL/min), and negative HIV test results. Any concomitant medications or herbal supplements for which there is a known risk of pharmacokinetic or pharmacodynamics drug interactions, including those that inhibit CYP3A family enzymes, were prohibited for 4 weeks prior to and during the study. The study was reviewed and approved by the institutional review board of The Johns Hopkins Medical Institutions and was conducted in compliance with national and local institutional guidelines. All participants gave written informed consent.

Healthy volunteers were screened by CYP3A5 genotyping (*1, *2, *3, *6, and *7) for enrollment into 3 groups of 8 research participants (24 total sample size) based on the status of CYP3A5 genotype: homozygous wild type (2 CYP3A5*1 alleles), heterozygous (1 CYP3A5*1 allele and 1 mutant allele), and without wild type genotype (2 mutant alleles). A single dose of 300 mg maraviroc tablet was given to the volunteers orally along with 200 mL water under direct observation. Ten mL of venous blood before (0 h) and 1, 2, 3, 4, 6, 8, 10, 24 and 32 h after the drug administration was drawn from each subject into heparinized tubes. Plasma was prepared by centrifugation of blood at 1,500 × g for 10 min at 4 °C and stored at -80 °C.

Preparation of stock solutions, calibration standards and quality control samples

An isotopically-labeled analog of maraviroc, $^{2}H_{6}$- maraviroc, was used as an internal standard in quantitative analysis of maraviroc and its metabolites. All master stock solutions were prepared in acetonitrile at 1 mg/mL. Working solutions were serial dilutions of master stocks into acetonitrile. Calibration standards and quality controls were prepared by spiking freshly-made working solutions into EDTA K_2 plasma. Since the true chemical standard of M1 is unavailable, 4-hydroxyphenyl maraviroc whose m/z ratios of precursor/daughter are similar to M1 was used to make calibrators and quality controls to determine the concentration of M1. The calibration range was linear from 0.5−1,000 ng/mL for maraviroc and 0.25−1,000 ng/mL for M1. Stock solutions, calibration standards and quality control samples were stored at −80°C until use.

Measurement of plasma concentrations of maraviroc and M1

Patient plasma samples, standards, and quality controls were thawed, vortexed, and processed at room temperature. Fifty microliters of plasma was mixed with 50 µl of acetonitrile containing 10 ng/mL internal standard, $^{2}H_{6}$- maraviroc.

For maraviroc, the 100 µL mixture was transferred to a filtration plate (Agilent Captiva 0.45 µm polypropylene, Lake Forest, CA). Then 500 µl of acetonitrile was added for protein precipitation. Following a period of 5-min incubation, vacuum was applied and filtrates were collected into a 96-well plate. Eluents were dried under a dry nitrogen stream and reconstituted in 100 µl of a 1:1 water containing 0.1% formic acid (mobile phase A): acetonitrile containing 0.1% formic acid (mobile phase B) mixture. The plate was sealed with a polypropylene mat caps (Waters) and put into the autosampler at 4 ºC. Ten microliters of reconstituted sample was injected onto a reversed-phase Waters BEH C_8 Ultra Performance Liquid Chromatography (UPLC) column (1.7 µm, 50 × 2.1 mm) at room temperature (20-24 ºC) and analytes were detected over 5 minute with a flow rate of 1 mL/min using AB SCIEX API 4000 mass spectrometer. Mobile phases were programmed at 20% B from 0 to 1 min, 50% B from 1.0 to 1.5 min, 95% B from 2 to 3.5 min, and 20% B from 3.8 to 5 min. The MRM transitions were determined by the direct infusion of the authentic standard and deuterated analogs into the mass spectrometer ion source by positive electrospray. Detection of the analytes and internal standards was achieved via multiple reaction monitoring. The mass-to-charge ratios of characteristic ion pairs (precursor > product), individually optimized voltages, and retention times of analytes and internal standards are presented in **Table 5-1**. Signal levels of carbon-12 maraviroc were too high to be monitored over the desired range so the carbon-13 isotope of maraviroc was chosen as the maraviroc transition. The multiple reaction monitoring

ions and transitions monitored were as follows: maraviroc m/z 515.3 > 390.2; $^{2}H_{6}$-maraviroc m/z 520.6 > 389.1. Via this method, maraviroc can be detected over an analytical measuring range of 0.5 − 1,000 ng/mL. Samples above the upper limit of quantitation were diluted, 1:3 sample:EDTA blank plasma, and re-evaluated. The method was developed and validated by the Clinical Pharmacology Analytical Laboratory in the Division of Clinical Pharmacology at The Johns Hopkins School of Medicine. Briefly, inter-and intra-assay precision was ≤ 5.38% and ≤ 5.98%, respectively; inter-and intra-assay accuracy was ≤ 10.2% and ≤ 8.44%, respectively. These validation results exceeded standards recommended by Food and Drug Administration (FDA) and a manuscript has been recently accepted for publication[152].

For measurement of plasma M1, 500 µl of acetonitrile was added into the 100 µl mixture of plasma and internal standard followed by 5 min incubation for protein precipitation and transfer to a filtration plate. Then vacuum was applied and filtrates were collected into a 96-well plate. Eluents were dried under a dry nitrogen stream and reconstituted in 75 µl of mobile phases A (5% acetonitrile – 0.1% formic acid in water) and B (5% water – 0.1% formic acid in acetonitrile) by vortexing for 30 s. Ten microliters of reconstituted sample was injected onto the same UPLC column (1.7 µm, 50 × 2.1 mm) used for maraviroc quantitation method but the analytes were detected over 8.0 minute using AB SCIEX API 5500 mass spectrometer under positive electrospray mode. The optimized parameters and settings for mass spectrometry are listed in **Table 5-1**. The program of the mobile phases is shown in **Table 5-2**. The flow rate was 1 mL/min.

Table 5-1. Retention times and mass spectrometric conditions.

	Retention Time	*m/z*[†] of Ions		Operating Parameters		
	(min)	Precursor	Product	DP[‡]	CE[§]	CXP[ll]
Method for maraviroc using API 4000						
Maraviroc	0.54	515.3	390.2	86	29	10
$^{2}H_{6}$-maraviroc	0.54	520.6	389.1	80	29	10
Method for M1 using API5500						
M1	3.1	530.2	405.2	161	29	12
$^{2}H_{6}$-maraviroc	5.2	520.2	389.2	71	29	28

[†]m/z, mass-to-charge ratio
[‡]DP, Declustering Potential, V
[§]CE, Collision Energy, eV
[ll]CXP, Collision Cell Exit Potential, V

Table 5-2. Mobile phases program for detection of M1.

Time (minutes)	% Mobile Phase B
0.0	4.0
0.5	4.0
4.0	6.0
4.1	15.0
5.0	15.0
5.1	100.0
6.5	100.0
7.0	4.0
8.0	4.0

Pharmacokinetic analysis and statistical considerations

Pharmacokinetic parameters of maraviroc and its metabolite M1, including area under the curve from time to infinity ($AUC_{0\text{-}inf}$), area under the curve from time 0 to 32 h ($AUC_{0\text{-}32}$), plasma peak concentration (C_{max}), time to reach C_{max} (T_{max}), half-life ($T_{1/2}$), oral apparent clearance (CL/F) and volume of distribution (V/F) were estimated by WinNonlin (version 6.1, Pharsight, Cary, NC) using non-compartmental analysis. The values of time to C_{max} were computed from the respective concentration–time curves. The metabolic ratio of maraviroc to metabolite M1 was calculated as the AUC ratio of maraviroc to M1 ($AUC_{maraviroc}/AUC_{M1}$). Statistical analyses were performed with software R (version 2.15.1). Pharmacokinetic parameters and metabolic ratios among the three groups were compared using Kruskal-Wallis test; and differences between the groups with different CYP3A5 genotypes were assessed using a nonparametric statistical Mann–Whitney–Wilcoxon test. In addition, CYP3A5 genotype was treated as an ordered categorical variable (0, 1, and 2, for the homozygous mutant genotype, the heterozygous, and homozygous wild genotype, respectively) to evaluate the linear trend as one of the possible genetic models. We also valuated genotype as a dichotomous variable, combining heterozygous and homozygous mutant allele carriers for comparison with homozygous wild type allele CYP3A5*1 carriers to test a recessive pattern of inheritance and combining homozygous and heterozygous CYP3A5*1 allele carriers for comparison with homozygous mutant allele carriers to test a dominant genetic model. $P < 0.05$ was considered statistically significant. Linear regression graph was generated in SigmaPlot (version 12.3).

CYP3A5 genotyping procedure

Genomic DNA was extracted from blood samples using QIAamp DNA Blood Mini Kit (Qiagen Inc, Valencia, CA). DNA fragments containing the polymorphic loci were amplified using iProof™ High Fidelity DNA polymerase obtained from Bio-Rad (Hercules, CA). Previously reported primers[15,153,154] for polymerase chain reactions (PCR) and sequencing were used and the sequences are shown in **Table 5-3**. Optimum annealing temperature was determined using gradient PCR. The following program were used for PCR: (1) 98 °C for 30 s; (2) 98°C for 10s; (3) 65.2 °C for CYP3A5*3, 59.0°C for *6, 57.8°C for *7; (4) 72 °C for 45 s; repeat (2)-(4) for 35 cycles; and finally 72°C for 10 min. The PCR products were purified using QIAquick PCR purification kit (Qiagen, Inc) and sequenced at Synthesis and Sequencing Facility of The Johns Hopkins University School of Medicine using Sanger sequencing. The genotype of CYP3A5 was determined by evaluation of the chromatograms for the specific variant locus.

Table 5-3. Sequence of oligonucleotides used for CYP3A5 genotyping.

	Oligonucleotide Sequence
PCR Primers	
CYP3A5*3	5'- CCTGCCTTCAATTTTTCACTG-3'
	5'- GCAATGTAGGAAGGAGGGCT-3'
CYP3A5*6	5'- GCTGCATGTATAGTGGAAGGAC-3'[†]
	5'- GGAATTGTACCTTTTAAGTGGATG-3'
CYP3A5*2/*7	5'- AAATACTTCACGAATACTATGATC-3'
	5'- CAGGGACATAATTGATTATCTTTG-3'
Sequencing Primers	
CYP3A5*3	5'- TAATATTCTTTTTGATAATG-3'
CYP3A5*2 or *7	5'-ACC ACC ATT GAC CCT TTG GG-3'

[†]Primer was also used for sequencing.

Results

Genotyping analysis

A total of 34 subjects were evaluated for CYP3A5 genotype screening. Ten subjects were found to be homozygous for the wild type (29.4%, CYP3A5*1/*1), 10 were heterozygous (29.4%, 7 CYP3A5*1/*3, 2 CYP3A5*1/*6, 1 CYP3A5*1/*7,) and 14 were the mutant type (41.2%, 10 CYP3A5*3/*3, 2 CYP3A5*3/*6, 1 CYP3A5*6/*7, and 1 CYP3A5*7/*7). No CYP3A5*2 was found. After genotypic screening, these potential study participants had a medical history, physical examination, and laboratory testing. Volunteers who were determined to be healthy were enrolled in the study with 8 people in each of the three CYP3A5 genotypic groups: (1) no CYP3A5*1 allele; (2) one CYP3A5*1 allele and one mutant allele; and (3) two CYP3A5*1 alleles. After receiving a single maraviroc dose, one volunteer in the homozygous wild type (CYP3A5*1/*1) was found to have no detectable maraviroc or maraviroc metabolites in any plasma samples. Consequently, this subject was excluded for data analysis and was replaced with another subject in the same genotype group. For the final 24 evaluable research participants the mutant group included 5 CYP3A5*3/*3, 2 CYP3A5*3/*6, and 1 CYP3A5*6/*7; the heterozygous group had 7 CYP3A5*1/*3 and 1 CYP3A5*1/*6; and the homozygous wild type group had 8 CYP3A5*1/*1.

Demographics of subjects

The age and weight of the 24 evaluable subjects ranged from 21 to 58 years (mean ± SD, 41 ± 11years) and from 51.5 to 100.0 kg (mean ± SD, 78.2 ± 15.1 kg), respectively. Age, weight, body mass index (BMI), creatinine clearance (CrCL), total protein, albumin, bilirubin, and aspartate transaminase (AST) activity were similar among different

genotypic groups (**Table 5-4**). Alkaline phosphatase (ALP) and alanine transaminase (ALT) were lower in groups of people who carry two CYP3A5*1 alleles compared to the other two groups but the differences were not statistically significant. There were 6 females with 2, 1, and 3 of them distributing in groups of people who carrying 0, 1 and 2 CYP3A5*1 alleles, respectively. Among the 24 volunteers, 17 of them were black, 6 were white, and one was Asian.

Effect of CYP3A5 polymorphism on the pharmacokinetics of maraviroc and M1

The mutant group had similar concentration-time profiles as the heterozygous group (**Figure 5-2**). In contrast, the homozygous wild type group exhibited lower mean plasma maraviroc concentrations at almost all blood collection times. The medians (interquartile range, IQR) of pharmacokinetic parameters of maraviroc and metabolite M1 are shown in **Table 5-5**. The biggest % of extrapolated AUC from the time of the last measurable concentration to infinity is 17.1%. The values of AUC_{0-32} are very close to values of AUC_{0-inf}. Compared with the mutant group of people who do not carry any CYP3A5*1 alleles, maraviroc median AUC_{0-inf} was 41% lower and CL/F was 66% higher in the homozygous wild type group of people who carry two CYP3A5*1 alleles ($p = 0.02$ for both, **Figure 5-2**); V/F was 78% higher ($p = 0.005$); and C_{max} was 33% lower but the difference was not statistically significant ($p = 0.33$). Compared to the other two groups, the heterozygous group who carry one CYP3A5*1 allele and one variant allele exhibited larger inter-individual variability. Median values of maraviroc C_{max}, AUC_{0-inf}, CL/F, and V/F in the heterozygous group were not statistically significant from those in either of the other two groups. T_{max} and $T_{1/2}$ were not statistically different among the three genotypic groups.

For metabolite M1, the plasma concentrations are lower in the mutant group compared with the other two groups (**Figure 5-3**). The M1 $AUC_{0\text{-}inf}$ in the homozygous wild type group is 157% relative to that in the mutant group with median (IQR) at 64.5 (57.4-82.9) h•ng/mL and 41.1 (32.2-53.1) h•ng/mL, p = 0.01), respectively. The M1 $AUC_{0\text{-}inf}$ of the heterozygous wild type group is 224% relative to that in the mutant group with median (IQR) of 91.9 (38.7-133.8) h•ng/mL but the difference was not statistically significant (p = 0.10). The M1 C_{max} values were not statistically different among the three genotypic groups. Although not statistically significant, median T_{max} in the homozygous wild type group was one hour earlier than that in the mutant group (p = 0.06).

The influence of the CYP3A5 genotype was more evident in the $AUC_{0\text{-}inf}$ ratio of maraviroc to metabolite M1 ($AUC_{maraviroc}/AUC_{M1}$), a parameter that is commonly used for comparing metabolizing enzyme activities. The three genotype groups were determined to be different populations for values of $AUC_{maraviroc}/AUC_{M1}$ using Kruskal-Wallis test ($p < 0.001$). Compared to the mutant group that has median (IQR) of $AUC_{maraviroc}/AUC_{M1}$ at 49.5 (35.3-64.4), the homozygous wild type group and the heterozygous group were 64% and 52% lower with median (IQR) at 17.8 (15.7-22.5) and 24.0 (19.8-25.7), respectively, and the differences are both statistically significant ($p < 0.001$ for both, **Figure 5-4**). The homozygous wild type group and the heterozygous group were not statistically different from each other in $AUC_{maraviroc}/AUC_{M1}$ (p = 0.13). Evaluation of genetic models with linear trend, recessive, and dominant assumption based on values of Bayesian Information Criterion (BIC) suggested that a dominant model for the CYP3A5*1 allele explained the data best.

The $AUC_{0\text{-inf}}$ ratio and plasma concentration ratio of maraviroc to metabolite M1 (examining ratios at each sample time from 4 h to 10 h) showed strong correlations with $R^2 > 0.87$ ($r > 0.93$). Starting at 6 h, some subjects had M1 plasma concentrations that are close to 0.25 ng/mL (within ± 20% for deviation), the lower limit of quantitation for M1 concentration measurement assay. The $AUC_{0\text{-inf}}$ ratios and plasma concentration ratios of maraviroc to metabolite M1 are highly correlated ($R^2 = 0.94$, $r = 0.97$, $p < 0.001$, **Figure 5-5**) at 4 h after the dose. Similar to $AUC_{0\text{-inf}}$ ratios, plasma concentration ratios were statistically different among the three genotype groups using Kruskal-Wallis test ($p < 0.001$). Compared to the mutant group that has median (IQR) of plasma concentration ratio of maraviroc to M1 at 41.6(36.4-64.9), the homozygous wild type group and the heterozygous group were 46% ($p = 0.001$) and 56% ($p < 0.001$) lower with median (IQR) at 22.6 (18.8-27.2) and 18.2(16.6-19.2), respectively, and the differences are both statistically significant (**Figure 5-6**). The homozygous wild type group and the heterozygous group were not statistically different from each other in plasma concentration ratio of maraviroc to M1 ($p = 0.13$). The effect of CYP3A5 genotype on the plasma concentration ratios of maraviroc to M1 had a similar pattern through all the times that samples were collected. It would be advantageous to use a single-point blood sample to assess CYP3A5 activity on maraviroc as a phenotyping probe.

Table 5-4. Demographic information of healthy volunteers.

Group[*]	No CYP3A5*1 (N=8)	One CYP3A5*1 (N=8)	Two CYP3A5*1 (N=8)
Age[#] (year)	45.1 ± 12.7	39.4 ± 11.7	38.0 ± 8.8
Weight[#] (Kg)	84.0 ± 15.6	76.7 ± 14.9	73.8 ± 14.5
BMI[†#] (Kg/m^2)	26.4 ± 4.5	24.9 ± 3.6	23.8 ± 3.6
CrCL[‡#] (mL/min)	114.3 ± 28.8	103.2 ± 15.2	100.1 ± 30.2
Total Protein[#] (g/dL)	7.0 ± 0.4	7.5 ± 0.4	7.1 ± 0.3
Albumin[#] (g/dL)	4.6 ± 0.3	4.6 ± 0.1	4.5 ± 0.3
Bilirubin[#] (mg/dL)	0.5 ± 0.2	0.4 ± 0.3	0.5 ± 0.2
ALP[#] (IU/L)	73.3 ± 16.7	74.9 ± 17.0	54.9 ± 14.3
ALT[‡#] (IU/L)	17.5 ± 4.5	18.5 ± 6.8	13.9 ± 3.4
AST[#] (IU/L)	19.6 ± 2.9	22.4 ± 4.9	20.0 ± 2.9
No. of Female/male	2/6	1/7	3/5

Abbreviations: BMI, body mass index; CrCL, creatinine clearance; ALP, alkaline phosphatase; ALT, alanine transaminase; AST, aspartate transaminase.

[#]Data are shown as mean ± SD.

[*]Three groups of people based on CYP3A5 genotype: mutant (no CYP3A5*1 allele), heterozygous (one CYP3A5*1 allele and one mutant allele), and homozygous wild type (two CYP3A5*1 alleles).

[†] Calculated as weight/(height × height).

[‡]Calculated as [(140-age(year)) × weight (kg)]/[72 × serum creatinine concentration (mg/dL)] (multiply by 0.85 for female).

Figure 5-1. The CYP3A5 homozygous wild type group has reduced plasma maraviroc concentrations. Mean (± SE) plasma concentrations of maraviroc after administration of a single dose of 300 mg maraviroc. Maraviroc concentrations are in linear-scale in (A) and log-scale in (B), respectively. N = 8 in each of the following groups: the mutant group who do not have CYP3A5*1 allele (blue line with diamonds), the heterozygous group who has one CYP3A5*1 allele and one nonfunctional allele (red line with squares), and the homozygous wild type group who have two CYP3A5*1 alleles (green line with triangles).

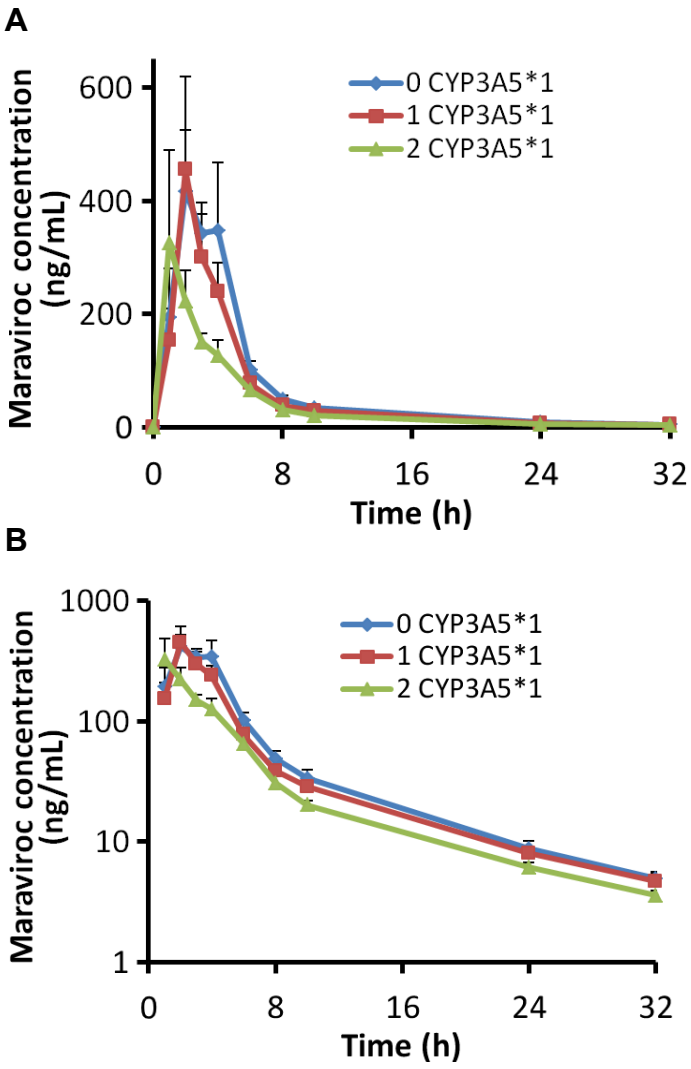

Table 5-5. Pharmacokinetic parameters (medians [interquartile range]) of maraviroc and metabolite M1.

Group*	No CYP3A5*1 (N=8)	One CYP3A5*1 (N=8)	Two CYP3A5*1 (N=8)
Maraviroc			
C_{max} (ng/mL)	505(348-959.25)	435(209.75-889)	339.5(237-551.5)
T_{max} (h)	2.5(2.0-3.8)	2.0(1.2-3.0)	2.0(1.0-3.5)
AUC_{0-32} (ng·h/mL)	2056(1454-2416)	1718(1200-2513)	1180(1038-1350)
AUC_{0-inf} (ng·h/mL)	2099(1422-2568)	1761(931-2640)	1238(1065-1407)
% extrapolated AUC	2.4(2.1-2.8)	2.5(2.3-4.3)	3.6(2.6-4.4)
$T_{1/2}$ (h)	7.6(7.1-8.7)	7.4(6.5-10.8)	8.7(8.0-9.7)
CL/F (L/h)	146(117-212)	173(114-343)	243(213-282)
V/F (L)	1757(1345-2235)	1697(1197-5234)	3126(2513-3711)
M1			
C_{max} (ng/mL)	10.1(6.5-18.5)	20.7(7.6-30.1)	15.9(15.2-18.9)
T_{max} (h)	3.0(2.3-3.8)	2.0(1.3-3.0)	2.0(1.0-2.0)
AUC_{0-32} (ng·h/mL)	40.4(36.0-48.2)	90.1(49.2-117.9)	61.0(56.2-70.6)
AUC_{0-inf} (ng·h/mL)	41.1(32.2-53.1)	91.9(38.7-133.8)	64.5(57.4-82.9)
% extrapolated AUC	2.4(1.3-5.9)	5.0(3.5-9.2)	4.2(2.6-6.6)
AUC_{0-32} ratio (marviroc/M1)	49.2(35.6-63.1)	24.2(20.2-26. 3)	17.9(15.8-23.4)
AUC_{0-inf} ratio $(marviroc/M1)_1$	49.5(35.3-64.4)	24.0(19.8-25.7)	17.8(15.7-22.5)

*Three groups of people based on CYP3A5 genotype: mutant (no CYP3A5*1 allele), heterozygous (one CYP3A5*1 allele and one mutant allele), and homozygous wild type (two CYP3A5*1alleles).

Figure 5-2. The CYP3A5 homozygous wild type group has increased maraviroc clearance and decreased exposure ($AUC_{0\text{-}inf}$). (**A**) Maraviroc $AUC_{0\text{-}inf}$. (**B**) Maraviroc oral apparent clearance (CL/F). N = 8 for each of the three groups.

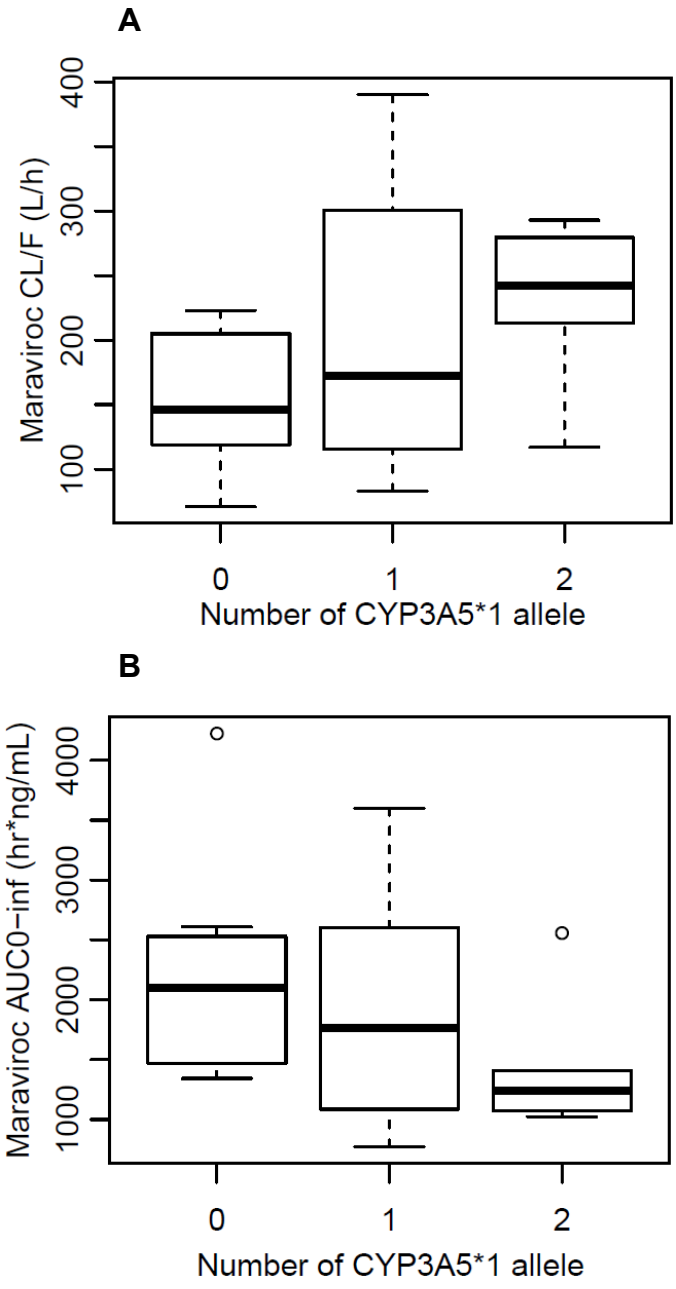

Figure 5-3. The CYP3A5 mutant group has reduced plasma M1 concentrations. Mean (± SE) plasma concentrations of M1 after administration of a single dose of 300 mg maraviroc. Metabolite M1 concentrations are in linear-scale in (A) and log-scale in (B), respectively. N = 8 in each of the following groups: the mutant group who do not have CYP3A5*1 allele (blue line with diamonds), the heterozygous group who has one CYP3A5*1 allele and one nonfunctional allele (red line with squares), and the homozygous wild type group who have two CYP3A5*1 alleles (green line with triangles).

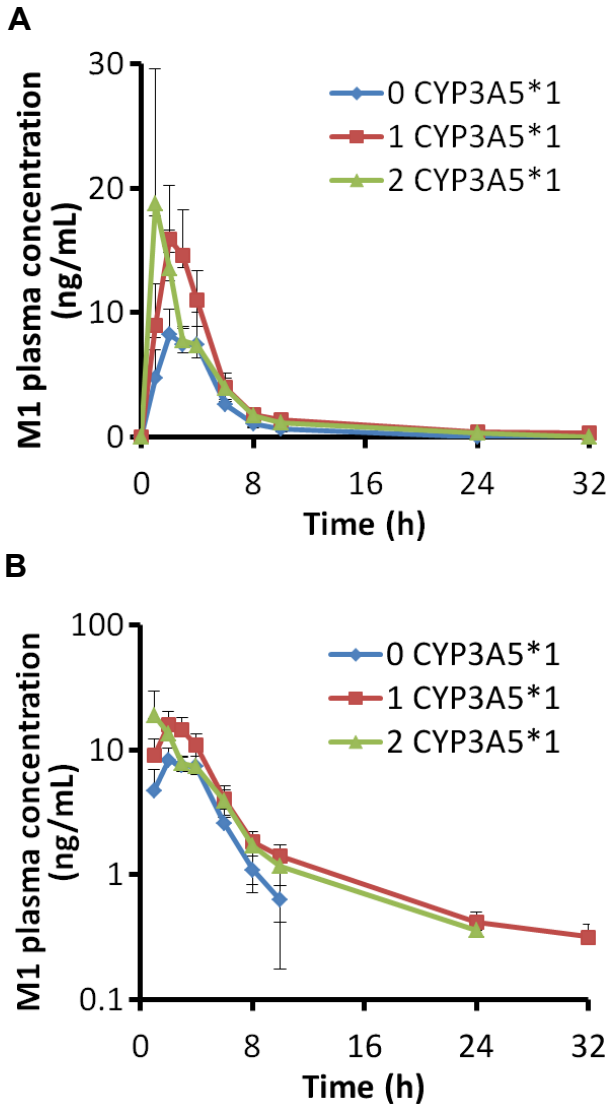

Figure 5-4. Carrying CYP3A5*1 allele caused reduction of area under the plasma concentration-time curve ratio of maraviroc to metabolite M1 ($AUC_{maraviroc}/AUC_{M1}$). Statistical test was performed using Wilcoxon rank sum test in R. Bonferroni post hoc test significance level $p < 0.017$.

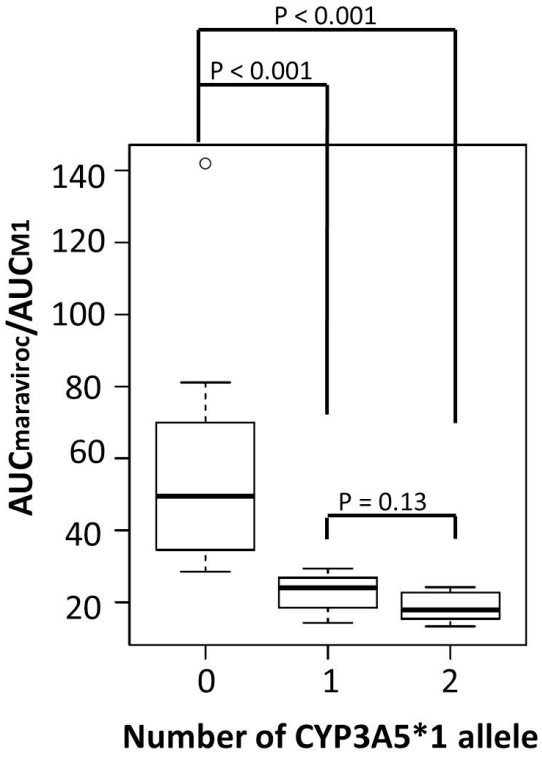

Figure 5-5. Correlations between $AUC_{0\text{-}inf}$ ratios to plasma concentration ratios of maraviroc to metabolite M1 at 4 h after the maraviroc dose. Observed values (black dots) are presented with fitted linear regression line (the middle thick red line), 95% confidence interval (next outer curved lines) and the prediction band (broken line). Filled, circles, opened circles, and filled triangles represent data from people with 0, 1, and 2 CYP3A5*1 allele, respectively. A data point (x = 310, y = 142) was determined to be an extreme value for data at both axes and thus excluded for the regression (R^2=0.87 when included). The excluded data point was from an individual who was determined to have two non-functional alleles (*3/*3) and had the lowest M1 $AUC_{0\text{-}inf}$ and the highest $AUC_{0\text{-}inf}$ ratio of maraviroc to M1, indicating that this individual had the lowest CYP3A5 activity compared with other subjects.

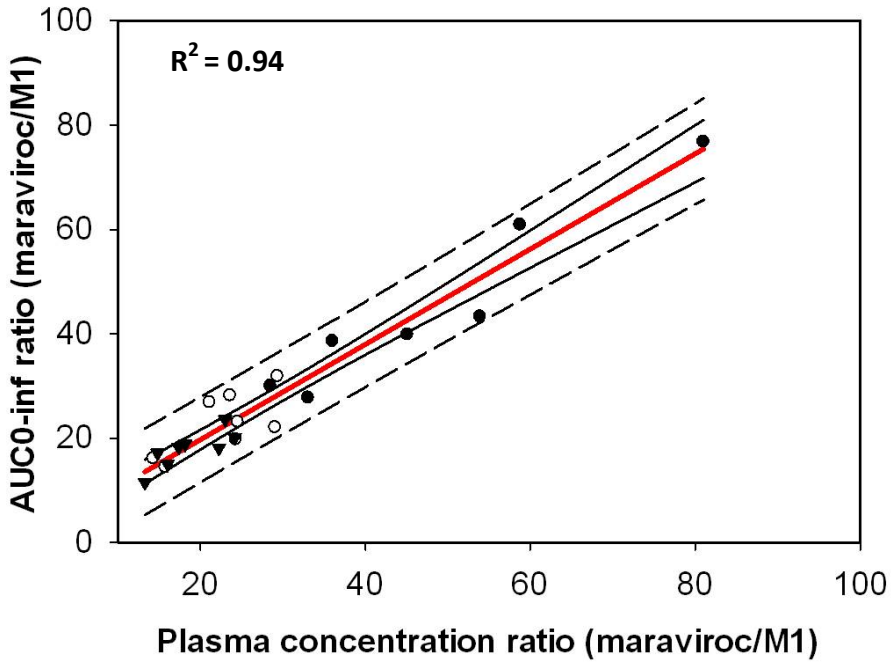

Figure 5-6. CYP3A5 genotype effect on plasma concentration ratios of maraviroc to M1 at 4 h. Individual data are shown with box-plot on the right for each group. Median values are shown as horizontal lines inside the boxes.

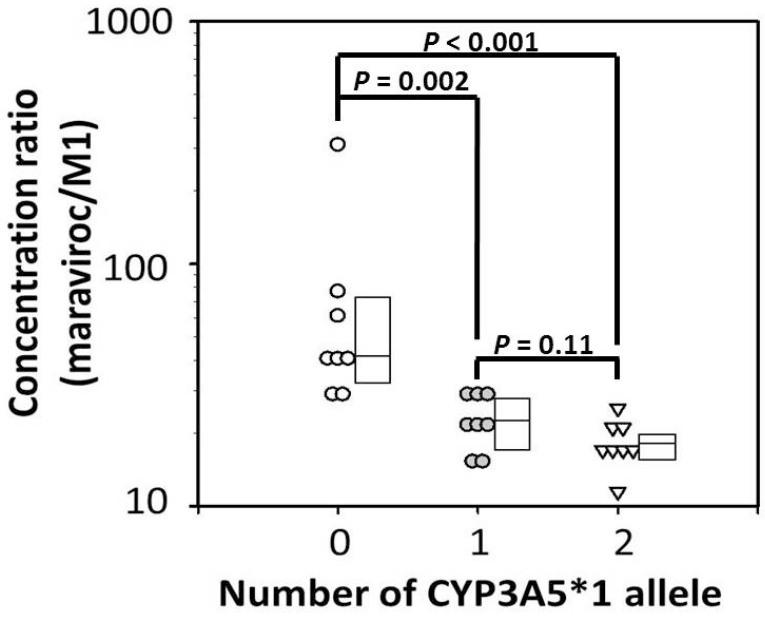

Discussion

The purpose of the investigation in this chapter was to extend our *in vitro* CYP3A5 studies to this clinical study to further evaluate the impact of CYP3A5 genotype on the pharmacokinetics of maraviroc and a major oxidative metabolite M1. The results show that maraviroc $AUC_{0\text{-inf}}$ in the CYP3A5*1 homozygous group decreased almost by half and oral apparent clearance increased significantly as compared to the subjects that do not carry the CYP3A5*1 allele; however, half-lives were similar between the two groups. The pharmacokinetic parameters of maraviroc in the mutant and heterozygous groups are similar to those reported values of previous studies in which CYP3A5 genotype was not characterized[155,156]. We observed large variability in maraviroc $AUC_{0\text{-inf}}$ in the heterozygous group, probably because when only one CYP3A5*1 is present, expression of CYP3A5 tends to be more easily influenced by other enzymes or transporters that play a role in absorption, disposition or elimination of maraviroc. CYP3A5 has been reported to be in linkage disequilibrium with CYP3A4 [157,158], the other important enzyme that is involved in maraviroc metabolism. Polymorphisms of CYP3A4 may also contribute to the pharmacokinetic variations of maraviroc. Epigenetic modifications are another potential reason for the variation of CYP3A4/5 expression although only a few studies have explored the mechanism in this field for CYP3A[159-164]. Besides CYP3A4 and CYP3A5, maraviroc is a substrate for P-glycoprotein (P-gp; also known as MDR1)[165], a drug efflux pump located on intestinal epithelial cells which limits drug absorption, and organic anion transporting polypeptide 1B1 (OATP1B1), an influx transporter located on the basolateral membrane of hepatocytes mediating hepatic uptake of drugs. Their polymorphism-dependent expression has been reported to affect maraviroc plasma

concentrations[165-169]. The polymorphisms in these genes may contribute to the large variability. We will be examining the polymorphisms in these genes for our next step.

The reduction of maraviroc exposure in the CYP3A5 wild type group supports our hypothesis that CYP3A5 genotype affects maraviroc pharmacokinetics. Our *in vitro* metabolism study suggested that CYP3A5 plays a major role in maraviroc oxidation[170]. Furthermore, in people who are CYP3A5 expressors, CYP3A5 represents at least half of CYP3A content in the jejunum and liver[15], where metabolism occurs for orally administered drugs before entering systemic blood circulation. Therefore, the reduced maraviroc exposure we observed here in the CYP3A5 homozygous wild type group may be, or at least partially, due to reduced bioavailability caused by enhanced biotransformation from maraviroc to oxidative metabolites mediated by CYP3A5. The reduced maraviroc exposure is an impactful finding since more than 60% of African Americans are CYP3A5 expressors while current dosing recommendations were derived in a predominantly white population[171]. In combination with the fact that African Americans are disproportionately infected with HIV and at greater risk of acquiring HIV infection[172], this finding may have implications for HIV treatment regimens and development of oral maraviroc for HIV prevention. When co-administered with strong CYP3A inducers like rifampin and efavirenz, maraviroc doses are recommended to be doubled to compensate the half-reduction in maraviroc AUC[173,174]. Because the CYP3A5 genotype results in a similar magnitude of change, a doubling of the maraviroc dose in individuals with CYP3A5*1/*1 genotype would be warranted.

In the previous chapter, we have demonstrated *in vitro* that using formation of one of the major monooxygenated metabolite M1 can be used to assess CYP3A5 activity. Since

maraviroc is an FDA-approved drug and has an excellent safety profile, maraviroc has great potential to assess CYP3A5 *in vivo* activity. Therefore, in this study, we also aimed to explore this utility of maraviroc in a clinical setting. In concordance with our hypothesis, we did find that people who carry CYP3A5*1 alleles had higher M1 $AUC_{0\text{-}inf}$ and C_{max} compared to those who do not carry CYP3A5*1 alleles. The status of CYP3A5 genotype status was well predicted by the $AUC_{0\text{-}inf}$ ratio of maraviroc to metabolite M1 with more than 2 times bigger in people who do not carry CYP3A5*1 allele compared with those who carry CYP3A5*1 allele. Plasma concentration ratios of maraviroc to M1 and the $AUC_{0\text{-}inf}$ ratios showed the strongest correlations at 4 h post maraviroc administration, indicating that single-point blood collections and plasma concentration measurement of maraviroc and M1 may be suitable to assess CYP3A5 activity to substitute intensive samplings for capture of the whole plasma concentration-time curve. This would add great value to the applicability of using maraviroc as a CYP3A5 phenotyping tool. Furthermore, maraviroc does not modulate other CYP enzymes at the range of therapeutic concentrations[124], it has the potential to be added to currently available phenotyping cocktails for other CYP enzymes.

This investigation involved a small number of subjects in each of the three CYP3A5 genotypic groups (N = 8). The results and optimal sampling times merit confirmation by studies with larger sample size. Future directions will include evaluation on changes of metabolic ratios of maraviroc to M1 in the presence of inducers and inhibitors that are ideally selective to CYP3A5 to confirm the utility of maraviroc to assess CYP3A5 *in vivo* activity.

In conclusion, despite the small size of the study groups, we observed a reduction of maraviroc $AUC_{0\text{-}inf}$ nearly by half and 66% higher maraviroc oral clearance in group of people who carry two wild type CYP3A5*1 allele compared to those who do not have CYP3A5*1 allele. Maraviroc to metabolite $AUC_{0\text{-}inf}$ ratios were more than 2 times higher in people who do not have CYP3A5*1 alleles relative to those who carry at least one CYP3A5*1 allele, indicating maraviroc has the potential to be used as a clinical phenotyping probe for CYP3A5. Moreover, measurement of plasma concentration ratio of maraviroc and metabolite M1 at 4 h following a single 300 mg oral dose of maraviroc could represent a useful surrogate measure for $AUC_{0\text{-}inf}$ ratio of maraviroc to M1 and an accurate indirect marker of the CYP3A5 phenotype in healthy volunteers. The clinical utility of using maraviroc as a CYP3A5 phenotyping probe drug, as supported by this study could be helpful for predicting drug-drug interactions and identifying individuals with various CYP3A5 enzymatic activities in order to prevent drug toxicity or treatment failure.

Chapter 6 – Conclusions

This thesis demonstrates pharmacokinetic variations of drugs related to three of the world's most devastating disease, HIV infection, tuberculosis, and malaria. We characterized drug-drug pharmacokinetic interactions mediated by the most important drug metabolizing enzymes CYP3A4/5 and identified the anti-HIV drug maraviroc as a phenotyping probe both *in vitro* and *in vivo* to assess the highly variable isoenzyme CYP3A5 caused by genetic polymorphisms.

In Chapter 2, we performed a dose escalation study for anti-tuberculosis drug rifapentine to evaluate its pharmacokinetics with new daily dosing regimens in healthy volunteers and found rifapentine had a less than dose-proportional increase in both AUC and C_{max} as dose increased. We used a chemical analogue that is also known as a CYP3A inducer, rifampin, as a comparator drug to study the effect on a CYP3A4/5 substrate drug, midazolam, and found that rifapentine strongly induced CYP3A4/5 enzyme in a dose-independent manner at a degree that was stronger than the induction caused by rifampin.

In chapter 3, we conducted a drug-drug interaction study to assess long-term use of a CYP3A4/5 inhibitor, ritonavir, containing anti-HIV drugs lopinavir/ritonavir (or LPV/r) on CYP3A substrate quinine, a drug used for treatment of malaria with a low therapeutic window. In the presence of steady-state LPV/r, we found significant decrease in the exposure (C_{max} and AUC) of quinine and its major active metabolite 3-hydroxyquinine (both total and protein bound free) as well as the metabolite to parent drug AUC ratio compared with those when quinine was administered alone.

The CYP3A substrate drugs as described above, midazolam and quinine, are metabolized by both CYP3A4 and CYP3A5. Therefore, the individual contributions of CYP3A4 and CYP3A5 cannot be differentiated due to the high similarity between the two enzymes. Since CYP3A5 expression exhibits high variability due to genetic polymorphisms, discovery of a CYP3A5 selective substrate will be helpful in assessment of CYP3A5 contribution in drug-drug interaction studies and identification of CYP3A5 substrates, inducers and inhibitors.

In chapter 4, through a comprehensive analysis of metabolism for the anti-HIV drug maraviroc, we determined that CYP3A5 was the principal enzyme responsible for the formation of an abundant metabolite of maraviroc, named M1, resulting from oxygenation of the dichlorocyclohexane ring. CYP3A5 has 23 times higher enzyme capacity for M1 formation compared with CYP3A4. We then confirmed the role of CYP3A5 in M1 formation by using human liver microsomes isolated from CYP3A5-genotyped donors. By exchanging divergent residues between CYP3A4 and CYP3A5 using site-directed mutagenesis followed by metabolic activity measurement of the mutated enzymes, we discovered an amino acid residue 57 that may play a role in the differential activities of these enzymes towards maraviroc biotransformation. From this study, we identified the anti-HIV drug maraviroc as a candidate for development as a CYP3A5 phenotyping probe and provided novel mechanistic insight into the role of divergent amino acids of CYP3A4 and CYP3A5 in influencing their catalytic activities. The favorable safety profile of maraviroc renders this drug an attractive candidate for future development as a clinical CYP3A5 phenotyping probe.

In Chapter 5, we conducted a clinical study in CYP3A5-genotyped healthy volunteers to further investigate the clinical value of maraviroc in assessing CYP3A5 activity by evaluating the influence of CYP3A5 genotype on pharmacokinetics of maraviroc and the metabolite M1 primarily formed by CYP3A5. Following a single oral dose of maraviroc, subjects in the homozygous wild type group had 41% lower maraviroc AUC, 66% higher maraviroc oral clearance, and 57% higher M1 AUC compared with the mutant group. The AUC ratio of maraviroc to M1 in mutant group doubled when compared to heterozygous and homozygous wild type groups, confirming the value of maraviroc as a substrate drug to assess CYP3A5 activity in a clinical setting. In addition, plasma concentration ratio of maraviroc to M1 correlated highly with the AUC ratio at 4 h after dose administration, suggesting that sing-point blood collection may be used for CYP3A5 activity measurement.

In summary, this thesis has identified pharmacokinetic variations of anti-infective agents, their effect on pharmacokinetics of CYP3A substrate drugs, and discovered the anti-HIV drug maraviroc as a phenotyping probe to assess the highly variable enzyme CYP3A5 both *in vitro* and *in vivo*. The results from this thesis will be helpful to inform dosing regimen selection to achieve treatment success while minimizing drug-related toxicity. Our discovery of maraviroc as a CYP3A5 probe will have a broad application from bench to bedside to identify CYP3A5 substrates, inducers, and inhibitors, which will help to increase efficiency of drug discovery/development and reduce the risk of developing side effects and the loss of drug efficacy among patients with some genotypes.

References

1. Klingenberg, M. Pigments of rat liver microsomes. *Archives of biochemistry and biophysics* **75**, 376-386 (1958).
2. Danielson, P.B. The cytochrome P450 superfamily: biochemistry, evolution and drug metabolism in humans. *Current drug metabolism* **3**, 561-597 (2002).
3. Anttila, S.*, et al.* Expression and localization of CYP3A4 and CYP3A5 in human lung. *Am J Respir Cell Mol Biol* **16**, 242-249 (1997).
4. Koch, I.*, et al.* Interindividual variability and tissue-specificity in the expression of cytochrome P450 3A mRNA. *Drug Metab Dispos* **30**, 1108-1114 (2002).
5. Estabrook, R.W. The remarkable P450s: a historical overview of these versatile hemeprotein catalysts. *FASEB journal : official publication of the Federation of American Societies for Experimental Biology* **10**, 202-204 (1996).
6. Nelson, D.R.*, et al.* P450 superfamily: update on new sequences, gene mapping, accession numbers and nomenclature. *Pharmacogenetics* **6**, 1-42 (1996).
7. Zanger, U.M. & Schwab, M. Cytochrome P450 enzymes in drug metabolism: regulation of gene expression, enzyme activities, and impact of genetic variation. *Pharmacology & therapeutics* **138**, 103-141 (2013).
8. Wrighton, S.A.*, et al.* The human CYP3A subfamily: practical considerations. *Drug Metab Rev* **32**, 339-361 (2000).
9. Pearson, J.T.*, et al.* Differential time-dependent inactivation of P450 3A4 and P450 3A5 by raloxifene: a key role for C239 in quenching reactive intermediates. *Chemical research in toxicology* **20**, 1778-1786 (2007).

10. Iyer, S.V., Lependu, P., Harpaz, R., Bauer-Mehren, A. & Shah, N.H. Learning signals of adverse drug-drug interactions from the unstructured text of electronic health records. *AMIA Summits on Translational Science proceedings AMIA Summit on Translational Science* **2013**, 83-87 (2013).

11. Lazarou, J., Pomeranz, B.H. & Corey, P.N. Incidence of adverse drug reactions in hospitalized patients: a meta-analysis of prospective studies. *JAMA : the journal of the American Medical Association* **279**, 1200-1205 (1998).

12. Liangpunsakul, S.*, et al.* Activity of CYP2E1 and CYP3A enzymes in adults with moderate alcohol consumption: a comparison with nonalcoholics. *Hepatology* **41**, 1144-1150 (2005).

13. Huang, S.M. & Lesko, L.J. Drug-drug, drug-dietary supplement, and drug-citrus fruit and other food interactions: what have we learned? *Journal of clinical pharmacology* **44**, 559-569 (2004).

14. Lin, Y.S.*, et al.* Co-regulation of CYP3A4 and CYP3A5 and contribution to hepatic and intestinal midazolam metabolism. *Molecular pharmacology* **62**, 162-172 (2002).

15. Kuehl, P.*, et al.* Sequence diversity in CYP3A promoters and characterization of the genetic basis of polymorphic CYP3A5 expression. *Nature genetics* **27**, 383-391 (2001).

16. Hustert, E.*, et al.* The genetic determinants of the CYP3A5 polymorphism. *Pharmacogenetics* **11**, 773-779 (2001).

17. Lamba, J.K., Lin, Y.S., Schuetz, E.G. & Thummel, K.E. Genetic contribution to variable human CYP3A-mediated metabolism. *Advanced drug delivery reviews* **54**, 1271-1294 (2002).

18. van Schaik, R.H., van der Heiden, I.P., van den Anker, J.N. & Lindemans, J. CYP3A5 variant allele frequencies in Dutch Caucasians. *Clin Chem* **48**, 1668-1671 (2002).

19. Kuehl, P.*, et al.* Sequence diversity in CYP3A promoters and characterization of the genetic basis of polymorphic CYP3A5 expression. *Nat Genet* **27**, 383-391 (2001).

20. Daly, A.K. Significance of the minor cytochrome P450 3A isoforms. *Clin Pharmacokinet* **45**, 13-31 (2006).

21. Lalovic, B., Phillips, B., Risler, L.L., Howald, W. & Shen, D.D. Quantitative contribution of CYP2D6 and CYP3A to oxycodone metabolism in human liver and intestinal microsomes. *Drug Metab Dispos* **32**, 447-454 (2004).

22. Xie, H.G., Wood, A.J., Kim, R.B., Stein, C.M. & Wilkinson, G.R. Genetic variability in CYP3A5 and its possible consequences. *Pharmacogenomics* **5**, 243-272 (2004).

23. Egbelakin, A.*, et al.* Increased risk of vincristine neurotoxicity associated with low CYP3A5 expression genotype in children with acute lymphoblastic leukemia. *Pediatric blood & cancer* **56**, 361-367 (2011).

24. Hooper, D.K.*, et al.* Risk of tacrolimus toxicity in CYP3A5 Nonexpressors treated with intravenous nicardipine after kidney transplantation. *Transplantation* **93**, 806-812 (2012).

25. Egbelakin, A.*, et al.* Increased risk of vincristine neurotoxicity associated with low CYP3A5 expression genotype in children with acute lymphoblastic leukemia. *Pediatr Blood Cancer* **56**, 361-367 (2011).

26. Takashina, Y.*, et al.* Impact of CYP3A5 and ABCB1 Gene Polymorphisms on Fentanyl Pharmacokinetics and Clinical Responses in Cancer Patients Undergoing Conversion to a Transdermal System. *Drug Metab Pharmacokinet* (2012).

27. Zaman, K. Tuberculosis: a global health problem. *Journal of health, population, and nutrition* **28**, 111-113 (2010).

28. Organization, W.H. Global Tuberculosis Control: WHO report 2010. (WHO Press; Geneva, Switzerland, 2010).

29. Rosenthal, I.M.*, et al.* Daily dosing of rifapentine cures tuberculosis in three months or less in the murine model. *PLoS medicine* **4**, e344 (2007).

30. Rosenthal, I.M., Zhang, M., Almeida, D., Grosset, J.H. & Nuermberger, E.L. Isoniazid or moxifloxacin in rifapentine-based regimens for experimental tuberculosis? *American journal of respiratory and critical care medicine* **178**, 989-993 (2008).

31. Zhang, M.*, et al.* Treatment of tuberculosis with rifamycin-containing regimens in immune-deficient mice. *American journal of respiratory and critical care medicine* **183**, 1254-1261 (2011).

32. Vernon, A., Burman, W., Benator, D., Khan, A. & Bozeman, L. Acquired rifamycin monoresistance in patients with HIV-related tuberculosis treated with once-weekly rifapentine and isoniazid. Tuberculosis Trials Consortium. *Lancet* **353**, 1843-1847 (1999).

33. Benator, D.*, et al.* Rifapentine and isoniazid once a week versus rifampicin and isoniazid twice a week for treatment of drug-susceptible pulmonary tuberculosis in HIV-negative patients: a randomised clinical trial. *Lancet* **360**, 528-534 (2002).

34. Roussel, H.M. Rifapentine. 21-24 (Center for Drug Evaluation and Research, FDA, New Drug Application, 1998).

35. Vital Durand, D., Hampden, C., Boobis, A.R., Park, B.K. & Davies, D.S. Induction of mixed function oxidase activity in man by rifapentine (MDL 473), a long-acting rifamycin derivative. *British journal of clinical pharmacology* **21**, 1-7 (1986).

36. Li, A.P.*, et al.* Primary human hepatocytes as a tool for the evaluation of structure-activity relationship in cytochrome P450 induction potential of xenobiotics: evaluation of rifampin, rifapentine and rifabutin. *Chemico-biological interactions* **107**, 17-30 (1997).

37. Dooley, K.*, et al.* Repeated administration of high-dose intermittent rifapentine reduces rifapentine and moxifloxacin plasma concentrations. *Antimicrobial agents and chemotherapy* **52**, 4037-4042 (2008).

38. Rosenthal, I.M.*, et al.* Potent twice-weekly rifapentine-containing regimens in murine tuberculosis. *American journal of respiratory and critical care medicine* **174**, 94-101 (2006).

39. Dumond, J.B.*, et al.* A phenotype-genotype approach to predicting CYP450 and P-glycoprotein drug interactions with the mixed inhibitor/inducer tipranavir/ritonavir. *Clinical pharmacology and therapeutics* **87**, 735-742 (2010).

40. Administration, F.a.D. Guidance for Industry: Bioanalytical Method Validation. (ed. US Department of Health and Human Services, F., Center for Drug Evaluation and Research.) (Rockville, MD, USA, 2001).

41. Weiner, M.*, et al.* Effects of tuberculosis, race, and human gene SLCO1B1 polymorphisms on rifampin concentrations. *Antimicrobial agents and chemotherapy* **54**, 4192-4200 (2010).

42. Burman, W.*, et al.* Acquired rifamycin resistance with twice-weekly treatment of HIV-related tuberculosis. *American journal of respiratory and critical care medicine* **173**, 350-356 (2006).

43. Weiner, M.*, et al.* Association between acquired rifamycin resistance and the pharmacokinetics of rifabutin and isoniazid among patients with HIV and tuberculosis. *Clinical infectious diseases : an official publication of the Infectious Diseases Society of America* **40**, 1481-1491 (2005).

44. Nuermberger E, R.I., Zhang M, Grosset J. Is it possible to cure TB in weeks instead of months? *Int J Tuberc Lung Dis.*, S167 (2007).

45. Gumbo, T.*, et al.* Concentration-dependent Mycobacterium tuberculosis killing and prevention of resistance by rifampin. *Antimicrobial agents and chemotherapy* **51**, 3781-3788 (2007).

46. Acocella, G. Clinical pharmacokinetics of rifampicin. *Clinical pharmacokinetics* **3**, 108-127 (1978).

47. Langdon, G.*, et al.* Population pharmacokinetics of rifapentine and its primary desacetyl metabolite in South African tuberculosis patients. *Antimicrobial agents and chemotherapy* **49**, 4429-4436 (2005).

48. Loos, U., Musch, E., Jensen, J.C., Schwabe, H.K. & Eichelbaum, M. Influence of the enzyme induction by rifampicin on its presystemic metabolism. *Pharmacology & therapeutics* **33**, 201-204 (1987).

49. Loos, U.*, et al.* Pharmacokinetics of oral and intravenous rifampicin during chronic administration. *Klinische Wochenschrift* **63**, 1205-1211 (1985).

50. Chen, J. & Raymond, K. Roles of rifampicin in drug-drug interactions: underlying molecular mechanisms involving the nuclear pregnane X receptor. *Annals of clinical microbiology and antimicrobials* **5**, 3 (2006).

51. Martin, P., Riley, R., Back, D.J. & Owen, A. Comparison of the induction profile for drug disposition proteins by typical nuclear receptor activators in human hepatic and intestinal cells. *British journal of pharmacology* **153**, 805-819 (2008).

52. Xu, C., Wang, X. & Staudinger, J.L. Regulation of tissue-specific carboxylesterase expression by pregnane x receptor and constitutive androstane receptor. *Drug metabolism and disposition: the biological fate of chemicals* **37**, 1539-1547 (2009).

53. Acocella, G., Mattiussi, R. & Segre, G. Multicompartmental analysis of serum, urine and bile concentrations of rifampicin and desacetyl-rifampicin in subjects treated for one week. *Pharmacological research communications* **10**, 271-288 (1978).

54. Watkins, P.B. Noninvasive tests of CYP3A enzymes. *Pharmacogenetics* **4**, 171-184 (1994).

55. Tsunoda, S.M., Velez, R.L., von Moltke, L.L. & Greenblatt, D.J. Differentiation of intestinal and hepatic cytochrome P450 3A activity with use of midazolam as

an in vivo probe: effect of ketoconazole. *Clinical pharmacology and therapeutics* **66**, 461-471 (1999).

56. Research, F.a.D.A.C.f.D.E.a. Guidance for Industry:Drug Interaction Studies-Study Design, Data Analysis, and Implications for Dosing and Labelling Recommendations. (ed. Services, U.D.o.H.a.H.) (2012).

57. Backman, J.T., Olkkola, K.T. & Neuvonen, P.J. Rifampin drastically reduces plasma concentrations and effects of oral midazolam. *Clinical pharmacology and therapeutics* **59**, 7-13 (1996).

58. Chung, E., Nafziger, A.N., Kazierad, D.J. & Bertino, J.S., Jr. Comparison of midazolam and simvastatin as cytochrome P450 3A probes. *Clinical pharmacology and therapeutics* **79**, 350-361 (2006).

59. Li, A.P. & Jurima-Romet, M. Applications of primary human hepatocytes in the evaluation of pharmacokinetic drug-drug interactions: evaluation of model drugs terfenadine and rifampin. *Cell biology and toxicology* **13**, 365-374 (1997).

60. Laufer, M.K. & Plowe, C.V. The Interaction between HIV and malaria in Africa. *Current infectious disease reports* **9**, 47-54 (2007).

61. German, P.*, et al.* Lopinavir/ritonavir affects pharmacokinetic exposure of artemether/lumefantrine in HIV-uninfected healthy volunteers. *J Acquir Immune Defic Syndr* **51**, 424-429 (2009).

62. Giao, P.T. & de Vries, P.J. Pharmacokinetic interactions of antimalarial agents. *Clinical pharmacokinetics* **40**, 343-373 (2001).

63. Soyinka, J.O*., et al.* Effects of concurrent administration of nevirapine on the disposition of quinine in healthy volunteers. *The Journal of pharmacy and pharmacology* **61**, 439-443 (2009).

64. Mirghani, R.A., Hellgren, U., Bertilsson, L., Gustafsson, L.L. & Ericsson, O. Metabolism and elimination of quinine in healthy volunteers. *European journal of clinical pharmacology* **59**, 423-427 (2003).

65. Pukrittayakamee, S*., et al.* A study of the factors affecting the metabolic clearance of quinine in malaria. *European journal of clinical pharmacology* **52**, 487-493 (1997).

66. Wanwimolruk, S., Wong, S.M., Zhang, H., Coville, P.F. & Walker, R.J. Metabolism of quinine in man: identification of a major metabolite, and effects of smoking and rifampicin pretreatment. *The Journal of pharmacy and pharmacology* **47**, 957-963 (1995).

67. Mukonzo, J.K., Waako, P., Ogwal-Okeng, J., Gustafsson, L.L. & Aklillu, E. Genetic variations in ABCB1 and CYP3A5 as well as sex influence quinine disposition among Ugandans. *Therapeutic drug monitoring* **32**, 346-352 (2010).

68. Pussard, E., Merzouk, M. & Barennes, H. Increased uptake of quinine into the brain by inhibition of P-glycoprotein. *European journal of pharmaceutical sciences : official journal of the European Federation for Pharmaceutical Sciences* **32**, 123-127 (2007).

69. Silamut, K., Molunto, P., Ho, M., Davis, T.M. & White, N.J. Alpha 1-acid glycoprotein (orosomucoid) and plasma protein binding of quinine in falciparum malaria. *British journal of clinical pharmacology* **32**, 311-315 (1991).

70. Oie, S., Jacobson, M.A. & Abrams, D.I. Alpha 1-acid glycoprotein levels in AIDS patients before and after short-term treatment with zidovudine (ZDV). *J Acquir Immune Defic Syndr* **6**, 531-533 (1993).

71. Graninger, W., Thalhammer, F., Hollenstein, U., Zotter, G.M. & Kremsner, P.G. Serum protein concentrations in Plasmodium falciparum malaria. *Acta tropica* **52**, 121-128 (1992).

72. Schon, A., del Mar Ingaramo, M. & Freire, E. The binding of HIV-1 protease inhibitors to human serum proteins. *Biophysical chemistry* **105**, 221-230 (2003).

73. Granfors, M.T.*, et al.* Differential inhibition of cytochrome P450 3A4, 3A5 and 3A7 by five human immunodeficiency virus (HIV) protease inhibitors in vitro. *Basic & clinical pharmacology & toxicology* **98**, 79-85 (2006).

74. Koudriakova, T.*, et al.* Metabolism of the human immunodeficiency virus protease inhibitors indinavir and ritonavir by human intestinal microsomes and expressed cytochrome P4503A4/3A5: mechanism-based inactivation of cytochrome P4503A by ritonavir. *Drug metabolism and disposition: the biological fate of chemicals* **26**, 552-561 (1998).

75. Foisy, M.M., Yakiwchuk, E.M. & Hughes, C.A. Induction effects of ritonavir: implications for drug interactions. *The Annals of pharmacotherapy* **42**, 1048-1059 (2008).

76. Ding, R.*, et al.* Substantial pharmacokinetic interaction between digoxin and ritonavir in healthy volunteers. *Clinical pharmacology and therapeutics* **76**, 73-84 (2004).

77. Perloff, M.D., Von Moltke, L.L., Marchand, J.E. & Greenblatt, D.J. Ritonavir induces P-glycoprotein expression, multidrug resistance-associated protein (MRP1) expression, and drug transporter-mediated activity in a human intestinal cell line. *Journal of pharmaceutical sciences* **90**, 1829-1837 (2001).

78. Soyinka, J.O*., et al.* Pharmacokinetic interactions between ritonavir and quinine in healthy volunteers following concurrent administration. *British journal of clinical pharmacology* **69**, 262-270 (2010).

79. Edstein, M.D., Prasitthipayong, A., Sabchareon, A., Chongsuphajaisiddhi, T. & Webster, H.K. Simultaneous measurement of quinine and quinidine in human plasma, whole blood, and erythrocytes by high-performance liquid chromatography with fluorescence detection. *Therapeutic drug monitoring* **12**, 493-500 (1990).

80. Orlando, R., De Martin, S., Pegoraro, P., Quintieri, L. & Palatini, P. Irreversible CYP3A inhibition accompanied by plasma protein-binding displacement: a comparative analysis in subjects with normal and impaired liver function. *Clinical pharmacology and therapeutics* **85**, 319-326 (2009).

81. Nettles, R.E*., et al.* Marked intraindividual variability in antiretroviral concentrations may limit the utility of therapeutic drug monitoring. *Clinical infectious diseases : an official publication of the Infectious Diseases Society of America* **42**, 1189-1196 (2006).

82. Diggle, P.L.K.Z., S. *Analysis of longitudinal data.*, (Oxford University Press, Oxford, UK, 2002).

83. Mirghani, R.A., *et al.* The roles of cytochrome P450 3A4 and 1A2 in the 3-hydroxylation of quinine in vivo. *Clinical pharmacology and therapeutics* **66**, 454-460 (1999).

84. Powell, R.D.a.M., J.V. . Quinine: Side-Effects and Plasma Levels. . *Proc. Helm. Soc. Wash.*, 331 (1972).

85. Krishna, S. & White, N.J. Pharmacokinetics of quinine, chloroquine and amodiaquine. Clinical implications. *Clinical pharmacokinetics* **30**, 263-299 (1996).

86. Dondorp, A.M., *et al.* Artemisinin resistance in Plasmodium falciparum malaria. *The New England journal of medicine* **361**, 455-467 (2009).

87. Oldfield, V. & Plosker, G.L. Lopinavir/ritonavir: a review of its use in the management of HIV infection. *Drugs* **66**, 1275-1299 (2006).

88. Lin, J.H. & Yamazaki, M. Role of P-glycoprotein in pharmacokinetics: clinical implications. *Clinical pharmacokinetics* **42**, 59-98 (2003).

89. Piscitelli, S.C. & Gallicano, K.D. Interactions among drugs for HIV and opportunistic infections. *The New England journal of medicine* **344**, 984-996 (2001).

90. Mansor, S.M., Ward, S.A., Edwards, G., Hoaksey, P.E. & Breckenridge, A.M. The influence of alpha 1-acid glycoprotein on quinine and quinidine disposition in the rat isolated perfused liver preparation. *The Journal of pharmacy and pharmacology* **43**, 650-654 (1991).

91. Taylor, W.R. & White, N.J. Antimalarial drug toxicity: a review. *Drug safety : an international journal of medical toxicology and drug experience* **27**, 25-61 (2004).

92. Administration., U.F.a.D. Kaletra™ (lopinavir/ritonavir). (2008).

93. Administration., U.F.a.D. Qualaquine (quinine sulfate). (2011).

94. Lefevre, G.*, et al.* Interaction trial between artemether-lumefantrine (Riamet) and quinine in healthy subjects. *Journal of clinical pharmacology* **42**, 1147-1158 (2002).

95. White, N.J., Chanthavanich, P., Krishna, S., Bunch, C. & Silamut, K. Quinine disposition kinetics. *British journal of clinical pharmacology* **16**, 399-403 (1983).

96. Na-Bangchang, K.*, et al.* Pharmacokinetic and pharmacodynamic interactions of mefloquine and quinine. *International journal of clinical pharmacology research* **19**, 73-82 (1999).

97. Supanaranond, W.*, et al.* Lack of a significant adverse cardiovascular effect of combined quinine and mefloquine therapy for uncomplicated malaria. *Transactions of the Royal Society of Tropical Medicine and Hygiene* **91**, 694-696 (1997).

98. Cubeddu, L.X. QT prolongation and fatal arrhythmias: a review of clinical implications and effects of drugs. *American journal of therapeutics* **10**, 452-457 (2003).

99. Drici, M.D. & Clement, N. Is gender a risk factor for adverse drug reactions? The example of drug-induced long QT syndrome. *Drug safety : an international journal of medical toxicology and drug experience* **24**, 575-585 (2001).

100. Makkar, R.R., Fromm, B.S., Steinman, R.T., Meissner, M.D. & Lehmann, M.H. Female gender as a risk factor for torsades de pointes associated with

cardiovascular drugs. *JAMA : the journal of the American Medical Association* **270**, 2590-2597 (1993).

101. Corbett, A.H., Lim, M.L. & Kashuba, A.D. Kaletra (lopinavir/ritonavir). *The Annals of pharmacotherapy* **36**, 1193-1203 (2002).

102. Chung, W.H.*, et al.* Medical genetics: a marker for Stevens-Johnson syndrome. *Nature* **428**, 486 (2004).

103. Hung, S.I.*, et al.* HLA-B*5801 allele as a genetic marker for severe cutaneous adverse reactions caused by allopurinol. *Proceedings of the National Academy of Sciences of the United States of America* **102**, 4134-4139 (2005).

104. Hsu, A., Granneman, G.R. & Bertz, R.J. Ritonavir. Clinical pharmacokinetics and interactions with other anti-HIV agents. *Clinical pharmacokinetics* **35**, 275-291 (1998).

105. Hsu, A.*, et al.* Pharmacokinetic-pharmacodynamic analysis of lopinavir-ritonavir in combination with efavirenz and two nucleoside reverse transcriptase inhibitors in extensively pretreated human immunodeficiency virus-infected patients. *Antimicrobial agents and chemotherapy* **47**, 350-359 (2003).

106. Ng, J.e.a. Pharmacokinetics of rifabutin 150 mg TIW plus lopinavir/ritonavir (LPV/r) 400/100 mg BID administered in healthy subjects. (10th International Workshop on Clinical Pharmacology of HIV Therapy. Amsterdam,Netherlands, 2009).

107. Boulanger, C.*, et al.* Pharmacokinetic evaluation of rifabutin in combination with lopinavir-ritonavir in patients with HIV infection and active tuberculosis. *Clinical*

infectious diseases : an official publication of the Infectious Diseases Society of America **49**, 1305-1311 (2009).

108. Fletcher, C.V. Drug interactions should be evaluated in patients. *Clinical pharmacology and therapeutics* **88**, 585-587 (2010).

109. Rendic, S. & Di Carlo, F.J. Human cytochrome P450 enzymes: a status report summarizing their reactions, substrates, inducers, and inhibitors. *Drug Metab Rev* **29**, 413-580 (1997).

110. Wang, H.*, et al.* Structure-function relationships of human liver cytochromes P450 3A: aflatoxin B1 metabolism as a probe. *Biochemistry* **37**, 12536-12545 (1998).

111. Roussel, F., Khan, K.K. & Halpert, J.R. The importance of SRS-1 residues in catalytic specificity of human cytochrome P450 3A4. *Archives of biochemistry and biophysics* **374**, 269-278 (2000).

112. Domanski, T.L., Liu, J., Harlow, G.R. & Halpert, J.R. Analysis of four residues within substrate recognition site 4 of human cytochrome P450 3A4: role in steroid hydroxylase activity and alpha-naphthoflavone stimulation. *Archives of biochemistry and biophysics* **350**, 223-232 (1998).

113. Khan, K.K., He, Y.Q., Domanski, T.L. & Halpert, J.R. Midazolam oxidation by cytochrome P450 3A4 and active-site mutants: an evaluation of multiple binding sites and of the metabolic pathway that leads to enzyme inactivation. *Molecular pharmacology* **61**, 495-506 (2002).

114. Khan, K.K. & Halpert, J.R. Structure-function analysis of human cytochrome P450 3A4 using 7-alkoxycoumarins as active-site probes. *Archives of biochemistry and biophysics* **373**, 335-345 (2000).

115. Harlow, G.R. & Halpert, J.R. Alanine-scanning mutagenesis of a putative substrate recognition site in human cytochrome P450 3A4. Role of residues 210 and 211 in flavonoid activation and substrate specificity. *The Journal of biological chemistry* **272**, 5396-5402 (1997).

116. He, Y.A., He, Y.Q., Szklarz, G.D. & Halpert, J.R. Identification of three key residues in substrate recognition site 5 of human cytochrome P450 3A4 by cassette and site-directed mutagenesis. *Biochemistry* **36**, 8831-8839 (1997).

117. Yano, J.K.*, et al.* The structure of human microsomal cytochrome P450 3A4 determined by X-ray crystallography to 2.05-A resolution. *The Journal of biological chemistry* **279**, 38091-38094 (2004).

118. Williams, P.A.*, et al.* Crystal structures of human cytochrome P450 3A4 bound to metyrapone and progesterone. *Science* **305**, 683-686 (2004).

119. Zawaira, A., Ching, L.Y., Coulson, L., Blackburn, J. & Wei, Y.C. An expanded, unified substrate recognition site map for mammalian cytochrome P450s: analysis of molecular interactions between 15 mammalian CYP450 isoforms and 868 substrates. *Curr Drug Metab* **12**, 684-700 (2011).

120. Sevrioukova, I.F. & Poulos, T.L. Structure and mechanism of the complex between cytochrome P4503A4 and ritonavir. *Proc Natl Acad Sci U S A* **107**, 18422-18427 (2010).

121. Dorr, P., *et al.* Maraviroc (UK-427,857), a potent, orally bioavailable, and selective small-molecule inhibitor of chemokine receptor CCR5 with broad-spectrum anti-human immunodeficiency virus type 1 activity. *Antimicrobial agents and chemotherapy* **49**, 4721-4732 (2005).

122. Fatkenheuer, G., *et al.* Efficacy of short-term monotherapy with maraviroc, a new CCR5 antagonist, in patients infected with HIV-1. *Nat Med* **11**, 1170-1172 (2005).

123. Abel, S., *et al.* Assessment of the absorption, metabolism and absolute bioavailability of maraviroc in healthy male subjects. *Br J Clin Pharmacol* **65 Suppl 1**, 60-67 (2008).

124. Hyland, R., Dickins, M., Collins, C., Jones, H. & Jones, B. Maraviroc: in vitro assessment of drug-drug interaction potential. *British journal of clinical pharmacology* **66**, 498-507 (2008).

125. Wright, P., Alex, A., Nyaruwata, T., Parsons, T. & Pullen, F. Using density functional theory to rationalise the mass spectral fragmentation of maraviroc and its metabolites. *Rapid Commun Mass Spectrom* **24**, 1025-1031 (2010).

126. V. P. Shevchenko, I.Y.N., and N. F. Myasoedov. Introduction of hydrogen isotopes into maraviroc and mass-spectrometric study of deuterium distribution. *Radiochemistry* **51**, 3 (2009).

127. Emoto, C. & Iwasaki, K. Enzymatic characteristics of CYP3A5 and CYP3A4: a comparison of in vitro kinetic and drug-drug interaction patterns. *Xenobiotica; the fate of foreign compounds in biological systems* **36**, 219-233 (2006).

128. Guo, Y., *et al.* Role of CYP2C9 and its variants (CYP2C9*3 and CYP2C9*13) in the metabolism of lornoxicam in humans. *Drug Metab Dispos* **33**, 749-753 (2005).

129. Walker, D.K., *et al.* Species differences in the disposition of the CCR5 antagonist, UK-427,857, a new potential treatment for HIV. *Drug metabolism and disposition: the biological fate of chemicals* **33**, 587-595 (2005).

130. Abel, S., *et al.* Assessment of the pharmacokinetics, safety and tolerability of maraviroc, a novel CCR5 antagonist, in healthy volunteers. *Br J Clin Pharmacol* **65 Suppl 1**, 5-18 (2008).

131. Boffito, M. & Abel, S. A review of the clinical pharmacology of maraviroc. Introduction. *Br J Clin Pharmacol* **65 Suppl 1**, 1-4 (2008).

132. Hardy, W.D., *et al.* Two-year safety and virologic efficacy of maraviroc in treatment-experienced patients with CCR5-tropic HIV-1 infection: 96-week combined analysis of MOTIVATE 1 and 2. *J Acquir Immune Defic Syndr* **55**, 558-564 (2010).

133. Dennison, J.B., *et al.* Selective metabolism of vincristine in vitro by CYP3A5. *Drug metabolism and disposition: the biological fate of chemicals* **34**, 1317-1327 (2006).

134. Dennison, J.B., Jones, D.R., Renbarger, J.L. & Hall, S.D. Effect of CYP3A5 expression on vincristine metabolism with human liver microsomes. *The Journal of pharmacology and experimental therapeutics* **321**, 553-563 (2007).

135. Dennison, J.B., Mohutsky, M.A., Barbuch, R.J., Wrighton, S.A. & Hall, S.D. Apparent high CYP3A5 expression is required for significant metabolism of

vincristine by human cryopreserved hepatocytes. *The Journal of pharmacology and experimental therapeutics* **327**, 248-257 (2008).

136. Kamdem, L.K.*, et al.* Contribution of CYP3A5 to the in vitro hepatic clearance of tacrolimus. *Clin Chem* **51**, 1374-1381 (2005).

137. Renders, L.*, et al.* CYP3A5 genotype markedly influences the pharmacokinetics of tacrolimus and sirolimus in kidney transplant recipients. *Clinical pharmacology and therapeutics* **81**, 228-234 (2007).

138. Min, D.I., Ellingrod, V.L., Marsh, S. & McLeod, H. CYP3A5 polymorphism and the ethnic differences in cyclosporine pharmacokinetics in healthy subjects. *Therapeutic drug monitoring* **26**, 524-528 (2004).

139. Guilhaumou, R.*, et al.* Impact of plasma and intracellular exposure and CYP3A4, CYP3A5, and ABCB1 genetic polymorphisms on vincristine-induced neurotoxicity. *Cancer Chemother Pharmacol* **68**, 1633-1638 (2011).

140. Levitt, L.P. & Prager, D. Mononeuropathy due to vincristine toxicity. *Neurology* **25**, 894-895 (1975).

141. Bennett, W.M. & Norman, D.J. Action and toxicity of cyclosporine. *Annu Rev Med* **37**, 215-224 (1986).

142. Naesens, M., Kuypers, D.R. & Sarwal, M. Calcineurin inhibitor nephrotoxicity. *Clin J Am Soc Nephrol* **4**, 481-508 (2009).

143. Mannu, J., Jenardhanan, P. & Mathur, P.P. A computational study of CYP3A4 mediated drug interaction profiles for anti-HIV drugs. *J Mol Model* **17**, 1847-1854 (2011).

144. Wienkers, L.C. & Heath, T.G. Predicting in vivo drug interactions from in vitro drug discovery data. *Nat Rev Drug Discov* **4**, 825-833 (2005).

145. Lin, Y.S.*, et al.* Co-regulation of CYP3A4 and CYP3A5 and contribution to hepatic and intestinal midazolam metabolism. *Mol Pharmacol* **62**, 162-172 (2002).

146. Lamba, J.K., Lin, Y.S., Schuetz, E.G. & Thummel, K.E. Genetic contribution to variable human CYP3A-mediated metabolism. *Adv Drug Deliv Rev* **54**, 1271-1294 (2002).

147. Le Meur, Y.*, et al.* CYP3A5*3 influences sirolimus oral clearance in de novo and stable renal transplant recipients. *Clin Pharmacol Ther* **80**, 51-60 (2006).

148. Katz, D.A.*, et al.* CYP3A5 genotype has a dose-dependent effect on ABT-773 plasma levels. *Clin Pharmacol Ther* **75**, 516-528 (2004).

149. Anderson, P.L.*, et al.* Atazanavir pharmacokinetics in genetically determined CYP3A5 expressors versus non-expressors. *J Antimicrob Chemother* **64**, 1071-1079 (2009).

150. Mouly, S.J.*, et al.* Variation in oral clearance of saquinavir is predicted by CYP3A5*1 genotype but not by enterocyte content of cytochrome P450 3A5. *Clin Pharmacol Ther* **78**, 605-618 (2005).

151. Wempe, M.F. & Anderson, P.L. Atazanavir metabolism according to CYP3A5 status: an in vitro-in vivo assessment. *Drug Metab Dispos* **39**, 522-527 (2011).

152. Emory, J.F., Seserko, L.A. & Marzinke, M.A. Development and bioanalytical validation of a liquid chromatographic-tandem mass spectrometric (LC-MS/MS) method for the quantification of the CCR5 antagonist maraviroc in human plasma.

Clinica chimica acta; international journal of clinical chemistry **431C**, 198-205 (2014).

153. Floyd, M.D.*, et al.* Genotype-phenotype associations for common CYP3A4 and CYP3A5 variants in the basal and induced metabolism of midazolam in European- and African-American men and women. *Pharmacogenetics* **13**, 595-606 (2003).

154. Chou, F.C., Tzeng, S.J. & Huang, J.D. Genetic polymorphism of cytochrome P450 3A5 in Chinese. *Drug metabolism and disposition: the biological fate of chemicals* **29**, 1205-1209 (2001).

155. Kakuda, T.N.*, et al.* Pharmacokinetic interactions of maraviroc with darunavir-ritonavir, etravirine, and etravirine-darunavir-ritonavir in healthy volunteers: results of two drug interaction trials. *Antimicrobial agents and chemotherapy* **55**, 2290-2296 (2011).

156. Abel, S., Davis, J.D., Ridgway, C.E., Hamlin, J.C. & Vourvahis, M. Pharmacokinetics, safety and tolerability of a single oral dose of maraviroc in HIV-negative subjects with mild and moderate hepatic impairment. *Antiviral therapy* **14**, 831-837 (2009).

157. Wojnowski, L.*, et al.* Re: modification of clinical presentation of prostate tumors by a novel genetic variant in CYP3A4. *Journal of the National Cancer Institute* **94**, 630-631; author reply 631-632 (2002).

158. Coto, E.*, et al.* Functional polymorphisms in the CYP3A4, CYP3A5, and CYP21A2 genes in the risk for hypertension in pregnancy. *Biochemical and biophysical research communications* **397**, 576-579 (2010).

159. Dannenberg, L.O. & Edenberg, H.J. Epigenetics of gene expression in human hepatoma cells: expression profiling the response to inhibition of DNA methylation and histone deacetylation. *BMC genomics* **7**, 181 (2006).

160. Pan, Y.Z., Gao, W. & Yu, A.M. MicroRNAs regulate CYP3A4 expression via direct and indirect targeting. *Drug metabolism and disposition: the biological fate of chemicals* **37**, 2112-2117 (2009).

161. Takagi, S., Nakajima, M., Mohri, T. & Yokoi, T. Post-transcriptional regulation of human pregnane X receptor by micro-RNA affects the expression of cytochrome P450 3A4. *The Journal of biological chemistry* **283**, 9674-9680 (2008).

162. Xie, Y.*, et al.* Epigenetic regulation of transcriptional activity of pregnane X receptor by protein arginine methyltransferase 1. *The Journal of biological chemistry* **284**, 9199-9205 (2009).

163. Assenat, E.*, et al.* Interleukin 1beta inhibits CAR-induced expression of hepatic genes involved in drug and bilirubin clearance. *Hepatology* **40**, 951-960 (2004).

164. Kim, I.W., Han, N., Burckart, G.J. & Oh, J.M. Epigenetic Changes in Gene Expression for Drug-Metabolizing Enzymes and Transporters. *Pharmacotherapy* **34**, 140-150 (2014).

165. Walker, D.K.*, et al.* Species differences in the disposition of the CCR5 antagonist, UK-427,857, a new potential treatment for HIV. *Drug metabolism and disposition: the biological fate of chemicals* **33**, 587-595 (2005).

166. Siccardi, M.*, et al.* Maraviroc is a substrate for OATP1B1 in vitro and maraviroc plasma concentrations are influenced by SLCO1B1 521 T>C polymorphism. *Pharmacogenetics and genomics* **20**, 759-765 (2010).

167. Fung, K.L. & Gottesman, M.M. A synonymous polymorphism in a common MDR1 (ABCB1) haplotype shapes protein function. *Biochimica et biophysica acta* **1794**, 860-871 (2009).

168. Hoffmeyer, S.*, et al.* Functional polymorphisms of the human multidrug-resistance gene: multiple sequence variations and correlation of one allele with P-glycoprotein expression and activity in vivo. *Proceedings of the National Academy of Sciences of the United States of America* **97**, 3473-3478 (2000).

169. Schaeffeler, E.*, et al.* Frequency of C3435T polymorphism of MDR1 gene in African people. *Lancet* **358**, 383-384 (2001).

170. Lu, Y., Hendrix, C.W. & Bumpus, N.N. Cytochrome P450 3A5 plays a prominent role in the oxidative metabolism of the anti-human immunodeficiency virus drug maraviroc. *Drug metabolism and disposition: the biological fate of chemicals* **40**, 2221-2230 (2012).

171. Schlecht, H.P., Schellhorn, S., Dezube, B.J. & Jacobson, J.M. New approaches in the treatment of HIV/AIDS - focus on maraviroc and other CCR5 antagonists. *Therapeutics and clinical risk management* **4**, 473-485 (2008).

172. Moore, R.D. Epidemiology of HIV infection in the United States: implications for linkage to care. *Clinical infectious diseases : an official publication of the Infectious Diseases Society of America* **52 Suppl 2**, S208-213 (2011).

173. Abel, S., Jenkins, T.M., Whitlock, L.A., Ridgway, C.E. & Muirhead, G.J. Effects of CYP3A4 inducers with and without CYP3A4 inhibitors on the pharmacokinetics of maraviroc in healthy volunteers. *British journal of clinical pharmacology* **65 Suppl 1**, 38-46 (2008).

174. Abel, S., Back, D.J. & Vourvahis, M. Maraviroc: pharmacokinetics and drug interactions. *Antiviral therapy* **14**, 607-618 (2009).

CURRICULUM VITAE

YANHUI LU

Born
Jan 27th, 1982
Yanggu, Shandong, China

Contact
ylu16@jhmi.edu
lvyanhui123@gmail.com

Education:

Ph.D. (expected), Department of Pharmacology and Molecular Sciences, The Johns Hopkins University School of Medicine, Baltimore, MD, USA. **Advisor:** Craig W. Hendrix

The Johns Hopkins University School of Medicine
August 2009 – July 2014 (expected)
Ph.D., Pharmacology and Molecular Sciences
Thesis: "Cytochrome P450 3A-mediated Pharmacokinetic Variations for Anti-infective Agents". Thesis Advisor – Craig W. Hendrix, M.D.

Ohio State University
June 2007-July 2009
M.S., College of Pharmacy

Chinese Academy of Sciences
September 2002-July 2005
M.S., Biochemistry and Molecular Biology, Shanghai Institutes for Biological Sciences

Shandong University
September 1998-June 2002
B.S., Biotechnology

Publications:

1. Savic RM, **Lu Y**, Bliven-Sizemore E, Weiner M, Nuermberger E, Burman W, Dorman SE, Dooley KE. Population pharmacokinetics of rifapentine and desacetyl rifapentine in healthy volunteers: nonlinearities in clearance and bioavailability. *Antimicrob Agents Chemother.* 2014 Mar 10. [Epub ahead of print]
2. Gupta SV, Hertlein E, **Lu Y**, Sass EJ, Lapalombella RT, Chen TL, Davis M, Woyach JA, Lehman A, Jarjoura D, Byrd JC, Lucas DM. The proteasome inhibitor carfilzomib functions independently of p53 to induce potent cytotoxicity and an atypical NF-κB response in chronic lymphocytic leukemia cells. *Clin Cancer Res.*

2013;19(9):2406-19.

3. **Lu Y**, Celum C, Wald A, Baeten JM, Cowan F, Delany-Moretlwe S, Reid SE, Hughes JP, Wilcox E, Corey L, Hendrix CW. Acyclovir achieves a lower concentration in African HIV-seronegative, herpes simplex virus 2-seropositive women than in non-African populations. *Antimicrob Agents Chemother.* 2012; 56(5): 2777-9.
4. **Lu Y**, Hendrix CW, Bumpus, NN. Cytochrome P450 3A5 plays a prominent role in the oxidative metabolism of the anti-HIV drug maraviroc. *Drug Metab Dispos.* 2012; 40(12):2221-30.
5. Nyunt MM, **Lu Y**, Yu Q, El-Gasim M, Parsons TL, Petty BG, Hendrix CW. Effects of ritonavir-boosted lopinavir on the pharmacokinetics of quinine. *Clin Pharmacol Ther.* 2012; 91(5): 889-95.
6. Dolley KE, Bliven-Sizemore EE, Weiner M, **Lu Y**, Nuermberger EL, Hubbard WC, Fuchs EJ, Melia MT, Burman WJ, Dorman SE. Safety and pharmacokinetics of escalating daily doses of the antituberculosis drug rifapentine in healthy volunteers. *Clin Pharmacol Ther.* 2012; 91(5): 881-8.
7. Li H[*], **Lu Y**[*], Piao L, Wu J, Yang X, Kondadasula SV, Carson WE, Lee RJ. Folate- immunoglobulin G as an anticancer therapeutic antibody. *Bioconjug Chem.* 2010; 21(5): 961-8 ([*]**The authors contributed equally to this work**).
8. Li H, **Lu Y**, Piao L, Wu J, Liu S, Marcucci G, Ratnam M, Lee RJ. Targeting human clonogenic acute myelogenous leukemia cells via folate conjugated liposomes combined with receptor modulation by all-trans retinoic acid. *Int J Pharm.* 2010; 402(1-2): 57-63.
9. Xiang G, Wu J, **Lu Y**, Liu Z, Lee RJ. Synthesis and evaluation of a novel ligand for folate-mediated targeting liposomes. *Int J Pharm.* 2008; 356(1-2): 29-36.
10. **Lu Y**, Wu J, Wu J, Gonit M, Yang X, Lee A, Xiang G, Li H, Liu S, Marcucci G, Ratnam M, Lee RJ. Role of formulation composition in folate receptor-targeted liposomal doxorubicin delivery to acute myelogenous leukemia cells. *Mol Pharm.* 2007; 4(5): 707-12.
11. Tong L, **Lu Y**, Lee RJ, Cheng JX. Imaging receptor-mediated endocytosis with a polymeric nanoparticle-based coherent anti-stokes Raman scattering probe. *J Phys Chem B*. 2007; 111(33): 9980-5.
12. Wu J, **Lu Y**, Lee A, Pan X, Yang X, Zhao X, Lee RJ. Reversal of multidrug resistance by transferrin-conjugated liposomes co-encapsulating doxorubicin and verapamil. *J Pharm Pharm Sci.* 2007; 10(3): 350-7.
13. Wu J, Lee A, **Lu Y**, Lee RJ. Vascular targeting of doxorubicin using cationic liposomes. *Int J Pharm.* 2007; 337(1-2): 329-35.
14. Fulci G, Dmitrieva N, Gianni D, Fontana EJ, Pan X, **Lu Y**, Kaufman CS, Kaur B,

Lawler SE, Lee RJ, Marsh CB, Brat DJ, van Rooijen N, Stemmer-Rachamimov AO, Hochberg FH, Weissleder R, Martuza RL, Chiocca EA. Depletion of peripheral macrophages and brain microglia increases brain tumor titers of oncolytic viruses. *Cancer Res.* 2007; 67(19): 9398-406.

Abstracts:

1. Nyunt MM, **Lu Y**, El-Gasim M, Parsons T, Petty BG, Hendrix CW. Effects of steady-state lopinavir/ritonavir on the pharmacokinetics of quinine in healthy volunteers. American Society of Tropical Medicine and Hygiene, Atlanta, Georgia, 2010. Abstract No.1242.

2. **Lu Y**, Hendrix CW, Celum C, Baeten J, Cowan F, Delany-Moretlwe S, Reid S, Hughes J, Wald A, Corey L. Acyclovir achieves lower concentration in African HIV^-, $HSV\text{-}2^+$ women compared to non-African populations, possibly explaining lower Herpes suppression. 19th Biennial Conference of the International Society for Sexually Transmitted Diseases Research. Québec City, Canada, 2011.
3. Bliven-Sizemore E, Burman W, Dooley K, Dorman S, Fuchs E, **Lu Y**, Nuermberger E, Weiner M. A phase I dose escalation trial of the pharmacokinetics, safety, and tolerability of rifapentine dosed daily in healthy volunteers: preliminary results from Tuberculosis Trials Consortium study 29B. American Thoracic Society International Conference, Denver, Colorado, 2011.
4. **Lu Y**, Hendrix CW, Bumpus NN. Identification of novel phase I and phase II metabolites of maraviroc using human liver microsomes. 17th North American Regional International Society for the Study of Xenobiotics Meeting, Atlanta, Georgia, 2011. Abstract No. P252.
5. **Lu Y**, Hendrix CW, Bumpus NN. P450 3A5 is primarily responsible for the formation of the most abundant oxidative metabolite of maraviroc. ASPET Annual Meeting, San Diego, California, 2012. Abstract No. 1738.

Seminars and Presentations:

1. Pharmacokinetic interactions between quinine and lopinavir/ritonavir in healthy volunteers. Department of Pharmacology and Molecular Sciences, The Johns Hopkins University School of Medicine, April 8th, 2010.
2. Cytochrome P450 3A and maraviroc metabolism. Division of Clinical Pharmacology, Department of Medicine, The Johns Hopkins University School of Medicine, March 21st, 2012.
3. P450 3A5 is primarily responsible for the formation of the most abundant

oxidative metabolite of maraviroc. ASPET Annual Meeting at Experimental Biology 2012, San Diego, California, April 23rd, 2012.

4. The role of CYP3A enzymes in oxidative metabolism of maraviroc. Department of Pharmacology and Molecular Sciences, The Johns Hopkins University School of Medicine, May 15th, 2012.

Research Experience:

The Johns Hopkins University School of Medicine, Department of Pharmacology and Molecular Sciences: (May 2010 – March 2014)
Cytochrome P450 3A-mediated pharmacokinetic variations for anti-infective agents
Mentor: Craig W. Hendrix, M.D.

The Johns Hopkins University School of Medicine, Department of Pharmacology and Molecular Sciences: (December 2009 – April 2010)
The anti-HIV activity of tenofovir
Mentor: Robert F. Siliciano, M.D.

The Johns Hopkins University School of Medicine, Department of Pharmacology and Molecular Sciences, Division of Clinical Pharmacology: (August 2009 – November 2009)
Effect of the anti-HIV drugs lopinavir/ritonavir on pharmacokinetics of an anti-malarial drug, quinine
Mentor: Craig W. Hendrix, M.D.

Ohio State University, Department of Medicinal Chemistry and Pharmacognosy, College of Pharmacy: (June 2007 – July2009)
The anti-leukemic mechanism of the proteasome inhibitor carfilzomib
Mentor: John C. Byrd, M.D.

Ohio State University, Department of Pharmaceutics, College of Pharmacy: (November 2005 – May 2007)
Development of targeted anti-cancer therapy using folate-conjugated liposomal drugs and/or human IgG
Mentor: Robert J. Lee, Ph.D.

Shanghai Institutes for Biological Sciences, Chinese Academy of Sciences: (September 2002 – June 2005)
The pharmacodynamics (anti-HIV effect) of the chemokine receptor CCR5 antagonist TD0232
Mentor: Gang Pei, Ph.D.

Academic Awards:

2011	Sheinberg Travel Award, Department of Pharmacology and Molecular Sciences, The Johns Hopkins University School of Medicine
2012	Graduate Student Best Abstract Award, American Society for Pharmacology and Experimental Therapeutics (ASPET) 2012
2012	Graduate Student Travel Award, ASPET 2012
2012	Junghea Park Memorial Travel Award, The Johns Hopkins University School of Medicine
2012	Chinese Government Award for Outstanding Self-financed Students Abroad
2014	The Bae Gyo Jung Research Award of Young Investigators' Day, The Johns Hopkins University School of Medicine

Professional/Scholastic Organizations:

American College of Clinical Pharmacology (2013-present)
American Society of Pharmacometrics (2011-present)
American Society for Pharmacology and Experimental Therapeutics (2011-present)
American Society for Clinical Pharmacology and Therapeutics (2011-present)
International Society for the Study of Xenobiotics (2011-present)